SYNTHESIS OF MAGNETIC NANOADSORBENTS DERIVED FROM MAIZE WASTE AND THEIR APPLICATION FOR THE ADSORPTIVE REMOVAL OF SELECTED HEAVY METAL IONS FROM WASTEWATER SAMPLES

by

LOUISAH MMABAKI MAHLAULE GLORY (63339536)

submitted in accordance with the requirements for
the degree of

MASTER OF SCIENCE

in Chemistry

at the

UNIVERSITY OF SOUTH AFRICA

SUPERVISOR: PROF N MKETO

CO-SUPERVISOR: DR ED MOEMA
CO-SUPERVISOR: PROF NC HINTSHO-MBITA

May 2024

DECLARATION

Name: Louisah Mmabaki Mahlaule Glory

Student number: 63339536

Degree: Master of Science in Chemistry

Exact wording of the title of the dissertation as appearing on the electronic copy submitted for examination:

Synthesis of magnetic nano-adsorbents derived from maize waste and their application for the adsorptive removal of selected heavy metal ions from wastewater samples

I declare that the above dissertation is my own work and that all the sources that I have used or quoted have been indicated and acknowledged by means of complete references.

I further declare that I submitted the dissertation to originality checking software and that it falls within the accepted requirements for originality.

I further declare that I have not previously submitted this work, or part of it, for examination at Unisa for another qualification or at any other higher education institution.

(The dissertation will not be examined unless this statement has been submitted.)

SIGNATURE DATE: 28 May 2024

UNIVERSITY OF SOUTH AFRICA

KEY TERMS DESCRIBING THE TOPIC OF A DISSERTATION/THESIS

The Executive Committee of Senate decided that in order to assist the library with retrieval of information, master's and doctoral students must list approximately ten key terms which describe the topic of the dissertation/thesis at the end of the summary of the dissertation/thesis.

If the dissertation/thesis is not written in English, the key terms in English must be listed at the end of the English summary.

The following is an example of key terms used for a thesis/dissertation:

Title of thesis/dissertation:

SYNTHESIS OF MAGNETIC NANOADSORBENTS DERIVED FROM MAIZE WASTE AND THEIR APPLICATION FOR THE ADSORPTIVE REMOVAL OF SELECTED HEAVY METAL IONS FROM WASTEWATER SAMPLES

KEY TERMS:

Nono-adsorbents, cellulose nano crystals (CNC), magnetic cellulose nanocrystal (MCNC), TEMPO crosslinked cellulose nanocrystals (TEMPO-CNC), TEMPO functionalised polyethyleneimine on CNC (TEMPO-CNC-PEI), magnetic cellulose nano crystals grated on PEI (MCNC-PEI), heavy metals ions (HMIs), adsorption, magnetic solid phase extraction (m-SPE), lead, chromium, nanocomposites, wastewater, multivariate optimization, central composite design, isotherms, kinetics, thermodynamics

ACKNOWLEDGEMENTS

I would like to thank my Lord and Saviour, Jesus Christ for the strength, protection, and courage to pursue my dreams. I give Him all the honour and Glory for He deserves the best in my life.

I appreciate my main supervisor, Prof. Nomvano Mketo for her kind heart, understanding, support, guidance, for believing in me, sharpening my thinking capacity, pushing me to be the best version of me and encouraging me to be ambitious and helping me to represent the department intentionally. You are the best! Furthermore, I would like to thank you to my co-supervisors Dr. Moema (University of South Africa) and Prof. Hintsho-Mbita (University of Limpopo) for their continuous support and guidance to ensure that I am always on the right track with my research project, I am grateful for everything you have done for me. I also grateful like to thank Dr. Zikona Tetana from the University of the Witwatersrand (Wits) for P-XRD and SEM analysis together with Ms. Orianda Sebabi from the University of Johannesburg (UJ) for the P-XRD analysis.

My gratitude also goes to all the Environmental and Food Analytical Chemistry Research Group members at UNISA for their continuous support and assistance when required. Special thanks go to Dr. Maxwell Thatyana, Mr Oluseyi Salami and Mr Njabulo Mdluli who went all out of their way to help me. From the same group, I would also like to thank Ms Thabang Kgoedi, Ms Musiwa Victoria Sengane, Mr Basil Munjanja and Mr Magwadi Alex Namame for going extra mile in assisting me.

I extend my gratitude to UNISA for giving me this opportunity to register for this degree and not forgetting the RPL co-ordinator Ms Eugene Nkhwashu for her assistance during the admission process.

To Carol Langa, thank you for your continued support and your help in sending the samples for analysis whenever I needed you to.

My deepest gratitude goes to Mr Neville Nyamutswa from the Capricorn District Municipality for the metal ion quantification using inductively coupled plasma-optical emission spectroscopy (ICP-OES).

Special thanks go to the University of Limpopo for financial assistance and time off, particularly to the Executive Dean of Science and Agriculture: Prof. HJ Siweya and the School Director Prof. HR Chauke for granting me a sabbatical leave and recommending financial assistance.

In him we live move and have our being.

Special thanks to my family members, my husband Morris Mahlaule Glory for taking care of the family in my absence to pursue this career. Not forgetting my precious princesses (Blessing, Nsaseko, Kgalalelo and Restoration) Mahlaule Glory for their love, courage, and their moral support.

PUBLICATION(S)

Papers

1. L.M Mahlaule-Glory, M Thatyana, E.D Moema, N.C. Hintsho-Mbita, N.Mketo*. Synthesis of magnetic cellulose nanocrystals derived from maize waste for the adsorptive removal of Pb (II) from wastewater samples. *Reviewr's comments recived with minor corrections.*
2. L.M Mahlaule-Glory[1], E.D Moema[1], N.C. Hintsho-Mbita[2], N.Mketo[1*]. Adsorbents applied for the adsorptive removal of Heavy Metal Ions from wastewater samples and their distribution and interactions using linear regression analysis. A review**.** *For submission*
3. L.M Mahlaule-Glory[1], N.S Mdluli[1], E.D Moema[1], N.C. Hintsho-Mbita[2], N.Mketo[*1]. Fabrication of polyethyleneimine-functionalized magnetic cellulose nanocrystals for selective adsorption of Cr (VI) from aqueous solutions. *Under review.*

Oral Presentation

1. L.M Mahlaule-Glory[1], E.D Moema[1], N.C. Hintsho-Mbita[2], N.Mketo[1*]. Synthesis of magnetic cellulose nanocrystals derived from maize waste for the adsorptive removal of Pb (II) from wastewater samples. The 1st Aristotle Conference of Chemistry (ACC 2023), 12th-15th November 2023, Thessalonikki, Greece.

ABSTRACT

Over the past few years, heavy metal ion (HMI) pollution has become a crucial matter due to their threat to human health and ecological systems.,. Furthermore, HMIs have been reported to be hazardous, persistent, and in some of the global health organizations reports, they have been declared as carcinogens. These HMIs include Pb (II) and Cr (VI) and they are very reactive and highly oxidizing in nature. Thus, the need to remediate these HMIs from wastewater using magnetic nano adsorbents.

In this study, three nano-adsorbents such as cellulose nano crystals (CNC), magnetite (M), and magnetic cellulose nanocrystal (MCNC) were synthesized for the removal of Pb (II) in wastewater. The magnetic cellulose nanocrystals (MCNCs) were synthesized using a co-precipitation method from the magnetite (Fe_3O_4) and cellulose nano crystals (CNCs) were used as a base for stability and easy dispersion of iron for the adsorptive removal of Pb (II) ions. Furthermore, to enhance the adsorption capacity and to improve selectivity of the CNC towards -targeting anionic Cr (VI) ions, the surface modification was conducted by crosslinking CNCs with 2,2,6,6-tetramethylpiperidinyloxy (TEMPO), thereby oxidising the material to form a bridge with the grafting of the polyethyleneimine (PEI). The surface of the CNC-TEMPO-PEI was further magnetised by introducing iron on to the surface material via a co-precipitation method.

Fourier-transform infrared spectroscopic (FTIR) analysis revealed the presence of C=O, COOH, CH, OH and FeO stretching frequencies in MCNC, while powder X-ray diffraction (P-XRD) confirmed the formation of MCNC and the monoclinic type 1 cellulose with 1β lattice and magnetite cubic spinel phases of the CNC. Ultraviolet-visible spectroscopy (UV-Vis) showed the presence of both CNC and magnetite at 400 nm. The scanning electron microscopy (SEM) indicated a smooth fibroid surface of CNCs while magnetite (M) displayed 2 morphologies, the rod like and spherical morphology, indicating the presence of iron and oxygen. The MCNC were stable after 600 ºC as shown on the thermograms generated from the thermogravimetric analyser (TGA). Last, the Brunauer-Emmett-Teller (BET) displayed surface area, pore size

and pore volume improvement of 56 m^2/g, 98 Å and 0,1465 cm^3/g. Å, respectively, for the MCNC.

Following the characterization of the MCNCs nanocomposites, the material was used for adsorptive removal of Pb (II). It was discovered that for the Pb (II) removal efficiency was 97 % with an acceptable precision of ≤ 3 %. The highest efficiency was obtained at optimal conditions of 60 mg dosage, 0,1 ppm concentration within a rapid contact time of 5 min at a temperature of 60 ºC and at a pH of 6. These parameters were optimised by using multivariate optimization tools (Minitab) and were also validated against the magnetite and the CNC. A maximum adsorption capacity of MCNC was also obtained at 47,70 mg/g for Pb (II) and the material was re-used for up to 4 cycles. The results revealed that the reaction followed Freundlich isotherms and Pseudo First Order kinetic model with a regression coefficient of 0,98 and 0,96 respectively. The adsorption thermodynamics studies indicated a spontaneous process and an exothermic reaction.

On the other hand, the MCNC-TEMPO-PEI was characterised with FTIR, P-XRD, TEM and SEM-EDS techniques. The FTIR confirmed a successful formation and the presence of COOH, OH, Fe-O band and NH_2 groups on the nanocomposite. The P-XRD confirmed the crystal structure of CNC-TEMPO and the amorphous structure of both the CNC-TEMPO-PEI and the MCNC-TEMPO-PEI. The SEM-EDS results demonstrated the rod-like, oval and irregular cubic morphology for successful preparation of MCNC-TEMPO-PEI nanocomposite.

The adsorption performance of MCNC-TEMPO-PEI on Cr (VI) ions was investigated by using univariate optimization tools. The MCNC-TEMPO-PEI was efficient at 5 ppm, using a 30 mg dosage at 25 ºC within the acidic conditions at pH 2 within a rapid contact time of 15 min. The optimised parameters were further validated using 5 various adsorbent materials and the results indicated that the MCNC-TEMPO-PEI was the most efficient by exhibiting the highest adsorption capacity of 4,4 mg/g with a 98% removal. The interaction between the MCNC-TEMPO-PEI and the Cr (VI) ions indicated a chemisorption of the electrostatic forces governing the magnetic and ionic exchange interaction between of the adsorbate and the analyte. The Langmuir adsorption isotherm displayed a correlation coefficient of 0,94 following

the PSO kinetic model against the adsorptive removal of Cr (VI) ions. The thermodynamic interaction indicated a non-spontaneous endothermic reaction with a favourable reaction. The adsorbent could be reused at least 8 times with a removal efficiency above 75 %. The results revealed that the real wastewater samples analysed from this study did not contain Cr (VI) ion.

Contents

LIST OF FIGURES

LIST OF TABLES

LIST OF EQUATIONS

LIST OF ABBREVIATIONS AND ACRONYMS

HMIS	: Heavy metal ions
Pb	: Lead
Pb (II)	: Divalent lead
Cr	: Chromium
Cr (VI)	: Hexavalent chromium
WWTPs	: Wastewater treatment plants
WHO	: World Health Organization
EPA	: Environmental Protection Agency
IARC	: International Agency for Research on cancer
CNC	: Cellulose nanocrystal
M	: Magnetite
MCNC	: Magnetic cellulose nanocrystal
TEMPO	: 2,2,6,6-tetramethylpiperidinyloxy
PEI	: Polyethyleneimine
MCNC-TEMPO-PEI	: Magnetic cellulose nanocrystal crosslinked with TEMPO and grated with polyethyleneimine.
H_2SO_4	: Sulphuric acid
HCl	: Hydrochloric acid
H_3PO_4	: Phosphoric acid
HF	: Hydrofluoric acid
MSPE	: Magnetic solid phase extraction
SPE	: Solid phase extraction
ICP-OES	: Inductive coupled plasma-optical emission spectroscopy
FTIR	: Fourier-Transform Infrared Spectroscopy

P-XRD	: Powder X-ray diffraction
TEM	: Transmission electron microscopy
SEM	: Scanning electron microscopy
EDS	: Energy dispersive X-ray spectrometer
UV-Vis	: Ultra-Violet Visible spectrophotometer
TGA	: Thermogravimetric analysis
BET:	: Brunauer–Emmett–Teller
MOs	: Metal oxides
MOF	: Metal organic framework
MIP	: Molecular imprinted polymer
IIP	: Ion imprinted polymers
PFO	: Pseudo First Order
PSO	: Pseudo Second Order

CHAPTER I (INTRODUCTION)

PREAMBLE

This chapter introduces the study with detailed information covering the background which includes the importance of having access to clean and drinkable water, factors affecting the quality of water, generation of wastewater effluents, toxins contained in wastewater, health effects caused by these pollutants, current and adsorbents used for the remediation of wastewater.

1.1. Background

Water is an essential element of life that is utilized by the ecosystem. From the 71 % available global water, the world has about 2.5 % of pure water [1-2]. Of that 2.5 %, less than 1% of fresh water is accessible for safe consumption by humans and animals [1]. Access to safe water for drinking for both humans and animals is a necessity which is required by the World Health Organization (WHO) as shown in **Fig. 1.1** [3].

Figure 1.1: Clean safe drinking water accessed globally [4]

Several factors have negatively influenced access to safe water globally over the past few years. These factors include low rainfall, climate change, population growth, economic growth, industrial expansion, poor water management and incorrect disposal of wastewater [5]. These factors have resulted in water scarcity, particularly in countries like South Africa. Amongst these factors, wastewater is a dominating factor in South Africa, particularly in urban areas like in Gauteng Province as the South African economic harbour. In as much as economic growth improves the country in acquiring necessary resources from industries, industries like farming, textile, mining, manufacturing, and hospitals are constantly releasing their waste into the nearest water streams as displayed in **Fig. 1.2**. The incorrect disposal adds different toxins and contaminate the neighbouring main water streams [5-6]. This affects the quality of water in various water bodies like rivers, dams etc. available for human consumption [7].

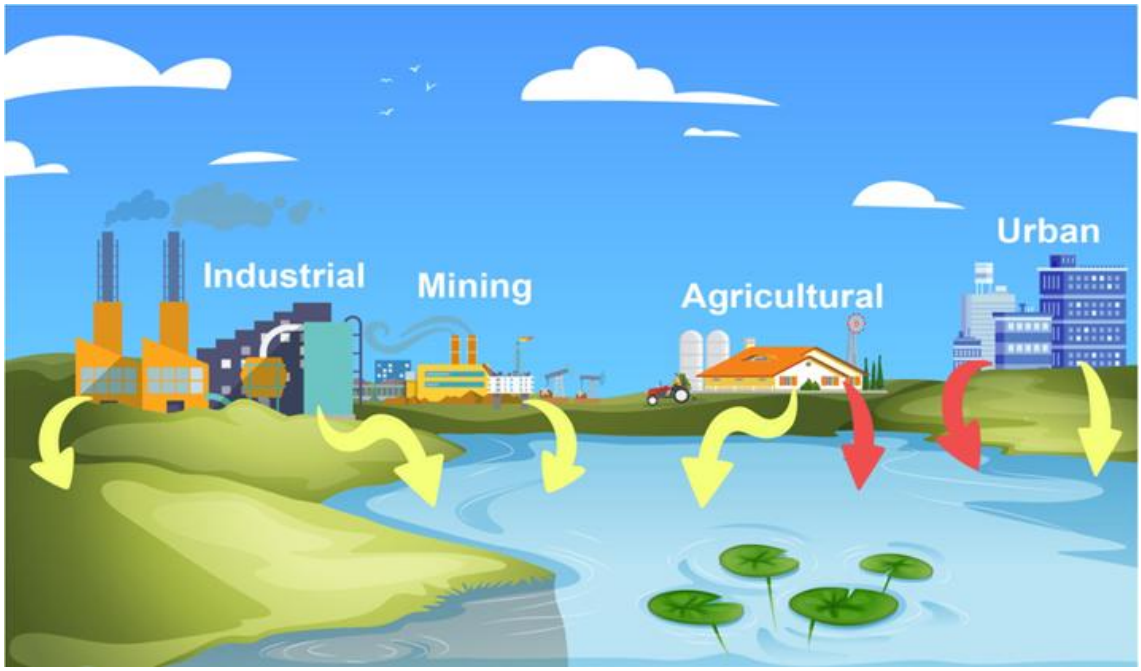

Figure 1.2: Wastewater contamination from various effluents [8]

In other countries, the seriousness of this conduct has compelled governments to place monitoring tools used to measure waste production to minimize water pollution [7]. Wastewater treatments plants (WWTPs) are established for the purpose of treating

wastewater. However, the WWTPs also generate wastewater effluents which also adds secondary pollution and further generates more pollutants when disposed. Noreen *et al* [9] reported that the majority of these pollutants are the HMIs with 70 % containment in wastewater [9]. The HMIs are considered a class of mutagenic, carcinogenic and hazardous pollutants [7]. On top of that, they have also been classified as persistent and destructive pollutants since they are soluble in water and can further be absorbed by the species within these water bodies [10]. This had led to serious health effects in humans ranging from acute to chronic diseases as shown in **Fig. 1.3**.

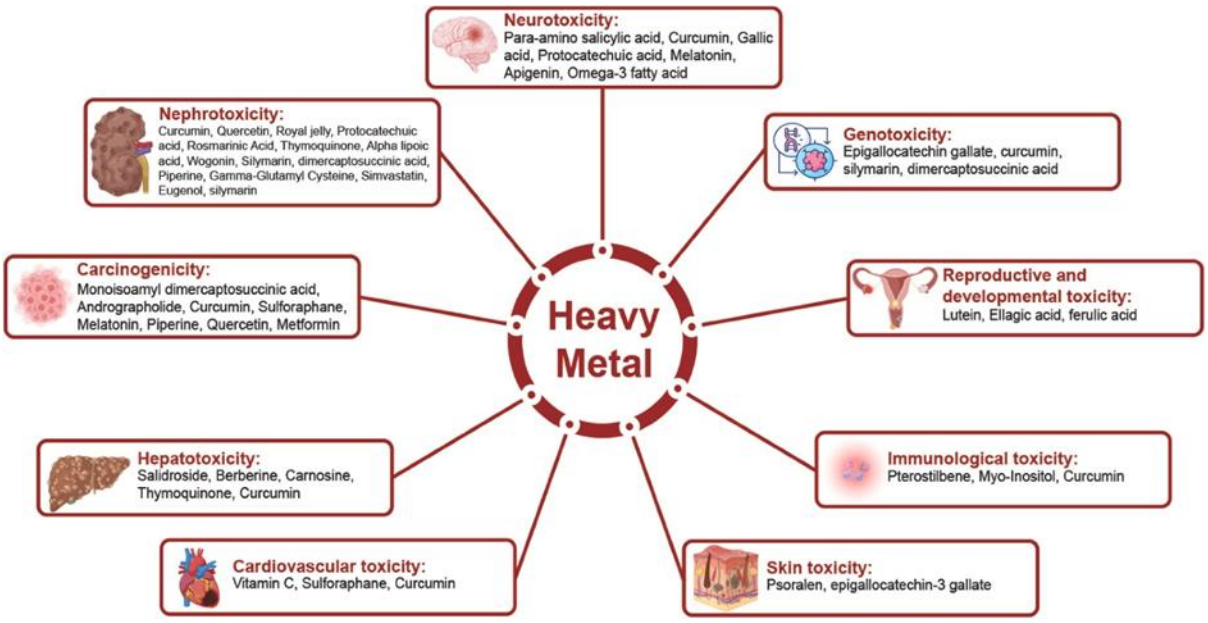

Figure 1.3: Diseases caused by Heavy metal ions (HMIs) consumption [8]

The acute illnesses include feeling tired, fatigued, nausea and body pain, whereas chronic diseases include hypertension, peripheral neuropathy, kidney, brain and nervous system failure also affecting plants and animals as well [11-12]. Thus, various wastewater remediation methods have received significant attention globally, as scientists have developed several techniques to address HMIs in wastewater [7,12]. These include ion exchange, flocculation, electrochemical, reverse osmosis and chemical precipitation [13-14]. Even though they have previously been reported to effectively treat wastewater, they have also

shown shortcomings, including the use of costly adsorbents, the need for multiple treatments, higher maintenance and higher energy-intensive methods [15].

A recent trend is the application of adsorptive materials for the removal of HMIs from wastewater because of their simplicity, high adsorption efficiency and easy removal steps [12]. This is due to the adsorbents having a high surface area, porosity and hence achieving high removal efficiency. However, the conventional adsorbents are known to have shown several setbacks such as being expensive and generating secondary pollutants after use. Furthermore, several researchers have attempted to use these adsorbents but failed to selectively remove their targeted analytes. Moreover, these adsorbents have been synthesized by different methods such as chemical and physical methods [6,10]. With chemical methods, toxic chemicals are used whilst physical methods use high temperature and pressure conditions. Nowadays research is geared towards the use of biosorbents (water remediation) from natural sources to preserve our ecological system [14-16].

Bio-polymeric materials are generally a perfect candidate for appropriate bio-sorbents since they possess a large surface area and can be produced at a low cost with numerous reusable cycles [16]. There is a need to substitute expensive adsorbents with cost-effective, environmentally friendly and locally available maize stalk adsorbents in line with the principles of green chemistry [17]. Maize waste is a preferred natural reductant due to its physicochemical properties and acts as a reducing, stabilizing and regeneration agent during the synthesis of the magnetic nanocomposite [15]. Moreover, maize waste contains a high content of cellulose that can assist in the synthesis of cellulose nanocrystal (CNC) adsorbent materials [16-17].

Cellulose nanocrystals as a biopolymer possesses large surface area but due to its hydrophobic nature and poor selectivity, CNC can result in low adsorption efficiency thus, hindering a higher percentage removal of HMIs from wastewater [18]. Yet these can be overcome by surface modification using the crosslinking process that involves the addition of other polymers to introduce other functional groups like (OH, COOH and NH_2) allowed to target

the analyte of interest [19-20]. The molecular imprinted polymers (MIPs) are the current interest for researchers in achieving higher adsorption capacity and higher selectivity better than the carboxy cellulose nanocrystal (CCNC) [21].

In addition to their vast selectivity, MIPs also have the ability to recognise active sites and receptors for a particular analyte of interest [22]. Nonetheless, these polymerized adsorbents have also exhibited some disadvantages drawn in the presence of UV radiation when polymers are present [23]. These include, breaking the polymer chain and reducing the molecular weight of the MIPs during adsorption [23]. On top of that, the methods for preparing bulk polymerization, tend to evoke the recognition sites that intensively overload the adsorbents (MIPs) inner structure, leading to the reduced mass transfer rate that can seriously affect the MIPs performance [24]. Moreover, the MIPs have also shown disadvantages of eliminating false similar structures of the analyte in question [24-25]. Therefore, the second surface modification of adding magnetite to the MIPs is required to overcome these challenges by introducing superparamagnetic properties, generate more active surface site and enhance the adsorption capacity and selectivity of the desired analyte [26].

In this study, the intention is to synthesize Magnetic Cellulose Nanocrystal (MCNC) and the Magnetic cellulose nanocrystals crosslinked with TEMPO and grafted on Polyethyleneimine (MCNC-TEMPO-PEI) derived from the maize stalk for the selective and removal of Pb (II) and Cr (VI) from wastewater. Thereafter, optimize the surface methodology for adsorption based on pH, dosage, concentration and contact time.

1.2. Problem statement

The indiscriminate discharge of wastewater effluents from WWTPs is not only contaminating the water streams but also leaves a large amount of unused and unavailable water that might have been utilised for human consumption after treatment. To remediate wastewater, various studies have used treatment methods like ion exchange, flocculation, reverse osmosis and chemical precipitation [27]. These methods have shown limitations like

generating secondary pollutants such as sludge, use of toxic and corrosive chemicals, requiring tedious treatment, energy-intensive consumption, requiring higher maintenance and use of expensive adsorbents when treating wastewater [13-14]. Adsorption has emerged as a method of choice for the removal of pollutants from WWTPs because adsorbents have a high surface area and porosity, and hence a high removal efficiency. However, conventional adsorbents applied have several setbacks such as being expensive and generating pollutants after use, low adsorption capacity, lack of selectivity and loss of material during the regeneration process. Thus, the need for eco-friendlier, less costly, effective adsorption, abundantly available adsorbents are required.

1.3. Aim and objectives.

1.3.1. *Aim*

This research project aims to synthesize, characterize and apply maize waste-derived magnetic cellulose nanocrystal (MCNC) and magnetic cellulose nanocrystal functionalised with TEMPO and polyethyleneimine (MCNC-TEMPO-PEI) for the adsorptive removal of Pb (II) and Cr (VI) ions, respectively from wastewater.

1.3.2. *objectives*

The specific objectives are to:

- ✓ *Synthesize the cellulose nanocrystal (CNC), magnetite (M), magnetic cellulose nanocrystal (MCNC), TEMPO mediated cellulose nanocrystal (CNC-TEMPO), cellulose nanocrystal crosslinked with TEMPO and grafted with polyethyleneimine (CNC-TEMPO-PEI), and the magnetic cellulose nanocrystal grafted with polyethyleneimine (MCNC-TEMPO-PEI) derived from maize stalk.*
- ✓ *Characterize the nanocomposites CNC, M, MCNC, CNC-TEMPO, CNC- TEMPO-PEI and MCNC-TEMPO-PEI using the FTIR, XRD, UV-Vis, BET, SEM, EDS, TEM and TGA.*

- ✓ *Optimize the most influential parameters (dosage, time, temperature, pH, concentration) against the Pb (II) and Cr (VI) using both multivariate and univariate optimization tools, respectively.*
- ✓ *Study kinetic, thermodynamic and adsorption isotherms under the optimum conditions.*
- ✓ *Investigate the adsorption mechanism.*
- ✓ *Evaluate the reusability of the studied of adsorbents and the leachability of the iron.*
- ✓ *Apply the proposed adsorbents in real wastewater samples.*

1.4. Justification of the study

Currently, researchers have opted to use eco-friendlier methods since they possess greens triple R's (recyclable, reusable and reduce) materials [20]. The renewable cellulose from the agricultural waste since it is cheaper and abundantly available for the synthesis of magnetic nanocomposites has been used to replace expensive materials [16]. Agricultural waste includes rice straws, nutshells, palm seeds, corn cob, corn stalk and corn pith [19-20]. The added advantage of crystalline cellulose derived from maize waste is its ability to possess good surface area and enhanced porosity making it a convenient water treatment material due to its hydrophilic and thermal properties [15,18]. Maize waste is used as a preferred natural reductant due to its physicochemical properties. It acts as a reducing, stabilizing and regeneration agent during the synthesis of the magnetic nanocomposite, it also can disperse iron to inhibit agglomeration from the iron-based materials [28].

For efficient adsorption of the required analyte, the nano adsorbents are recommended to perform a surface modification with the expectation of selectivity. Researchers have used the TEMPO to connect the PEI since CNC mainly have OH groups. This makes it difficult to selectively target the anionic analytes. Thus, the PEI is required to be grafted with the help of the TEMPO oxidised material. The use of TEMPO comes with added advantages such as selectively converting the primary OH groups, particularly on the C6 position of the CNC

surface to the COOH groups without alteration of the original CNC crystallinity [29-30]. This compels it to produce functionalised CNC with smaller particle sizes and diameters [31]. Thus, resulting in an increased number of carboxylic groups, having specific higher surface area, high crystallinity, and high specific strength [32]. Moreover, it facilitates the introduction of the amino groups useful for enhanced adsorption capacity from the addition of another polymer (PEI).

1.5. Hypothesis

The nano composite adsorbents (MCNC and MCNC-PEI) from this study are expected to remediate wastewater effluents to remove selected HMIs from WWTPs. Owing to their selectivity, sensitivity, magnetic properties making them to easily attach their analytes and easier desorption afterwards. Furthermore, our materials are also porous, selective towards the analyte and possess higher surface area that increases the chances of having many active sites during adsorption and enhance the adsorption capacity. Moreover, because of these properties, their stability during interaction reaction with the adsorbate is increased, generating numerous recyclable cycles.

1.6. Research questions

1.6.1. Will the cellulose provide efficient support on the magnetite for the adsorptive removal of HMIs?

1.6.2. Will the synthetic methods achieve the desired nano adsorbent?

1.6.3. How will the amine groups be introduced on the adsorbent for the removal of Cr (VI)?

1.6.4. Which analytical techniques will be used to check the formation, crystallinity of the nano adsorbents?

1.6.5. At what optimal conditions will the nano adsorbent be the most effective adsorbent for the removal of HMIs?

1.6.6. Which methods can be developed to optimize the adsorbent when interacting with the analyte?

1.7. Dissertation outline

Chapter 1

In this chapter, the study is introduced by covering the background that includes wastewater and the significance of having safe drinking water. The chapter further gave a summarised problem statement, justification, hypothesis, aims and objectives, and the research questions.

Chapter 2

In this chapter, the focus is on literature review which includes, wastewater, HMIs and remediation methods used by researchers over the years. The advantages and disadvantages affecting the treatments, adsorption process, isotherms, kinetic, thermodynamic studies and the comparison of other published studies.

Chapter 3

In this chapter, the focus was on the first nano adsorbent (MCNC), the extraction of CNC and the synthesis of CNC, magnetite and MCNC production. The characterization methods, the results of magnetite, CNC and the MCNC materials are discussed. The MCNC application against the adsorptive removal of Pb (II) ions is evaluated and reported. The surface response methodology affecting the adsorbent and the adsorbate are explained and discussed. The optimal conditions' of MCNC on Pb (II), validation and the reusability results are also discussed. The adsorptive results obtained from isotherms, kinetics, thermodynamics are evaluated and reported, the chapter conclusion is also elaborated. The references are listed at the end.

Chapter 4

In this chapter the CNC was modified by crosslinking it with the TEMPO by introducing the carboxylic group on CNC for easy binding of the PEI then functionalizing it with Fe_3O_4. The synthesis and characterization methods of CNC-TEMPO, CNC-TEMPO-PEI and MCNC-

TEMPO-PEI were investigated, and the results were also discussed. Then the MCNC-TEMPO-PEI was applied for the adsorptive removal of Cr (VI) from wastewater. The optimization studies, validation studies, reusability studies, isotherms, kinetics and thermodynamics methods were discussed, also the conclusion is also summarised.

Chapter 5

In this chapter, general conclusion with specific achieved objectives were outlined in detail. The limitations incurred from the study were also elaborated with necessary future work recommendation.

Appendix

The supplementary information is presented in this section.

1.8. References

1. Joseph N.M, J.N.., Dr.S. Mahendrakumar, D.S.M.: An Analysis of Demand and Supply of Water Resource in Karnataka – An Empirical Study. Int. J. Sci. Res. 3, 96–98 (2012).

2. Saravanan, A., Senthil Kumar, P., Jeevanantham, S., Karishma, S., Tajsabreen, B., Yaashikaa, P.R., Reshma, B.: Effective water/wastewater treatment methodologies for toxic pollutants removal: Processes and applications towards sustainable development. Chemosphere. 280, 130595 (2021).

3. Yi, Y., Zhao, Y., Zhang, Z., Wu, Y., Zhu, G.: Recent developments in electrochemical detection of cadmium. Trends Environ. Anal. Chem. 33, e00152 (2022).

4. Getty Images.: Access to clean water: Blue pump water flow equipment, agriculture. iStock, Stock photos/water. https://www.istockphoto.com/photos/access-to-clean-water

5. Otero, M., Coimbra, R.N.: Current Trends and Perspectives in the Application of Polymeric Materials for Wastewater Treatment.

6. Motloung, M.T., Magagula, S.I., Kaleni, A., Sikhosana, T.S., Lebelo, K., Mochane, M.J.: Recent Advances on Chemically Functionalized Cellulose-Based Materials for Arsenic Removal in Wastewater: A Review. Water. 15, 793 (2023).

7. Soares, E. V., Soares, H.M.V.M.: Bioremediation of industrial effluents containing heavy metals using brewing cells of Saccharomyces cerevisiae as a green technology: A review. Environ. Sci. Pollut. Res. 19, 1066–1083 (2012).

8. Kolya, H., Kang, C.W.: Toxicity of Metal Oxides, Dyes, and Dissolved Organic Matter in Water: Implications for the Environment and Human Health. Toxics. 12, 111 (2024).

9. Noreen, U., Ahmed, Z., Khalid, A., Di Serafino, A., Habiba, U., Ali, F., Hussain, M.: Water pollution and occupational health hazards caused by the marble industries in district Mardan, Pakistan. Environ. Technol. Innov. 16, 100470 (2019).

10. Mitra, S., Chakraborty, A.J., Tareq, A.M., Emran, T. Bin, Nainu, F., Khusro, A., Idris, A.M., Khandaker, M.U., Osman, H., Alhumaydhi, F.A., Simal-Gandara, J.: Impact of heavy metals on the environment and human health: Novel therapeutic insights to counter the toxicity. J. King Saud Univ. - Sci. 34, 101865 (2022).

11. Ayangbenro, A.S., Babalola, O.O.: A new strategy for heavy metal polluted environments: A review of microbial biosorbents. Int. J. Environ. Res. Public Health. 14, (2017).

12. Bilal, M., Ihsanullah, I., Ul Hassan Shah, M., Younas, M.: Enhanced removal of cadmium from water using bio-sorbents synthesized from branches and leaves of Capparis decidua and Ziziphus mauritiana. Environ. Technol. Innov. 24, 101922 (2021).

13. Shukla, S., Khan, R., Daverey, A.: Synthesis and characterization of magnetic nanoparticles, and their applications in wastewater treatment: A review. Environ. Technol. Innov. 101924 (2021).

14. Baratta, M., Mastropietro, T.F., Bruno, R., Tursi, A., Negro, C., Ferrando-Soria, J., Mashin, A.I., Nezhdanov, A., Nicoletta, F.P., De Filpo, G., Pardo, E., Armentano, D.: Multivariate Metal-Organic Framework/Single-Walled Carbon Nanotube Buckypaper for Selective Lead Decontamination. ACS Appl. Nano Mater. 5, 5223–5233 (2022).

15. Ayub, S., Changani Khorasgani, F.: Adsorption Process for Wastewater Treatment by using Coconut Shell. Res. J. Chem. Sci. 4, 1–8 (2014)

16. Motaung, T.E., Linganiso, L.Z.: Critical review on agrowaste cellulose applications for biopolymers. Springer India (2018)

17. Mahmoud, M.E., Abdou, A.E.H., Sobhy, M.E.: Engineered nano-zirconium oxide-crosslinked-nanolayer of carboxymethyl cellulose for speciation and adsorptive removal of Cr(III) and Cr(VI). Powder Technol. 321, 444–453 (2017).

18. Velempini, T., Pillay, K., Mbianda, X.Y., Arotiba, O.A.: Epichlorohydrin crosslinked carboxymethyl cellulose-ethylenediamine imprinted polymer for the selective uptake of Cr(VI). Int. J. Biol. Macromol. 101, 837–844 (2017).

19. Xing, X., Li, W., Zhang, J., Wu, H., Guan, Y., Gao, H.: TEMPO-oxidized cellulose hydrogel for efficient adsorption of Cu^{2+} and Pb^{2+} modified by polyethyleneimine. Cellulose. 28, 7953–7968 (2021).

20. Jebali, Z., Nabili, A., Majdoub, H., Boufi, S.: Cellulose nanofibrils (CNFs) from Ammophila arenaria, a natural and a fast growing grass plant. Int. J. Biol. Macromol. 107, 530–536 (2018).

21. Chen, L., Wang, X., Lu, W., Wu, X., Li, J.: Molecular imprinting: Perspectives and applications, (2016)

22. Ansari, S.: Application of magnetic molecularly imprinted polymer as a versatile and highly selective tool in food and environmental analysis: Recent developments and trends. TrAC - Trends Anal. Chem. 90, 89–106 (2017).

23. Neolaka, Y.A.B., Lawa, Y., Naat, J.N., Pau Riwu, A.A., Darmokoesoemo, H., Supriyanto, G., Holdsworth, C.I., Amenaghawon, A.N., Kusuma, H.S.: A Cr(VI)-imprinted-poly(4-VP-co-EGDMA) sorbent prepared using precipitation polymerization and its application for selective adsorptive removal and solid phase extraction of Cr(VI) ions from electroplating industrial wastewater. React. Funct. Polym. 147, (2020).

24. Huang, R., Ma, X., Li, X., Guo, L., Xie, X., Zhang, M., Li, J.: A novel ion-imprinted polymer based on graphene oxide-mesoporous silica nanosheet for fast and efficient removal of chromium (VI) from aqueous solution. J. Colloid Interface Sci. 514, 544–553 (2018).

25. Turiel, E., Martín-Esteban, A.: Molecularly imprinted polymers-based microextraction techniques. TrAC - Trends Anal. Chem. 118, 574–586 (2019).

26. Kumar, S., Alveroğlu, E., Balouch, A., Talpur, F.N., Jagirani, M.S., Abdullah, Mahar, A.M., Pato, A.H., Mal, D., Lal, S.: Fabrication of chromium-imprinted polymer: A real magneto-selective sorbent for the removal of Cr(vi) ions in real water samples. New J. Chem. 44, 18668–18678 (2020).

27. Kerur, S.S., Bandekar, S., Hanagadakar, M.S., Nandi, S.S., Ratnamala, G.M., Hegde, P.G.: Removal of hexavalent Chromium-Industry treated water and Wastewater: A review. In: Materials Today: Proceedings. pp. 1112–1121. Elsevier Ltd (2020)

28. Mahlaule-Glory, L.M., Mapetla, S., Makofane, A., Mathipa, M.M., Hintsho-Mbita, N.C.: Biosynthesis of iron oxide nanoparticles for the degradation of methylene blue dye, sulfisoxazole antibiotic and removal of bacteria from real water. Heliyon. 8, e10536 (2022).

29. Appenzeller, L., Doblin, M., Barreiro, R., Wang, H., Niu, X., Kollipara, K., Carrigan, L., Tomes, D., Chapman, M., Dhugga, K.S.: Cellulose synthesis in maize: isolation and expression analysis of the cellulose synthase (CesA) gene family. Cellulose. 11, 287–299 (2004).

30. Meng, Q., Li, H., Fu, S., Lucia, L.A.: The non-trivial role of native xylans on the preparation of TEMPO-oxidized cellulose nanofibrils. React. Funct. Polym. 85, 142–150 (2014).

31. Abou-zeid, R.E., Dacrory, S., Ali, K.A., Kamel, S.: International Journal of Biological Macromolecules Novel method of preparation of tricarboxylic cellulose nano fi ber for ef fi cient removal of heavy metal ions from aqueous solution. Int. J. Biol. Macromol. 119, 207–214 (2018).

32. Xi, C., Wang, R., Rao, P., Zhang, W., Yan, L., Li, G., Chai, F., Cai, Y., Luo, T., Zhou, X.: The fabrication and arsenic removal performance of cellulose nanocrystal-containing absorbents based on the “bridge joint” effect of iron ions. Carbohydr. Polym. 237, (2020).

CHAPTER (II) (LITERATURE REVIEW)

PREAMBLE

In this chapter, wastewater is summarised with its contained toxins and provides a thorough discussion of the heavy metal ions (HMIs). The nature, source, and toxicity of the HMIs to the environment and to human beings is also discussed. Moreover, the remediation methods, the advantages and disadvantages are further elaborated. Furthermore, the principles, uses and functions of the adsorption process are also outlined. Various adsorbents and their properties and limitations are also discussed. The effect of the adsorption parameters used to optimize these adsorbents during the adsorption process is also discussed. The mechanism and the type of interaction, the adsorbate and the adsorbents, the optimizing methods, adsorption isotherms, kinetics and the thermodynamics reaction obtained are compared with other studies and further discussed.

2.1 Background

Wastewater is explained as the disposed water from various effluents, these include mining industries, farming, hospital, pharmaceuticals, and household effluents [1-2]. Feeding towards diverse water streams such as lakes, rivers, oceans, and many others. This then has caused global health concerns especially when they influence the eco-system and impact the environment negatively [3]. Thus, studies from authors like Crini *et al* [4], reported that in their country (Switzerland), the European legislations and framework policies have been established in efforts to monitor and control indiscriminate discharge of wastewater to various water bodies [4]. Therefore, it is imperative that wastewater effluents are treated since they carry a lot of different toxins from heavy metal ions (HMIs), organic dyes, pharmaceuticals and many others to the different water bodies as displayed in **Fig. 2.1**.

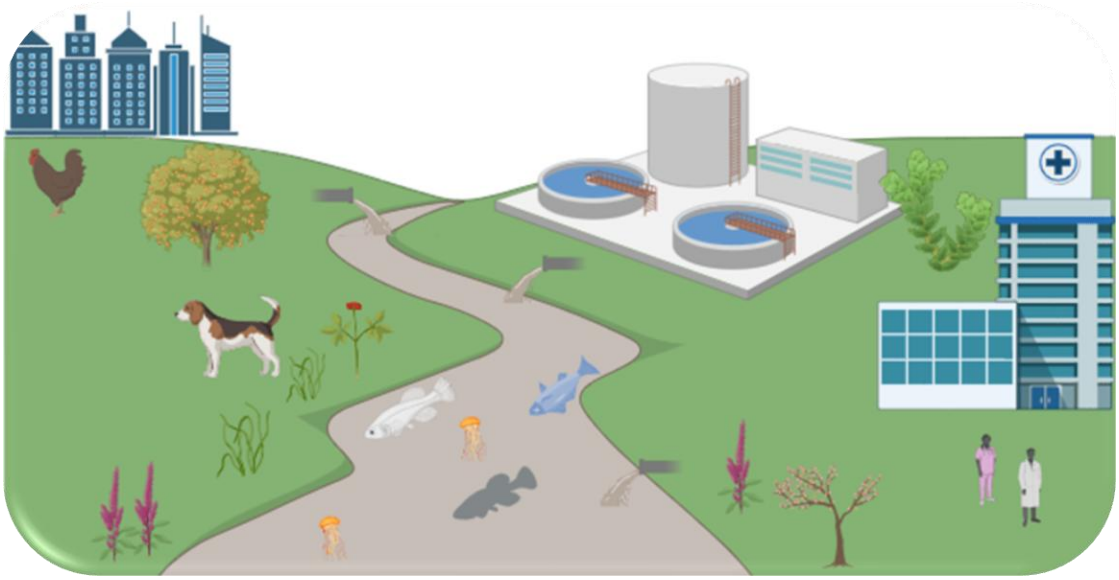

Figure 2.1: Incorrect disposal of wastewater into a river from different effluents.

Thus, in this study, the focus is on the HMIs as they were reported of being the superior contributors of wastewater, with an estimation of over 70 % containment of HMIs presently in the wastewater effluents [5]. The HMIs toxicity within the human system through polluted water consumption that leads to severe health effects. This has prompted severe sicknesses throughout the human system and affecting the brain, heart, blood, reproductive system and the vascular system as exhibited in **Fig. 2.2** [6-7]. Thus, several health organisations like the Environmental Protection Agency (EPA), World Health Organization (WHO) and International Agency for Research on Cancer (IARC) have declared HMIs as carcinogenic and toxic to the human health [8-9]. Moreover, HMIs are stable in natural environment and soluble across a wide pH range [10].

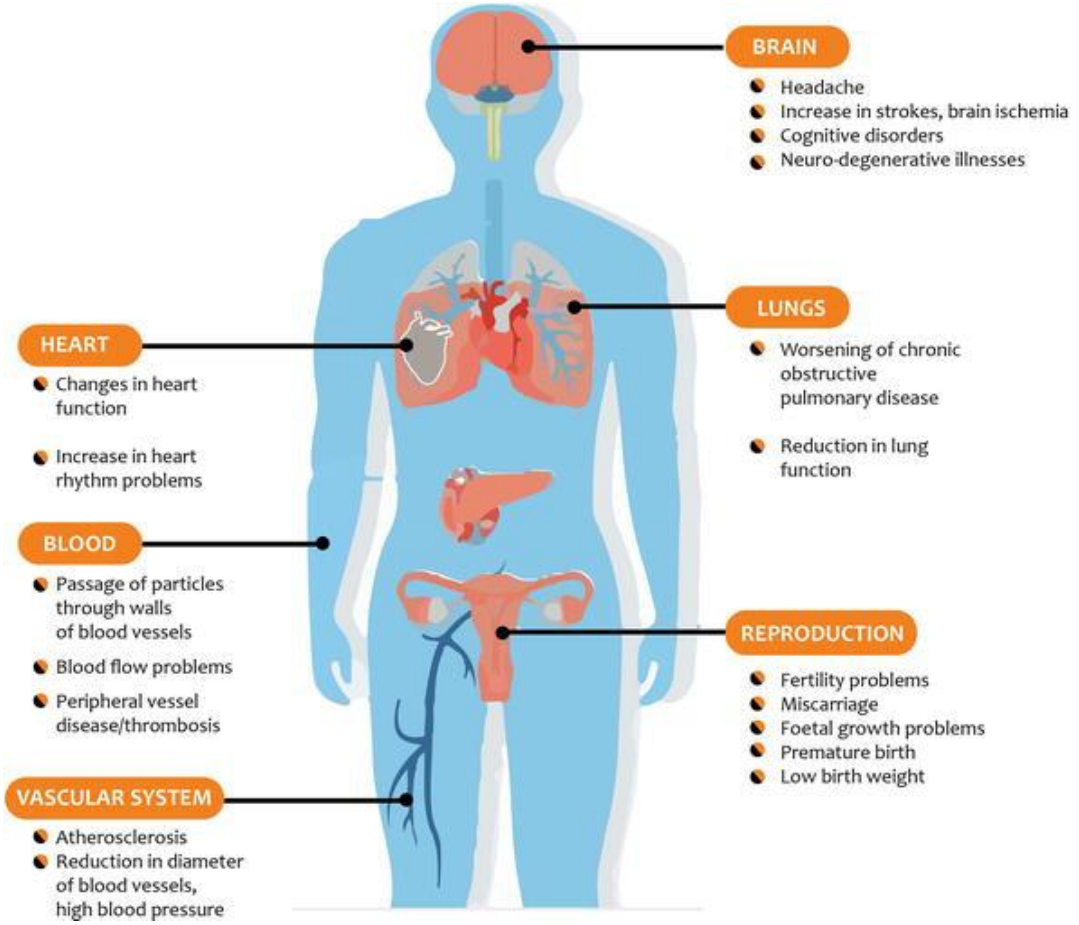

Figure 2.2: Diseases caused by the consumption of high concentration of HMIs [6]

2.1.1 Heavy metal ions (HMIs).

The physicochemical properties of HMIs such as slow dissolution in water, softness and malleability, account for their widespread use [6-10]. Furthermore, industrial development expansion particularly in urban areas and the increase in population growth globally has also accelerated the use of these metals. Their sources over the years have been from various anthropogenic applications including mining, cosmetics, fossil fuel, paints, fertilizers and industries (smelting, combustion, manufacturing and many more [11-12]. Moreover, they appear in different oxidation states like the divalent, trivalent, pentavalent and the hexavalent ions [10,13]. The toxicity of these HMIs depends on their composition and their oxidation states [14-16]. The divalent lead ion [Pb (II)] and the hexavalent chromium ion [Cr (VI)] are the most common, abundant elements within the natural environment (water and soil) [17-18]. Their toxicity affects both adults and children negatively as exhibited in **Fig. 2.2**.

This makes these HMIs persistent, hazardous, carcinogenic and non-biodegradable even at lower concentrations [19-20]. Thus, the health organisations like the EPA and WHO have recommended that the maximum containment level (MCL) of Pb (II) for human consumption should not exceed the range of 1-15 ppb in drinking water [21-22]. Whereas the MCL of Cr in drinking water, should not exceed 20 ppb and can only be permissible for human consumption at concentrations lower than 20 ppb [21-22]. This then necessitates researchers to treat wastewater effluents for the removal of these pollutants deteriorating the water quality within the eco-system.

2.2 Remediation methods

Researchers have demonstrated the essential need to use of adsorption process for the remediation of wastewater. Thus, various treatment methods have been utilised over the past decade in an effort to remediate wastewater from selective HMIs [23]. These include, flocculation, chemical precipitation, ion exchange methods and many more [23-24]. However, these methods have their shortcomings, like generation of secondary pollutants, use of harsh conditions, require regular maintenance thereby increasing their operational costs [25-25]. Owing to these outcomes, the adsorption method has become a suitable alternative because of its chemical and physical properties which provide a higher removal efficiency than other treatment methods. Different treatment methods have been summarized in **Table 2.1** with the emphasis on their disadvantages.

Adsorption is a surface phenomenon where an adsorbent is used to hold the adsorbate through the formation of either a physical or chemical bond [26-27]. This process is controlled by the mobility of the adsorbate from the adsorbent under optimal/experimental parameters such as pH, the concentration of the analyte, adsorbent dosage, contact time and temperature distribution to provide effective removal of pollutants as illustrated in **Fig. 2.3** [30-31].

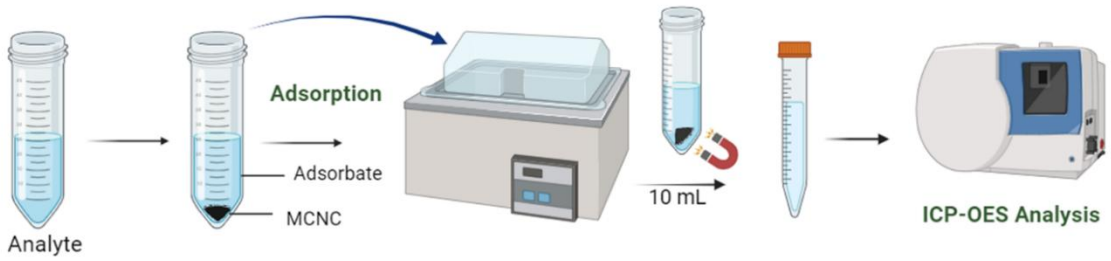

Figure 2.3: The adsorption process of the analyte adsorbing HMIs at optimal parameters.

The advantage of adsorption is that it is versatile, economically efficient, has low energy consumption and produces fewer by-products that are harmful [17]. To provide an effective adsorption capacity, adsorbents that have a higher surface area, porous and crystalline nature are required for the removal of HMIs in wastewater [26].

Table 2.1: Wastewater treatment methods used by various researchers for wastewater treatment purposes.

Remediation methods	Disadvantage	Refs
Reverse osmosis	Membrane fouling	[3]
	Energy-intensive	
	High maintenance	
Ion exchange	Expensive resin	[28]
	Require pre-treatment method	
	Ionic completion	
	Sensitive to pH	
Flocculation	High sludge generation	[29]
	require multiple treatments	
Coagulation	Require multiple treatments	[30]
Chemical precipitation	Use of toxic chemicals	[31]
	Generate secondary pollutants.	
	Separate with difficulty	

2.3 Adsorbents

Current adsorbents used within adsorption process includes metal oxides, carbon-based materials, polymers, metal organic frameworks, imprinted polymers, agriculturally based materials, and many others as indicated in **Fig. 2.4**.

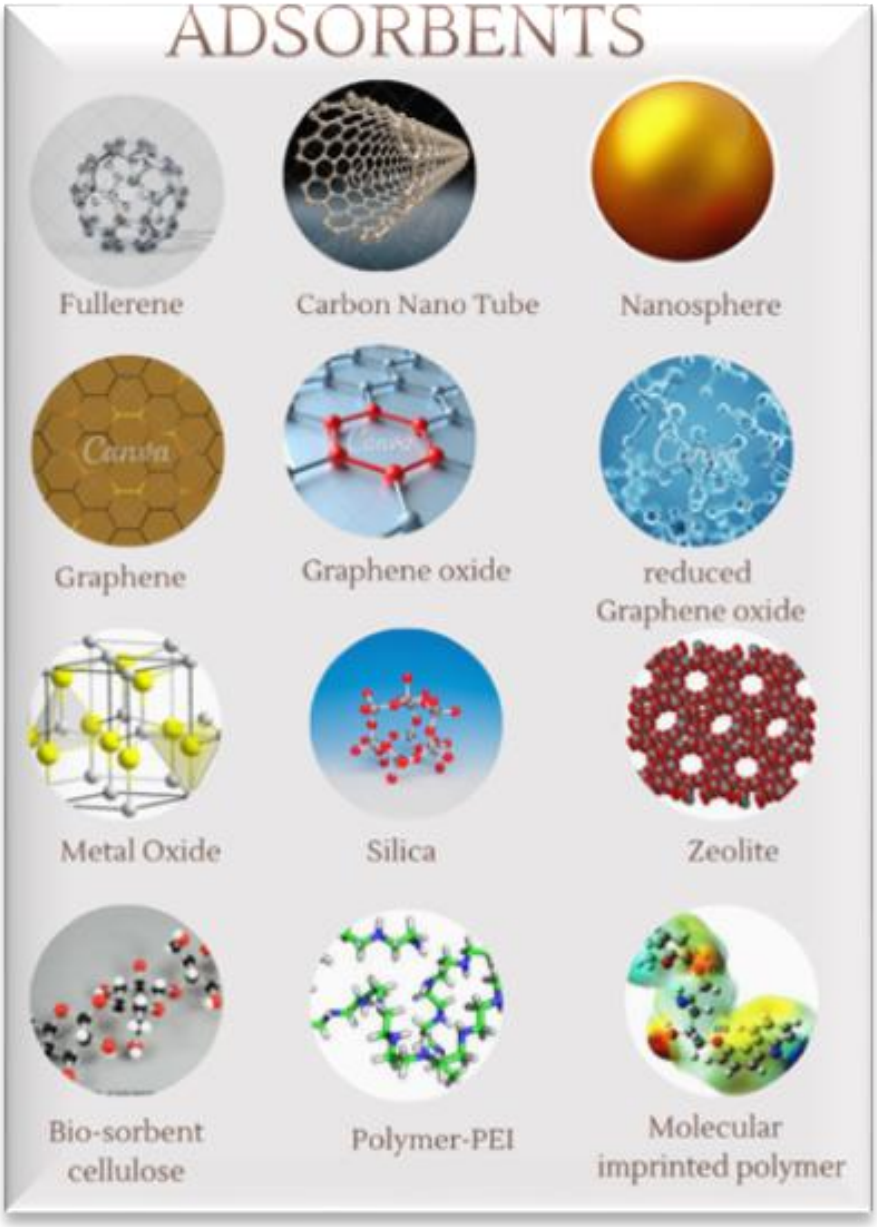

Figure 2.4: Various adsorbents used for the adsorptive removal of HMIs [32-33]

These adsorbents are extensively used due to the unique properties they possess like higher purity, good crystal structure, excellent surface area, larger pore sizes and pore volume [32,34]. Because of these traits, adsorbents have gained a lot of attention in research recently. Moreover, ensuring effective adsorbents, maintained good adsorption capacity, and sometimes demonstrated fast adsorption rate for HMIs removal in wastewater [33-34]. The exploration of these adsorbents is further discussed in the next section starting with the metal oxides (MOs).

2.3.1 Metal oxides-based adsorbents

Metal oxides such as ZnO, NiO, CuO, AgO, TiO_2, MnO_2, AlO_2 and many others have been applied for the removal of HMIs in aqueous solutions [27,35]. This could be due to the amphoteric feature of metal oxides (MOs) that allows them to react with both acids and bases during adsorption [36]. For an example, Shaik et al [37] synthesized ZnO nanoparticles for the removal of Cr (VI) and obtained an 82 % removal as displayed in **Table 2.2** [37]. Furthermore, metal oxides can be functionalised or synthesized with ease aiming to improve its adsorption capacity [21-22]. Saravanakumar et al [38] functionalised NiO with biochar for the adsorptive removal of Pb (II) ions where they obtained the adsorption capacity of 43 mg/g with the highest removal efficiency of 95 %, under the following optimized parameters: 30 ppm, 27 ºC and pH=6 as displayed in **Table 2.2** [38]. In other studies, MO like Al_2O_3 were also used for the removal of various HMIs especially the cationic metals such as Pb (II), Cd (II) and Cu (II) as exhibited on **Table 2.2** [39]. This might be due to the diatomic molecules from the negatively charged surface (oxygen) attacking the cationic analytes in suitable pH medium [39]. It is also noticeable that in addition to these aforementioned MOs, other studies are using iron and its derivatives [(α Fe_2O_3), maghemite (γ Fe_2O_3) and magnetite (Fe_3O_4)] in the adsorption process, making them by far the leading metal oxide applied for adsorptive removal of various HMIs in various water types, particularly for modification purposes [40]. Owing to its superior magnetic properties that easily attract metal ions using the magnetic field with the help of an external magnet during the adsorption processes is easily obtained [40-41]. Furthermore, the iron reduces the use of tedious steps required during adsorption, thus, the need recommended for usage during the adsorptive removal of HMIs.

Table 2.2 below gives a summary of various adsorbents used for the removal of HMIs. Moreover, **Table 2.2** also shows the optimal conditions and active functional moieties for the removal of HMIs from water.

Table 2.2: Various adsorbents that were modified and used for the adsorptive removal of HMIs from different water samples.

Adsorbent	Water type	Functional group	HMI	Parameters	Adsorption capacity mg/g Or % removal	Recyclability Cycles	Year Published	Ref
$MnFe_2O_4$/G-AC	Simulated water	COOH, OH, C=O	Pb (II)	pH=6, 150 min, 50 mg, 50 ppm	625	5	2021	[11]
Fe_3O_4	Waste water	Fe	Cr (II)& Pb (II)	100 ppm	347,63 317,62	3	2022	[21]
MgO-Biochar	Wastewater	NH_2	Pb (II) & Cd (II)	600 min, pH=5, 0,5 g	384.08 207.02	3	2022	[29]
ZnO	Simulated water	M-O	Cr (VI)	1 g/L; 8 hrs, 120 rpm	81,17 %	-	2020	[37]
NiO/biochar (PJONC)	Simulated water	M-O	Pb (II)	50 mg, pH=63, 4 min, 30 ppm, 27 ºC	43,0	-	2019	[38]
Al_2O_3/Cu_2O	Simulated water	M-O	Cd (II)	0,3 g; pH=8; 90 min 90 ppm	4,48	-	2023	[39]
Fe_2O_3@UIO-66-NH_2	Simulated water	NH_2, OH	Cd (II) & Pb (II)	pH=6	666.7 833.3	4	2019	[41]
D-Fe3O4-NC	Drinking water	M-O, OH	Cd (II) Cr (II) & Pb (II)	pH=4, 40 min, 8 ppm, 10 mg	74,5 76 75,2	20	2023	[42]
FeCo@BDC	Waste water	COOH	Pb (II)	15 min, pH=3, 500 ppm	220,48	5	2022	[43]
MTV-MOF/SWCNT-BP	Waste water	NH_2, -S-H, COOH, C=O	Pb (II)	10 ppb, 16 hrs, pH=6,6	310	5	2022	[44]
MNP-GAC			- Cu (II)	100 ppm	23,61	10	2021	[45]
MWCNT-Au-Fe_3O_4	Waste water	COOH	Pb (II)	60 min, pH=10, 0,1 g	7.266	-	2022	[46]
I-Al_2O_3	Simulated water	M-O	Ni (II), Cd (II) & Pb (II)	0,3 mg, pH= 8 10 ppm, 40 min	60,0 66,0 66,4	-	2023	[47]
Al_2O_3	Ground water	M-O	As(v)	2g/L; pH=6,5; 200 min 500 ppb, 125 rpm	500 µg/g	3	2017	[48]
Fe_3O_4	Simulated water	Fe	Hg (II)	1g; pH=6, 45 min. 2, 40 ppm	101,01	-	2023	[49]
Fe_3O_4	Simulated water	Fe	Pb (II) Cr (III)	0,5 g/L; 30 min, 25 ppm 0,2g/L; 100 min,25 ppm pH=4	95,56 mg/g 46,05 mg/g	-	2017	[50]
GO-EDTA-CS	Complexed Wastewater	COOH, OH, NH_2	Hg (II) Cu (II)	pH>4, 50 min, <100 ppm,	324 130	7	2022	[51]
CNC-Fe_3O_4	Simulated water	COOH, OH	Pb (II)	240 min, pH=5, 50 ppm, 0,05 g	63.78	5	2016	[52]

CCN PEI	Simulated water	OH, COOH, NH_2	Cr (VI)	240 min, pH=3, 300 ppm	358,42	5	2017	[53]
GO-MCWT-DETA	Waste water	COOH, C=O, OH	Cr (II), Pb (II)	30 min, pH=4, 30 mg	5,4 9,5	-	2016	[54]
Go-NH_2@CA-NH_2	Simulated water	COOH, C-O-C & NH_2	Cr (VI)	60 min, pH=2,	410	7	2022	[55]
Pb-MCGO	Simulated water	NH_2, COOH	Pb (II)	40 min, pH=5	79	5	2022	[56]
TZFNC	Waste water	-S-	Pb (II)	14,5 min, pH=6,5 60 ppm, 40 mg	554.4	2	2020	[57]
Fe_3O_4/G-AC	Simulated water	COOH, OH, C=O	Pb (II)	pH=5, 0,25 g, 400 ppm, 150 min	153,2	-	2022	[58]
PVC-PPD-GO	Simulated water	COOH, OH, C-O-C	Pb (II) Zn (II)	-	462,421 336	15	2021	[59]
FLMGO	Tannery industrial water	C=O, C-O-C	Cd (II) Cu (II)	pH=7, 100 mg, 500 ppm	401,1 1114,22	5	2021	[60]
GCF	Simulated water	COOH	Cr (VI)	pH=7, 7 min, 600 min, pH=2, 0,5g/L 50 ppm	270	10	2018	[61]
CLCh/MWCNT/Fe	Electroplating effluent	COOH	Cr (III) Cr (VI)	60 min, 150 min,	66,25 449,30	10	2019	[62]
UIO-66-EDTMPA	Simulated water	PO_3, H_2	Cd (II) Pb (II)	pH=1, pH=5,5	98,21	-	2022	[63]
CFP	Simulated water	-	As (III)	80 min, pH=6, 2 ppm, 60 mg,	1,13	-	2022	[64]
BGAC	Simulated water	OH	Cr (VI)	pH=2, 0,5g/L,	403,23	-	2020	[65]
MCGON	Simulated water	NH_2, COOH, OH	Cu (II)	120 MIN, pH=4, 1g, 40 ppm	217,4	-	2020	[66]
AC	Simulated water	-	Cr (VI)	2,5g/L, pH=4,5	89,5	-	2020	[67]
FFT	Simulated water		Cu(II) Pb(II) Zn(II)	60 min, pH=4, 4g/L and 5g/L	97,4 % 79 % 73,28 %	-	2017	[68]
RH	Wastewater	-	Pb(II) Cu(II) Ni(II)	60mg. 1.17 ppm, 50mg, 11.78 ppm 60 mg, 0.48 ppm	87,17 % 98,0 % 67,0 %	-	2013	[69]
PC	Simulated water	≡Si-O^- ≡Al-O^-	Cd (II) Co (II) Cu (II)	pH= 8 – 10 pH= 6 – 10 pH= 8 – 10	25 28 20	-	2019	[70]
PHP	Industrial wastewater	-	Pb (II) Cd (II)	120 ppm, 3 hrs, 6,5g/L	100 % 41 %	-	2016	[71]
Magnetic Ferrite	Copper ammonia wastewater	-	Cu (II)		124,80	-	2018	[72]

GO-EDTA-CS= Graphene oxide ethylene diamine tetra acetic acid Chitosan
CCN-Fe_3O_4= Carboxylic cellulose nanocrystal modified by magnetite
$MnFe_2O_4$/G-AC= Manganese Ferrite/graphene oxide magnetic activated carbon
TZFNC= Thiourea Zinc functionalised cellulose nanocrystal
CMC= Cellulose microcrystal
PEI= Polyethyleneimine
GO-EDTA-CS= EDTA-Graphene oxide –chitosan
ZIF= Zeolite imidazolate
DETA= Diethylenetriamine
BDC= Dicarboxyl benzene
MTV= multivariate amino
FFT= Flax Fiber tows

$GO\text{-}NH_2@CA\text{-}NH_2$ = Animated graphene oxide functionalised with cellulose acetate and amine beads

RH= Rice husk

CS-AC=Carbon sphere/Activated carbon

$GO\text{-}Fe_3O_4$ =Graphene oxide/Magnetite

Janus PF&PM =Janus phenol formaldehyde resin & periodic mesoporous

GCF

$MWCNT/AuFe_3O_4$= Multiwalled carbon nanotube coated with gold and iron oxide

PVC-PPD-GO=

Fe_3O_4= Magnetite

AC = Activated carbon

PHP = Peanut husk powder

PC = Pillare clays

MNP-GAC = Magnetic nanoparticle – granular activated carbon

Fe_3O_4/G-AC =

CFP = Cassia fistula pod

$MnFe_2O_4$/G-AC =Manganese Ferrite/graphene oxide magnetic activated carbon

Al_2O_3 /Cu_2O= Aluminium oxide Modified by copper oxide

According to the observation from the reviewed summary from **Table 2.2**, it looked as though the MOs are effective adsorbents for HMIs removal in model water samples. However, reports have also stated that MOs have displayed setbacks as lacking selectivity towards the targeted analytes particularly in wastewater samples [41,43]. Moreover, they showed minimal adsorption capacity just as displayed where the highest captured capacity is 95 mg/g and lowest of 43 mg/g particularly for removing Pb (II) [38,50]. The second adsorbent currently utilised as an effective adsorbent from different studies is carbon especially for the adsorptive removal of HMIs in wastewater.

2.3.2 Carbon-based adsorbents

Carbon based adsorbents and their derivatives are adsorbents that are purely consisting of carbon as their major constituent and the examples are Activated carbon (AC), CNTs (carbon nanotubes) [single wall carbon nanotube (SWCNT and MWCNT)- Multiwalled carbon nanotubes, CNF (carbon nano fibres, fullerene), CNSs (carbon nano sphere), CND (carbon nano diamond), CNC (carbon nano-cones), charcoal, graphene and its derivatives [45-46]. They are stable in nature and known as good adsorbents for HMIs removal. Moreover, they have ease of applicability, electrical conductivity, controllable pore structure, thermos-stability and have demonstrated excellent % removal capacity of HMIs [64-65]. By virtue of these qualities, these adsorbents have been the most used adsorbents at present, particularly for the removal of HMIs in wastewater. In addition to their high cost and use of chemicals, they tend to show low adsorptivity and lose a lot of material during the regeneration process [74]. Zhou *et al* [73], reported a 26 % removal for Cd (II) unmodified Multiwalled CNT as an adsorbent [73]. Literature reports have it that based on the aforementioned limitations, they can still be compensated by further surface modification where other functional groups like the oxygen based [carboxylic (COOH), carbonyl (C=O) and hydroxyl (OH-)] groups are required to enhance the adsorption efficiency and strengthen its stability [74-75]. This was also shown when carbon was modified with oxygen containing functional groups to increase selectivity for the removal of Cr (VI). In a study done by Liu *et al* [76], the pore structure size was developed

to enhance the adsorption capacity and for that 0.4834 mmol g^{-1} was achieved, resulting in 4 times more efficiency than the unmodified AC of 0,1236 mmol g^{-1} [76]. Other types of carbon-based adsorbents are graphene-based and their derivatives which contains the carbonyl, carboxyl, epoxy functional groups attached to the carbon atom which also provides them with the ability to bind the HMIs via electrostatic and co-ordination interaction [74]. In addition to the aforementioned properties, they also possess good mechanical strength, adequate functional groups, high crystallinity, a higher surface area and charge transfer capability [73-74]. Even though it has exhibited desirable properties, they are deemed costly, and their production involves tedious methods [75-76]. Moreover, with its reported properties, they have also showed low adsorption capacity and might also require surface modification. Zeng *et al* [12] modified GO with Fe_3O_4 and Yan *et al* [63] modified graphene with Fe_3O_4 and they obtained 153 mg/g for the removal of Pb (II) from wastewater [12,58].

2.3.3 Polymers based adsorbents

Polymer-based adsorbents are normally synthesized from primary polymers like polyacrylamide (PAM) or polystyrene (PS) and the most common polymers are polyacrylic acid (PAA), polyethylenimine (PEI) and polyvinyl alcohol (PVA) [77-78]. Polyacrylic acid is often used to adsorb cationic heavy metals like Cu (II) and Pb (II), while on the other hand PEI adsorb both cationic and anionic heavy metals like Hg (II), Cd (II), Cr (VI) and as (V). Whereas polyvinyl alcohol is used to adsorb anionic heavy metals ions like as (VI) and Cr (VI). Polymers efficiency vary depending on the interaction of the polymer and the targeted analyte. Furthermore, polymers are customised during synthesis when modifying other adsorbents to possess specific functional groups, suitable for the adsorption process particularly for HMIs. For example, the polymeric adsorbents functionalised with COOH groups can efficiently remove cationic HMIs like the (Pb, Cu, Cd and many others). Whereas polymeric adsorbents containing NH_2 groups are preferred for targeting anionic HMIs like the oxidated metals (Cr VI & III), As (V & III). This is observed various studies from literature, studies like Hu *et al* [79] where the polyacrylic acid was grafted on the magnetic chitosan nanocomposite (MCS) and obtained an adsorption removal of 204,89 mg/g against Pb (II) [79]. In another study reported

by Liu *et al* [53], CNC-TEMPO-PEI was used remove Cr (VI) and the results obtained adsorption capacity of 358,42 mg/g [53]. This enhanced the adsorption capacity when the carboxylic groups were introduced on the surface adsorbent of CNC to bridge the amine from the functionalised (PEI) and the hydroxyl groups when modifying the surface adsorbent. While Omer *et al* [55] used carboxylic and the amine functional groups to successfully functionalize the adsorbent that initially had cellulose to target the Cr (VI) [55]. This is because Cr in an anionic form as $Cr_2O_4^{2-}$ and CrO_4^- are easily attracted by the amine bound surface modified adsorbents [65,74]. Nitrogen atom in the amine has 5 valence electrons available to surround and easily forms 3 bonds with other lone pairs resulting in the interaction with the lone pair from the HMIs triggering interaction between the two [80]. Moreover, these studies suggest that to remove the desired analyte effectively and selectively, like Cr (VI) from other species, researchers must consider binding carboxylated and amine functional groups onto the surface material. Studies reported polymers having properties such as high surface areas and high chemical stability, specific sizes, and shapes for adsorption. Moreover, they are hydrophilic in nature (water-loving), they can be recyclable and reusable leading to high adsorption capacity [53-56]. Nonetheless, looking at studies listed in **Table 2.2**, we can also note that for the divalent ions, oxygen-based functional groups like hydroxyl (OH), carboxyl and carbonyl groups were also used for selectivity towards the cationic analytes [80]. Ahmad *et al* [81], reported that cationic metals like divalent ions (Pb (II), Cu (II), Hg (II) and Cd (II)) in the aqueous media, have been attracted to the surface-modified oxygen-based adsorbents [81]. This is due to the negatively charged ions on the surface of the adsorbent caused by the lone pairs from the oxygen, which attracts the vulnerable divalent metal ions because of the oxidation-reduction and the electrostatic interaction [81,66]. Furthermore, the secondary polymer-based adsorbents include the metal organic framework (MOF).

2.3.3.1 Metal organic framework (MOF)

The MOF are a type of porous polymers formed by a combination of secondary building units co-ordinated to the organic ligands or linkers and the metal clusters to form dimensional

structures [59,63]. Studies on the adsorptive removal of HMIs have used the MOF because they possess a crystal structure and structural diversity, large surface area, smaller porosity and adjustable framework [63]. The MOF contains fillers within its structure that provides an additional advantage over other inorganic fillers used in polymer matrix by easily controlling the interface and the interactions of HMIs and the MOFs polymer [82]. Studies have included MOFs as their adsorbent by virtue of these properties. However, limitations have also been reported where they possess smaller pore sizes, poor stability, weak selectivity, and low adsorption capacity [82-83]. To overcome these, surface modification is required. Thus, some studies, add another polymer like ethylene diamine (EDA) to enhance the adsorption capacity through the formation of complexes with metal ions [83]. Arya *et al* [84] modified a PUC (MOF) by functionalizing it with the 1,3 aminopropyl Imidazole linkers to produce a nanocomposite of 3D-Zn-MOF in an effort to increase the amine groups within the structure that removed the three HMIs (Fe(II), Pb(II) and V(v)) with the adsorption capacity of 208,7 mg/g, 192, 6 mg/g and 203 mg/g, respectively [84]. Ren *et al* [85] modified MOF with EDA to form HKUDT-1-EDA (high specific surface MOF loaded with EDA) to increase the density of NH_2 when it's functionalised by reason of removing of Pb (II) and Cd (II) from wastewater [85]. Other studies modified their surface by adding functional groups to increase the adsorption capacity and enhance the selectivity of their adsorbents. Thus, **Table 2.2** exhibits these studies and their functional groups. This is where the tertiary polymers are introduced for selectivity, these include the imprinted polymers (IP).

2.3.3.2 Imprinted polymers (IP) based adsorbents

Imprinted polymers have two main types of polymers, these include the molecular imprinted polymers (MIP) and the ion imprinted polymers (IIP). The MIP are classified as polymers that uses similar properties with molecular memory or recognition to undergo polymerization of a suitable functional monomer in the presence of a model analyte or template molecule [86]. The ion imprinted polymers (IIP) use a ligand instead of molecules to form complexes that copolymerize with the metal ion in the presence of a crosslinker to form

a suitable template memory or recognition of similarly properties [88-89]. When designing an imprinted polymer that can best fit the size, the shape and functional group of the model analyte, it is required to facilitate the recognition site formation during removal interaction when the surface chemistry is conducted [89]. This makes it an ideal adsorbent that is sensitive and selective towards the targeted analyte in the presence of other pollutants in wastewater [86]. Liu *et al* [87] synthesized nanocellulose grafted on molecular printed polymers as Pb (II)MIP-NC and Hg (II)MIP-NC for the selective adsorptive removal of Pb (II) and Hg (II) [87]. In another study, the synthesis of a hallow mesoporous silica loaded with molecular imprinted polymers (H-MIP-Pb) was designed to adsorb Pb (II) from wastewater treatment [88]. Recently, most studies are using the MIPs by virtue of the previously mentioned qualities as an ideal adsorbent particularly for the selectivity towards the target analyte [88-89]. Amongst the other MIPs, the magnetic molecular imprinted polymers (MMIPs) seem to be the most currently used, owing to its magnetic properties, reproducibility, reduced affinity, and aggregation [88-89]. That allows increased adsorption capacity, easier separation, and fast binding kinetics due to their large surface area they possess [88-89]. Furthermore, its irregular shape is preferred by researchers since it has the potential to increase the monodispersed [88,33]. Moreover, MIPs have also been reported as costly hence researchers are currently moving away towards cost effective natural polymers from the agricultural waste for similar reasons [33]. The biosorbents or agriculturally based adsorbents are currently used due to their possession of the triple R's (recyclable, reusable and reduce) in line with the principles of green chemistry [90].

2.3.4 Agriculturally based adsorbents

Agricultural waste is from maize waste (stalk, corn and pith), wheat and rice waste (straw and husk), coconut, nutshells, palm seeds and many others [91]. Agricultural waste contains biosorbents compounds from polysaccharides such as cellulose, carbon, chitosan, chitin, keratin, biochar and many more extracted from these wastes [91]. It has been proven by various studies adsorbents from the agricultural wastes. For an example, a study was reported

by Boyrazli *et al* [92] where carbon was extracted from maize stalk [93]. Furthermore, another study was done using magnetic nanocomposite (eggshell/starch/Fe_3O_4) as bio-sorbents for adsorbing Cd (II) and Pb (II) ions from wastewater [93]. In this case, an adsorption removal of 96 and 98 %, for Cd (II) and Pb (II), respectively, was obtained at the optimal conditions of 25 ºC, 60 min, 10 ppm, and a dosage of 1 g/L at pH 7 and 6, respectively [96]. Nethaji *et al* [94] extracted carbon from corn cob for the removal of Cr (VI) with the adsorption capacity of 57 mg/g [94]. In addition, cellulose is one of the biosorbents from the agricultural waste and is a natural polymer extracted from various agricultural waste as already explained from the previous section. It possesses an abundance of -OH functional groups which has the ability to attach themselves with HMIs through chemical bonding and change the bio-sorbent surface charge, therefore, this surface charge affects the affinity during adsorption [57-58]. Moreover, the stability of the adsorbed complex can also be altered to improve the adsorption process [93-94]. Added properties of bio-sorbents are cost effectiveness, renewability, they also possess mechanical strength, have high surface area and can act as a reducing agent [93-95]. However, they have difficulty in dissolving in ordinary solvents due to the strong mechanical strength [90]. Various studies have used the CNCs as an adsorbent. Vivian Abiaziem *et al* [96] extracted cellulose from the Cassava peel and obtained 6,4 mg/g as their adsorption capacity for Pb (II) [96]. Literature has also reported setbacks like low porosity, low molecular weight, less selectivity and low adsorption capacity when using CNC for the removal of HMIs [51]. Thus, surface modifications where other functional groups like thiols(-S-H), amine (NH_2), carbonyl (C=O), and carboxylic (COOH), phosphate ($PO4^{-3}$) groups and magnetite (Fe_3O_4) have been applied to bind these groups to their adsorbents and to improve selectivity towards their desired analyte in wastewater effluents and increase the adsorption capacity [96-97]. This happens by using different methods like cross-linking, ligand complexation and ion exchange or ion pairing especially when trying to remove HMIs. This can also assist with the interaction between the adsorbent and the adsorbate via complexation, electrostatic attraction and many more [97]. Wang *et al* [82] modified CNC with Fe_3O_4 and MOF to form MCNC@Zn-BTC and obtained a higher adsorption capacity of 558,66

mg/g for the removal of Pb(II) [82]. In another study, a carboxylated CNC functionalised with Fe_3O_4 was used for the removal of Pb (II) and it was reported that they obtained 63 mg/g [52].

2.3.5 Composite nano-adsorbents

Composites, are materials comprised of more than two compounds aiming to produce excellent adsorption efficiency, maintain good reproducible results, effective stability and selectivity [77]. Many studies have combined more than two or more adsorbents to form a composite by modifying the surface material with oxygen, nitrogen or sulphate based functional groups or even functionalise it with the iron and its derivative, MIP or any of the aforementioned adsorbent in an effort to obtain higher adsorption capacity. Khan et *al* [59], modified GO using polyvinyl chloride (PVC) and *p*-Phenylenediamine to form a nano composite of PVC/PPD/GO for the removal of Cr (II) and they obtained a 93 % removal from wastewater as exhibited in **Table 2.2** [59]. Liu *et al* [72] functionalised AC with CS to remove Cr (VI) and obtained 0,48 mmol/g for their adsorption capacity [72], while others have functionalised GO-CS with EDTA against Hg (II) and Cu (II) and obtained 324 ± 3.30 and 130 ± 2.80 for Hg (II) and Cu (II), respectively [51].

In other instances, iron was also used to modify the surface of the adsorbent like in the study where Yan *et al* [58], used magnetite with graphene nanocomposite coupled with activated carbon (Fe_3O_4/G-AC). The nanocomposite gave a higher surface area of 485.8 m^2/g with a pore size of 0.302 cm^3/g than bare AC adsorbent. The overall nanocomposite performance provided an adsorption capacity of 153.2 mg/g with a total amount of 97 % removal of Pb (II) ions from wastewater [58]. In another study, the adsorption method was performed by using a Manganese ferrite/graphene oxide magnetic nanocomposite ($MnFe_2O_4$-GO) where the removal efficiency was almost 99 %, by removing Pb (II) and giving the adsorption capacity of 625 mg/g. Taking that into consideration, these magnetic nano-adsorbents were effectively involved within the adsorption process.

2.3.6 Summary

Table 2.2 was systemized by evaluating about 50 published manuscripts within a duration of 10 years stating from 2013 until 2023. These articles were extracted from Elsevier, MDPI, Wiley, Springer, Taylor and Francis publishing houses. Where similar research study interest from this study were pooled. For an example, studies working with various adsorbents for the adsorptive removal of Pb (II) and Cr (VI) from different water samples. A summary of adsorbents presented in **Table 2.2,** then **Fig 2.5** was generated by compiling the most used and efficient adsorbents between 2013 and 2023, where the reports were evaluated according to the year they were published. According to the results presented **in Fig. 2.5** from the extracted reports, the results indicates that 2022 had the most published articles in terms of adsorption, adsorbents, and the desired HMIs. Besides, when reviewing these adsorbents during this period (2013-2023), it appears that the nanocomposites have been the most used and efficient nano-adsorbents for the removal of HMIs over the years as exhibited in **Fig. 2.5**. This could be attributed to various factors such as a combination of various adsorbents, addition of other functional groups as already described along with the iron derivatives. Followed by the agricultural-based adsorbents, MOs, the least being, and the carbon based as shown in the year of 2022 as displayed in **Fig. 2.5.**

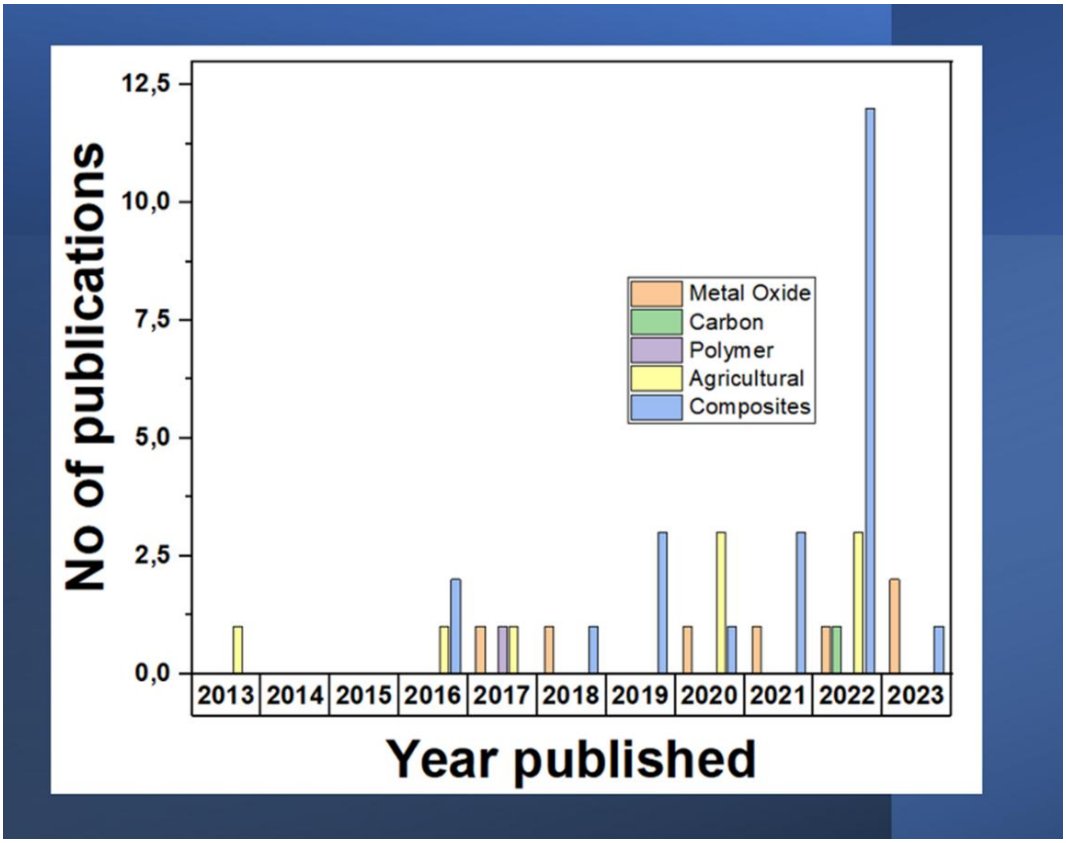

Figure 2.5: The number of reviewed articles published in ten years per adsorbent category.

The agricultural adsorbents are the second most used adsorbents, by reason of having the carboxylic, the hydroxyl, the epoxy and some containing amine groups which assist with the electrostatic attraction of the HMIs with the agricultural waste adsorbents [53,55]. The third mostly used adsorbents are the metal oxides and the least are the carbon and the polymers. This could be because researchers prefer to functionalise adsorbents with either polymers or carbon for stability and easy dispersion. Moreover, for efficient or higher adsorptive removal it is viable when adsorbents are combined for an enhanced combination of properties resulted from functional groups present within the material. The different parameters affecting the adsorption capacity are further discussed.

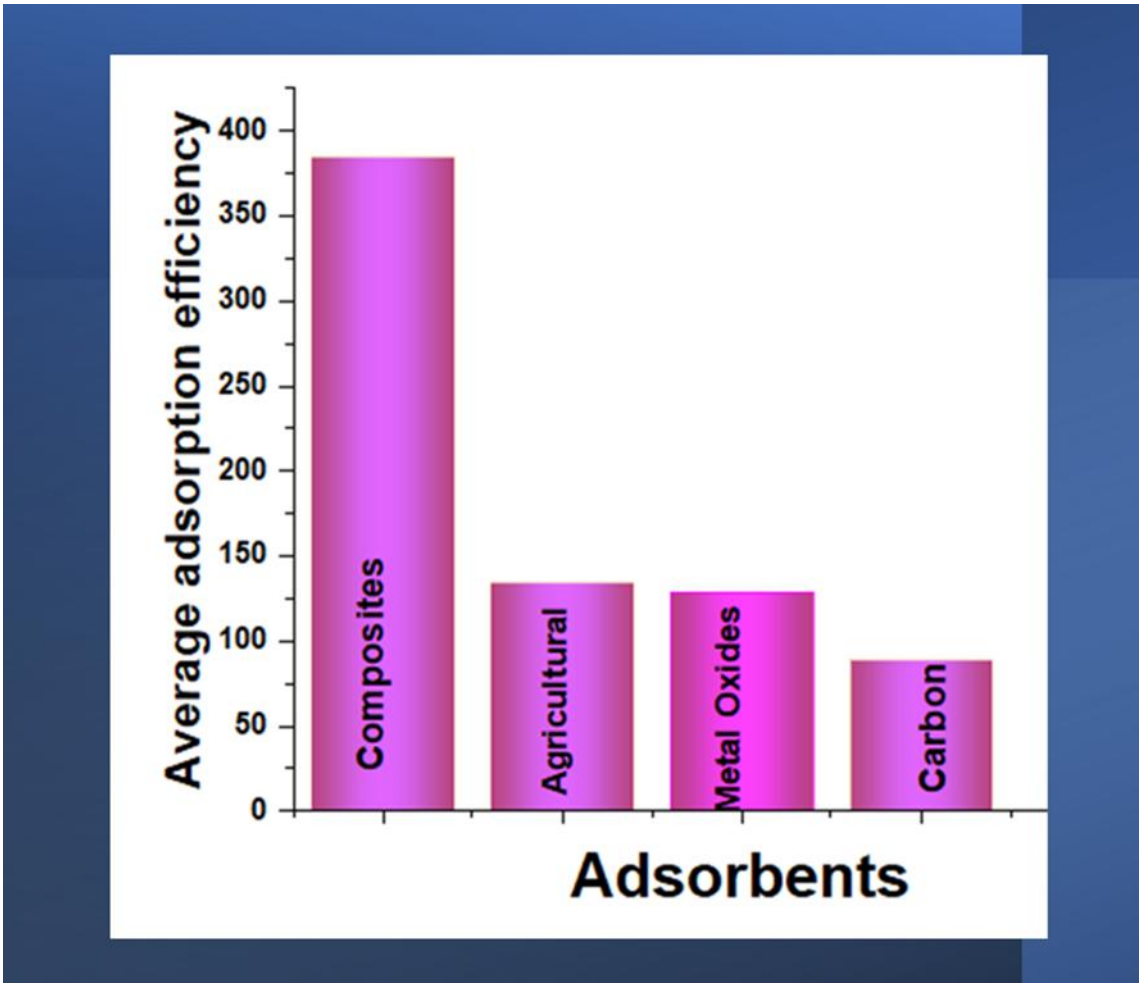

Figure 2.6: The most efficient adsorbents and less efficient adsorbents from the same articles

2.4 Adsorption

2.4.1 Factors affecting adsorption.

There are factors affecting adsorption and these also determine the adsorption interaction between the analyte and the adsorbent. These factors include the concentration of the analyte, dosage of the adsorbent, pH, contact time and temperature [52-59]. Depending on the nature of the adsorbent and of the analyte, they contribute towards the removal of the metal ions during the adsorption process. When the concentration of the adsorbate is less, then there is a possibility of higher adsorption capacity based on the adsorbent surface area that might have been higher. This can lead to an increase of active sites on the surface material governed by its permeability, or the surface are. This leads to an enhanced adsorption

capacity. This is observed when the pH of the solution is normally associated with the electrostatic interaction of the analyte versus the adsorbent. When ionic metals encounter negatively or positively charged surface materials in an acidic or alkaline environment. This was evident when a cationic metal Pb (II) had a higher adsorption capacity from various studies at a less acidic conditions of the average pH was between 5-6, since at pH 8, it tends to precipitate [56]. When anionic metals are adsorbed, the conditions are set in such a way that they fit the strong acidic conditions between the pH range of 1- 3 [53,62]. The contact time affects the surface adsorbent and the time efficiency where it allows the interaction to occur within that time, if the surface area and its porosity are higher, this can trap the adsorbate on to the surface adsorbent using its active binding sites [77].

2.4.2 Multivariate and univariate methods

Previously, researchers were optimizing one adsorbent's parameters at a time by performing univariate analysis as displayed on **Table 2.3** [23,52]. To be specific, the univariate method is a method where one parameter is optimised, and the rest of the conditions are kept constant. **Table 2.3** shows various studies since 2013 until 2023 where most research were still performing adsorption process using the univariate method. Even though the univariate was applied and preferred by various researchers, it has however, showcased a few limitations such as the method being ancient, requiring a lot of experiments which uses more reagents and leading to a lot of time consumption, focusses on one parameter at a time. Thus, simultaneous multivariate analysis has been the topic in the forefront because it has the ability to examine more than one analyte with a variation of all parameters in one setting on different experiments depending on the factorial design the researcher is adopting.

To get the precise experimental designs, Minitab, a mathematical tool has been widely used to monitor the process. The objective of performing simultaneous multivariate analysis is to minimize countless number of experiments while designing and developing experiments based on the minimal and maximum conditions of the parameters [98]. This includes, using first or second order models applied for the factorial designs which controls the interaction

effect of these factors where they are investigated and observed at 2 levels [99]. This is also represented or calculated by 2^{n-1}, where n represents the number of variables applied either on half factorial or full-factorial experimental design (FFED) [98-100]. The analysis of variance is applied too, by either using ANOVA or DOE to predict the significant factors influencing the response surface [98,109]. This leads to predicting the interactions between the analyte and the adsorbate as shown in **Table 2.3.** The table only focuses on selected analytes, namely the Pb (II) and the Cr (VI), which are the core analytes of this study.

Table 2.3: Various adsorption studies, isotherms, and kinetics using different adsorbents for the adsorptive removal of Pb (II) and Cr (VI).

No	*Adsorbent*	*Type of method*	*Analyte*	*Mechanism*	*Adsorption isotherms*	*Adsorption kinetics*	*Year published*	*Ref*
1	CCN-Fe_3O_4	Univariate	Pb	OH, C=O, Fe	Isotherms Langmuir 0,9998 q_{max}= 72,83 mg/g	PSO 0,759	2016	[52]
2	Pb-MCGO	Univariate	Pb	Pb, OH, C=O, Fe	Isotherms Langmuir 0,9956 q_{max} = 79,8 mg/g	PSO0,99	2016	[98]
3	PAC/Cell@Fe_3O_4	Univariate	Pb	OH, NH_2 and Fe	Isotherms Langmuir 0,98 q_{max} = 314,47 mg/g	PSO0,89	2019	[99]
4	MCNC@Zn-BTC	Univariate	Pb	OH, C=O, Fe	Isotherms Langmuir 0.9890 q_{max} x= 558.66 mg/g	PSO0,999	2017	[82]
5	M-Ch/CNF-Fe (III)	Univariate	Pb	OH, C=O, NH_2 and Fe	Isotherms Langmuir 0,9967 q_{max} = 0,4232 mg/g	PSO0,999	2023	[77]
6	NaSCNC	Univariate	Pb	COOH and ion exchange	Isotherms Langmuir 0,9967 q_{max} = 259,7 mg/g	PSO0,999	2013	[101]
7	GO-TETA-DAC	Univariate	Pb	OH, NH_2 and Fe	Isotherms Langmuir 0,9967 q_{max} = 69,98 mg/g	PSO0,999	2020	[102]
8	MCMGO	Univariate	Cr (VI)	NH_2 and Fe	Langmuir = 0,73 Freundlich = 0,99 q_{max} = 0,75 mg/g	-	2023	[23]
9	RGO/NiO	Univariate	Cr (VI)	NiO- ion exchange	Langmuir = 0,83 Freundlich = 0,99 q_{max} = 198 mg/g	PSO	2018	[103]
10	Chitosan/Fe_3O_4	Multivariate	Cr (VI)	NH_2 and Fe	Langmuir = 0,99 Freundlich = 0,90 Temkin = 0,86 q_{max} = 162mg/g	PFO 0,87 PSO 0,99	2019	[104]
11	GCF	Univariate	Cr (VI)	OH, NH_2 and Fe	Langmuir = 0,98 Freundlich = 0,97 q_{max} = 270mg/g	PFO 0,97 PSO 0,99	2018	[61]
12	CLCh/MWNCT/Fe	Univariate	Cr (VI)	C, NH_2 and Fe	Langmuir = 0,992 Freundlich = 0,980 q_{max} = 449 mg/g	PFO 0,971 PSO 0,987	2019	[62]
13	SBMGO	Univariate	Cr (VI)	OH, C=O, COOH and Fe	Langmuir = 0,998 Freundlich = 0,993 q_{max} =66 mg/g	PFO 0,782 PSO 0,999	2017	[66]

14	GO-Fe_3O_4	Multivariate	Cr (VI)	COOH, OH, NH2, C-O-C	Langmuir 0,996	PSO 0,999	2018	[105]

SBMGO = Chitosan Schiff Base-Magnetite-Graphene oxide nanocomposite

CCN-Fe_3O_4 = Magnetic carboxylated cellulose nanocrystal

MCMGO- Magnetic melamine functionalised chitosan modified by graphene oxide

Pb-MCGO = Magnetic chitosan functionalised by graphene oxide imprinted by lead

RGO/NIO = reduced graphene oxide coupled with Nickel oxide

PAM/Cell@Fe_3O_4 = Poly(acrylamide) crafted on the magnetic cellulose nanocrystals

M-Ch/CNF-Fe (III) = Magnetic chitosan cellulose nanofibre

GCF = Graphene oxide functionalised with Chitosan on ferrite nanocomposite

NaSCNC = Modification of cellulose with succinic anhydride

MCNC@Zn-BTC = Magnetic cellulose nanocrystals coupled with Metal−organic framework based on Zn (II) and benzene-1,3,5-tricarboxylic acid (Zn-BTC),

GO-TETA-DAC = Graphene oxide (GO) and dialdehyde cellulose (DAC) cross-linked with triethylenetetramine (TETA)

CLCh/MWCNT/FE = Cross linked Chitosan doped wit magnetic iron oxide on multiwalled carbon nanotube

Table 2.3 was compiled for the studies reported over the period of 10 years from 2013 until 2023. Looking at **Table. 2.3,** nanocomposites seem to be the most efficient adsorbents over 10 years as displayed on **Table 2.3.** Based on the presented reports it can also be observed the average adsorption capacity from these reports is above 385 mg/g. It could be attributed to the use of additional adsorbents like polymers, iron, carbon and many others. Moreover, it is evident that iron plays a major role within the adsorption process and can be clearly observed that the majority of these adsorbents contains iron in one way or the other. With respect to the results obtained from **Table 2.3**, the majority of researchers were practicing the use of univariate. The mechanism and interaction of the adsorbate and the analytes are also the key factors that requires reviewing since they have the potential to inform the researcher on how the material adapts to the environment.

2.4.3 Mechanism and interaction

The equilibrium of the adsorption process can be reached in three primary ways, used by researchers via the linear regression analysis tool to identify the equilibrium characterisation processes, apply these variables, and offer data sets that best fit the adsorption model.[74]. These ways include interaction of the adsorbate and the adsorbent at a variation of a certain parameter, examples are none other than the isotherms (concentration), kinetics (time) and thermodynamics (heat) [101-105]. **Table 2.3** displays a further review taken from studies presented in **Table 2.2** but now focuses further on the adsorption isotherms and kinetics study results particularly, with Pb (II) and Cr (VI) projected and further explained.

2.4.4 Adsorption Isotherms, Kinetics and thermodynamics

2.4.4.1 Adsorption Isotherms

By definition the adsorptive isotherms are known and used to determine the relationship or distribution between the adsorbent and the adsorbate [23]. The key goal is to use the surface properties to determine how the adsorbate and the adsorbent interact [10]. It also reveals the interactive surface feature of the adsorbent and the adsorption mechanism of the

adsorbent affinity using various isotherms [100]. These include the Langmuir, Freundlich, Temkin, Redlick Peterso, Dubinin-Radush Kevish, BET and many others [106].

Langmuir isotherm model (with the isotherm linear plot of $\frac{1}{q_e}$ against $\frac{1}{C_e}$) indicates monolayer and homogeneous adsorption process and the adsorption type is mainly chemisorption [105-106].

Langmuir's non- linear equation:

$$q_e = \frac{q_m k_L C_e}{1 + K_L C_e} \qquad 2.1$$

Langmuir's -linear equation

$$\frac{1}{q_e} = \frac{1}{q_{max}} + \left(\frac{1}{K_L q_{max}}\right)\frac{1}{C_e} \qquad 2.2$$

where the qe= amount of analyte adsorbed per mass (mg/g), qm/K=adsorption capacity (mg/g), K_L=Langmuir constant (L/mg), Ce= equilibrium concentration (mg/L). Many adsorptive studies prefer to use the Langmuir and Freundlich isotherm to identify the mechanism and interaction reactions. Investigation from **Table 2.3** has shown that a majority of the adsorbents had favoured Langmuir isotherms for both the Pb (II) and the Cr (VI) analytes. Moreover, for the kinetics it is also observed that the majority also favoured PSO kinetics. This is shown by the studies reported by Lu *et al* [52], Wang *et al* [98] and Hassan *et al* [99], where in their reports, they observed a Langmuir isotherm for the adsorptive removal of Pb [52,98-99]. According to literature, the Langmuir isotherms can assume that each adsorption site can only hold one adsorbate molecule and that the adsorbate molecules do not interact with each other, hence it has a homogeneous and a monolayer mechanism. Moreover, it can also mean that the reaction is physical and could be due to their surface areas and their porosity which allowed the Pb (II) molecules to be trapped within their surface sites. The second most popular adsorption isotherm is the Freundlich isotherm.

Freundlich isotherm model (with the isotherm linear plot of $\ln q_e$ against $\ln C_e$) indicates multilayer and heterogeneous adsorption process and the adsorption type is mainly physisorption. This assuming that the adsorbate molecules can interact with each other, also these adsorption site can hold more than one adsorbate molecule. The equation for this model is described as follows:

Freundlich's non-linear equation:

$$ln\, q_e = ln\, K_f + \frac{1}{n\, ln\, Ce} \qquad 2.3$$

Freundlich's linear equation:

$$qe = K_f ce^{1/n} \qquad 2.4$$

where 1/n and K_F are the empirical constant of the Freundlich isotherm = K_F (affinity constant in L/mg) and n(heterogeneity) obtained by calculating the slope and intercept of the calibration curve for the corelation coefficient. A study by Bagheri *et al* [23] for the removal of Cr (VI) obtained Freundlich isotherms which suggested a multilayer adsorption, meaning that several layers could have contributed without a uniform surface. The rate of the reaction was also investigated using kinetics studies from different reports as displayed in **Table 2.3**

2.4.4.2 Adsorption Kinetics

Adsorption kinetics is the process of studying the rate of adsorption over time at a constant concentration and pressure to evaluate the interaction of the adsorbate and the diffusion of the adsorbent pores [99,102]. There are various types of kinetics models which includes the Pseudo First order (PFO), Pseudo Second order (PSO), Pseudo order *n*, Bangham, Boyd, Crank, Elovich, Morris and Weber models [105-106]. Literature has focused mainly on the PFO and PSO models, where these two models were used during the adsorptive removal against Pb (II) and Cr (VI) ions from various studies reported on the same table. The PFO can be explained as follows:

Pseudo-first order (PFO) kinetic model (with the kinetic linear plot of $\ln(q_e - q_t)$ against t) indicates one active site of the adsorbent binds one adsorbate molecule. Where the equation below is used to calculate the PFO.

Pseudo-first order (PFO) kinetic model

PFO's non-linear equation

$$q_t = q_e(1 - 1\,exp(-k_1 t)) \qquad 2.5$$

PFO linear curve formula

$$\ln(qe - qt) = lnqe - K_1 t \qquad 2.6$$

Pseudo-second order (PSO) kinetic model (with the kinetic linear plot of t/q_t against *t*) indicates two active sites of the adsorbent bind one adsorbate molecule. The PSO linear equation is defined as followed:

PSO's non-linear equation

$$q_t = \frac{q_e^2 k_2 t}{q_e k_2 t + 1} \qquad 2.7$$

PSO linear equation

$$\frac{t}{q_t} = \frac{1}{k_2 q_e{}^2} + \frac{t}{q_e} \qquad 2.8$$

Where K_1 and K_2 are the PFO and PSO rate constants measured at g/(mg.min). According to the first studies as reported in **Table 2.3,** it is observed that most of them followed pseudo second order kinetics which assumes a chemisorption reaction. This means that the functionalization of these adsorbents enhanced their adsorption capacities. Hasan *et al* [99] and Wang *et al* [82] in their studies, reported a maximum adsorption capacity of 314 and 558 mg/g, respectively [82,99]. Moreover, there could have been factors that influences the

adsorption of Pb(II), such as the surface area and the electrostatic attraction caused by the adsorbents to the cationic Pb (II). The porous adsorbents caused by the incorporation of functional groups present in their surface, could have negatively charged the surface sites that can attract positively charged Pb (II) ions by electrostatic interaction [13]. The mechanism was formed in which the adsorbate was attached to the adsorbent, by the OH, COOH, NH_2 and the Fe groups particularly in water treatment for HMIs removal. That could also suggest that the adsorbents had a large surface for the chemisorption to occur.

2.4.4.3 Thermodynamics

Adsorption thermodynamics is a process that occurs spontaneously, and it is also accompanied by a decrease in the system's free energy. The decrease in free energy is due to the increase in entropy that occurs when the adsorbate molecules are adsorbed onto the adsorbent's surface and used frequently in water treatment methods for the removal of HMIs [55-60]. Adsorption is an exothermic process, which means that it is accompanied by a release of heat. Thus, when investigating thermodynamics, all the other factors remain constant while the temperature is varied. Thus, making temperature the key factor in thermodynamic adsorption [61-62]. The amount of heat released depends on the type of adsorption process and the specific adsorbent and adsorbate.

as determined by the following equations:

$$\Delta G = \Delta H - T\Delta S \quad 2.9$$

$$\Delta G = -RTLnK_L \quad 2.10$$

$$lnKd = \frac{\Delta S}{R} - \frac{\Delta H}{RT} \quad 2.11$$

$$Kd = \frac{qe}{ce} \quad 2.12$$

$$lnK_L = \Delta\frac{H}{T} + \Delta\frac{S}{R} \quad 2.13$$

Where ΔG = Gibbs energy change, ∆H = enthalpy change and ∆S = entropy change, R= gas constant (8,314 J/mol/K) and T=temperature measured in Kelvins=298 K [51]. It has also been reported to be reversible with low activation energy between 20–40 kJmol-1. Study after study has categorised the interaction between the adsorbent and the analyte as stronger or weaker, depending on the adsorbent's behaviour. Largitte *et al* [107] reported in their study, that the chemical model displayed the weakest interaction at the slowest rate [107]. Whereas other studies have classified chemical adsorption as the strongest model and Abdel-Magied as [110]. Chemical adsorption, (chemisorption) on the other hand, is a process in which the adsorbate molecules are held to the surface of the adsorbent by chemical interaction or bonding. Examples include the chelation, covalent, ion exchange and co-ordination bonds [106,110].

2.5 Overall summary

In **Table 2.3,** 14 studies were reported and amongst the 14, the leading method preferred by researchers since 2013 are the univariate methods with 12 conducted studies and only 2 studies were reported on multivariate analysis. This was reported in 2018 by Moges *et al* [105] and Pourmortazavi *et al* [108] in 2019 where both of these studies were adsorbing Cr (VI). This suggests that the method has not been explored enough and maybe since the method is recent, the researchers are slowly coming towards utilizing it. Thus, in this study, the exploration of this method will be put to service. Furthermore, **Fig. 2.7** exhibits that the adsorption Langmuir isotherm is primarily ruling over the Freundlich adsorption based on the aforementioned reasons. It has also been observed that the majority of the adsorbents used for the Pb (II) adsorption, were modified either with OH or COOH or both to target this analyte. Moreover, for the Cr (VI), the common functional group effective for adsorbing this analyte, seems to be the NH_2 in combination with COOH and OH as exhibited on **Table 2.3**

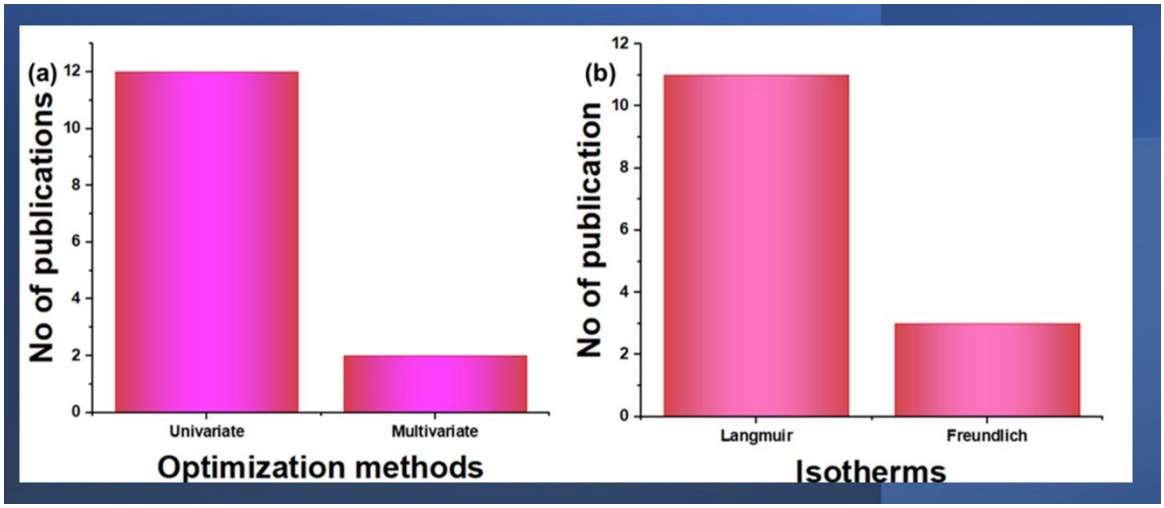

Figure 2.7: (a) the optimization methods and (b) isotherms used

2.6 Conclusion

In this study several adsorbents were investigated and reviewed it was discovered that the majority of the utilised adsorbents were reported with limitations, particularly, requiring the surface modification to improve the adsorption capacity. This was also noted with the derived agricultural waste cellulose and most studies opted to either use polymers since they possess other additional functional groups such as the oxygen based, nitrogen, sulphate based functional groups or iron for its superior magnetism. It was also discovered that among these adsorbents, the most efficient and used is the nano composites owing to their superior properties such as selectivity and the superior magnetism. The enhanced adsorption capacity was observed, not to mention that amongst the remediation methods, the adsorption process has been actively involved for the HMIs removal. The adsorption optimisation methods were also explored, and it was observed that the univariate has been the used method over the years and now researchers are currently starting to utilise the multivariate methods. For the removal of Pb (II) and Cr (VI), it was also observed that the majority of the interactions best fitted the Langmuir adsorption isotherms and the PFO kinetics during the adsorption experiments as highlighted in **Table 2.3** of this chapter.

2.7 References

1. Adekunle, A., Raghavan, V., Tartakovsky, B.: On-line monitoring of heavy metals-related toxicity with a microbial fuel cell biosensor. Biosens. Bioelectron. 132, 382–390 (2019).

2. Năstăsescu, V., Mititelu, M., Goumenou, M., Docea, A.O., Renieri, E., Udeanu, D.I., Oprea, E., Arsene, A.L., Dinu-Pîrvu, C.E., Ghica, M.: Heavy metal and pesticide levels in dairy products: Evaluation of human health risk. Food Chem. Toxicol. 146, (2020).

3. Saravanan, A., Senthil Kumar, P., Jeevanantham, S., Karishma, S., Tajsabreen, B., Yaashikaa, P.R., Reshma, B.: Effective water/wastewater treatment methodologies for toxic pollutants removal: Processes and applications towards sustainable development. Chemosphere. 280, 130595 (2021).

4. Crini, G., Lichtfouse, E.: Advantages and disadvantages of techniques used for wastewater treatment. Environ. Chem. Lett. 17, 145–155 (2019).

5. Noreen, U., Ahmed, Z., Khalid, A., Di Serafino, A., Habiba, U., Ali, F., Hussain, M.: Water pollution and occupational health hazards caused by the marble industries in district Mardan, Pakistan. Environ. Technol. Innov. 16, 100470 (2019).

6. Dagdag, O., Quadri, T.W., Haldhar, R., Kim, S.-C., Daoudi, W., Berdimurodov, E., Akpan, E.D., Ebenso, E.E.: An Overview of Heavy Metal Pollution and Control. Heavy Met. Environ. Manag. Strateg. Glob. Pollution, Part 1 - An Overv. Heavy Met. Pollut. Control. 3–24 (2023).

7. Philip, R.S., N, A., Mathew, M.: Hexavalent chromium removal using reduced graphene oxide-zinc oxide composite fabricated via simple pyrolysis method. Appl. Surf. Sci. Adv. 19, 100535 (2024).

8. Lian, M., Wang, J., Sun, L., Xu, Z., Tang, J., Yan, J., Zeng, X.: Profiles and potential health risks of heavy metals in soil and crops from the watershed of Xi River in

Northeast China. Ecotoxicol. Environ. Saf. 169, 442–448 (2019).

9. Ahmad, P., Alam, P., Balawi, T.H., Altalayan, F.H., Abass, M., Ashraf, M.: Chemosphere Sodium nitroprusside (SNP) improves tolerance to arsenic (As) toxicity in Vicia faba through the modi fi cations of biochemical attributes , antioxidants , ascorbate-glutathione cycle and glyoxalase cycle. Chemosphere. 244, 125480 (2020).

10. Dubey, R., Bajpai, J., Bajpai, A.K.: Green synthesis of graphene sand composite (GSC) as novel adsorbent for efficient removal of Cr (VI) ions from aqueous solution. J. Water Process Eng. 5, 83–94 (2015

11. Katubi, K.M.M., Alsaiari, N.S., Alzahrani, F.M., Siddeeg, S.M., Tahoon, M.A.: Synthesis of Manganese Ferrite / Graphene Oxide Magnetic Nanocomposite for Pollutants Removal from Water. (2021)

12. Zeng, K., Hachem, K., Kuznetsova, M., Chupradit, S., Su, C.H., Nguyen, H.C., El-Shafay, A.S.: Molecular dynamic simulation and artificial intelligence of lead ions removal from aqueous solution using magnetic-ash-graphene oxide nanocomposite. J. Mol. Liq. 347, 118290 (2022).

13. Kerur, S.S., Bandekar, S., Hanagadakar, M.S., Nandi, S.S., Ratnamala, G.M., Hegde, P.G.: Removal of hexavalent Chromium-Industry treated water and Wastewater: A review. In: Materials Today: Proceedings. Elsevier Ltd. pp. 1112–1121. (2020)

14. Jiang, Y., Zhou, J., Zhang, Q., Zhao, G., Heng, L., Chen, D., Liu, D.: Preparation of cellulose nanocrystals from Humulus japonicus stem and the influence of high temperature pretreatment. Carbohydr. Polym. 164, 284–293 (2017).

15. Ghorbani, M., Seyedin, O., Aghamohammadhassan, M.: Adsorptive removal of lead (II) ion from water and wastewater media using carbon-based nanomaterials as unique sorbents: A review. J. Environ. Manage. 254, 109814 (2020).

16. Sahoo, S.K., Panigrahi, G.K., Sahoo, J.K., Pradhan, A.K., Purohit, A.K., Dhal, J.P.: Electrospun magnetic polyacrylonitrile-GO hybrid nanofibers for removing Cr(VI) from water. J. Mol. Liq. 326, 115364 (2021).

17. Alija, A., Gashi, D., Plakaj, R., Omaj, A., Thaçi, V., Reka, A., Avdiaj, S., Berisha, A.: A theoretical and experimental study of the adsorptive removal of hexavalent chromium ions using graphene oxide as an adsorbent. Open Chem. 18, 936–942 (2020).

18. Alipour, A., Zarinabadi, S., Azimi, A., Mirzaei, M.: Adsorptive removal of Pb(II) ions from aqueous solutions by thiourea-functionalized magnetic ZnO/nanocellulose composite: Optimization by response surface methodology (RSM). Int. J. Biol. Macromol. 151, 124–135 (2020).

19. Khan, A., Khan, S., Khan, M.A., Qamar, Z., Waqas, M.: The uptake and bioaccumulation of heavy metals by food plants, their effects on plants nutrients, and associated health risk: a review. Environ. Sci. Pollut. Res. 22, 13772–13799 (2015).

20. Al osman, M., Yang, F., Massey, I.Y.: Exposure routes and health effects of heavy metals on children. BioMetals. 32, 563–573 (2019).

21. Venkatraman, Y., Priya, A.K.: Removal of heavy metal ion concentrations from the wastewater using tobacco leaves coated with iron oxide nanoparticles. Int. J. Environ. Sci. Technol. 19, 2721–2736 (2022).

22. Saleh, T.A., Gupta, V.K.: Column with CNT/magnesium oxide composite for lead(II) removal from water. Environ. Sci. Pollut. Res. 19, 1224–1228 (2012).

23. Bagheri, V., Naseri, A., Sajedi-Amin, S., Soylak, M., Zhang, Z.: Using Fe3O4-graphene oxide-modified chitosan with melamine magnetic nanocomposite in the removal and magnetic dispersive solid-phase microextraction of Cr (VI) ion in aquatic samples. Chem. Pap. (2023).

24. Samuel, M.S., Jose, S., Selvarajan, E., Mathimani, T., Pugazhendhi, A.:

Biosynthesized silver nanoparticles using Bacillus amyloliquefaciens; Application for cytotoxicity effect on A549 cell line and photocatalytic degradation of p-nitrophenol. J. Photochem. Photobiol. B Biol. 202, 111642 (2020).

25. Alalwan, H.A., Kadhom, M.A., Alminshid, A.H.: Removal of heavy metals from wastewater using agricultural byproducts. J. Water Supply Res. Technol. - AQUA. 69, 99–112 (2020).

26. Perera, H.M., Rajapaksha, A.U., Liyanage, S., Ekanayake, A., Selvasembian, R., Daverey, A., Vithanage, M.: Enhanced adsorptive removal of hexavalent chromium in aqueous media using chitosan-modified biochar: Synthesis, sorption mechanism, and reusability. Environ. Res. 231, 115982 (2023).

27. Azizi, S., Shahri, M.M., Mohamad, R.: Green synthesis of zinc oxide nanoparticles for enhanced adsorption of lead Ions from aqueous solutions: Equilibrium, kinetic and thermodynamic studies. Molecules. 22, (2017).

28. Silva, B., Martins, M., Rosca, M., Rocha, V., Lago, A., Neves, I.C., Tavares, T.: Waste-based biosorbents as cost-effective alternatives to commercial adsorbents for the retention of fluoxetine from water. Sep. Purif. Technol. 235, 116139 (2020).

29. Cheng, S., Zhao, S., Guo, H., Xing, B., Liu, Y., Zhang, C., Ma, M.: High-efficiency removal of lead/cadmium from wastewater by MgO modified biochar derived from crofton weed. Bioresour. Technol. 343, 126081 (2022).

30. Dutta, A., Datta, S., Ghosh, M., Sarkar, D., Chakrabarti, S.: Sunlight-assisted photo-fenton process for removal of insecticide from agricultural wastewater. In: Trends in Asian Water Environmental Science and Technology (2016)

31. Costa, T.C., Hendges, L.T., Temochko, B., Mazur, L.P., Marinho, B.A., Weschenfelder, S.E., Florido, P.L., da Silva, A., Ulson de Souza, A.A., Guelli Ulson de Souza, S.M.A.: Evaluation of the technical and environmental feasibility of adsorption

process to remove water soluble organics from produced water: A review. J. Pet. Sci. Eng. 208, (2022).

32. Alka, S., Shahir, S., Ibrahim, N., Ndejiko, M.J., Vo, D.V.N., Manan, F.A.: Arsenic removal technologies and future trends: A mini review. J. Clean. Prod. 278, (2021).

33. Sharma, G., Kandasubramanian, B.: Molecularly Imprinted Polymers for Selective Recognition and Extraction of Heavy Metal Ions and Toxic Dyes. J. Chem. Eng. Data. 65, 396–418 (2020).

34. Maraveas, C.: Production of sustainable and biodegradable polymers from agricultural waste. Polymers (Basel). 12, (2020).

35. Rathi, B.S., Kumar, P.S.: Application of adsorption process for effective removal of emerging contaminants from water and wastewater. Environ. Pollut. 280, 116995 (2021).

36. Gupta, K., Joshi, P., Gusain, R., Khatri, O.P.: Recent advances in adsorptive removal of heavy metal and metalloid ions by metal oxide-based nanomaterials. Coord. Chem. Rev. 445, 214100 (2021).

37. Shaik, A.M., David Raju, M., Rama Sekhara Reddy, D.: Green synthesis of zinc oxide nanoparticles using aqueous root extract of Sphagneticola trilobata Lin and investigate its role in toxic metal removal, sowing germination and fostering of plant growth. Inorg. Nano-Metal Chem. 50, 569–579 (2020).

38. Saravanakumar, R., Muthukumaran, K., Selvaraju, N.: Enhanced Pb (II) ions removal by using magnetic NiO/Biochar composite. Mater. Res. Express. 6, (2019).

39. Hassen, Y.E., Gedda, G., Assen, A.H., Kabtamu, D.M., Girma, W.M.: Dodonaea angustifolia Extract-Assisted Green Synthesis of the Cu2O/Al2O3 Nanocomposite for Adsorption of Cd(II) from Water. ACS Omega. 8, 17209–17219 (2023).

40. Patra, J.K., Baek, K.H.: Green biosynthesis of magnetic iron oxide (Fe3O4)

nanoparticles using the aqueous extracts of food processing wastes under photo-catalyzed condition and investigation of their antimicrobial and antioxidant activity. J. Photochem. Photobiol. B Biol. 173, 291–300 (2017).

41. Abdel-Magied, A.F., Abdelhamid, H.N., Ashour, R.M., Fu, L., Dowaidar, M., Xia, W., Forsberg, K.: Magnetic metal-organic frameworks for efficient removal of cadmium(II), and lead(II) from aqueous solution. J. Environ. Chem. Eng. 10, 1–10 (2022).

42. Samejo, S., Baig, J.A., uddin, S., Kazi, T.G., Afridi, H.I., Hol, A., Ali, F.I., Hussain, S., Akhtar, K., Perveen, S., Bhutto, A.A.: Green synthesis of iron oxide nanobiocomposite for the adsorptive removal of heavy metals from the drinking water. Mater. Chem. Phys. 303, 127807 (2023).

43. Hong, J., Kang, L., Shi, X., Wei, R., Mai, X., Pan, D., Naik, N., Guo, Z.: Highly efficient removal of trace lead (II) from wastewater by 1,4-dicarboxybenzene modified Fe/Co metal organic nanosheets. J. Mater. Sci. Technol. 98, 212–218 (2022).

44. Baratta, M., Mastropietro, T.F., Bruno, R., Tursi, A., Negro, C., Ferrando-Soria, J., Mashin, A.I., Nezhdanov, A., Nicoletta, F.P., De Filpo, G., Pardo, E., Armentano, D.: Multivariate Metal-Organic Framework/Single-Walled Carbon Nanotube Buckypaper for Selective Lead Decontamination. ACS Appl. Nano Mater. 5, 5223–5233 (2022).

45. Shahrashoub, M., Bakhtiari, S.: The efficiency of activated carbon/magnetite nanoparticles composites in copper removal: Industrial waste recovery, green synthesis, characterization, and adsorption-desorption studies. Microporous Mesoporous Mater. 311, 110692 (2021).

46. Zondo, B.Z., Sadare, O.O., Simate, G.S., Moothi, K.: Removal of Pb 2 + ions from synthetic wastewater using functionalized multi-walled carbon nanotubes decorated with green synthesized iron oxide – gold nanocomposite. 48, 304–316 (2022)

47. Bhutto, A.A., Baig, J.A., uddin, S., Kazi, T.G., Sierra-Alvarez, R., Akhtar, K., Perveen,

S., Afridi, H.I., Ali, H.E., Hol, A., Samejo, S.: Biosynthesis of aluminium oxide nanobiocomposite and its application for the removal of toxic metals from drinking water. Ceram. Int. 49, 14615–14623 (2023).

48. Prabhakar, R., Samadder, S.R.: Low cost and easy synthesis of aluminium oxide nanoparticles for arsenite removal from groundwater: A complete batch study. J. Mol. Liq. 250, 192–201 (2018).

49. Gindaba, G.T., Demsash, H.D., Jayakumar, M.: Green synthesis, characterization, and application of metal oxide nanoparticles for mercury removal from aqueous solution. Environ. Monit. Assess. 195, (2023).

50. Lingamdinne, L.P., Chang, Y.Y., Yang, J.K., Singh, J., Choi, E.H., Shiratani, M., Koduru, J.R., Attri, P.: Biogenic reductive preparation of magnetic inverse spinel iron oxide nanoparticles for the adsorption removal of heavy metals. Chem. Eng. J. 307, 74–84 (2017).

51. Verma, M., Lee, I., Oh, J., Kumar, V., Kim, H.: Synthesis of EDTA-functionalized graphene oxide-chitosan nanocomposite for simultaneous removal of inorganic and organic pollutants from complex wastewater. Chemosphere. 287, 132385 (2022).

52. Lu, J., Jin, R.N., Liu, C., Wang, Y.F., Ouyang, X. kun: Magnetic carboxylated cellulose nanocrystals as adsorbent for the removal of Pb(II) from aqueous solution. Int. J. Biol. Macromol. 93, 547–556 (2016).

53. Liu, C., Jin, R.N., Ouyang, X. kun, Wang, Y.G.: Adsorption behavior of carboxylated cellulose nanocrystal—polyethyleneimine composite for removal of Cr(VI) ions. Appl. Surf. Sci. 408, 77–87 (2017).

54. Zhu, X., Cui, Y., Chang, X., Wang, H.: Selective solid-phase extraction and analysis of trace-level CR(III), Fe(III), pb(II), and Mn(II) Ions in wastewater using diethylenetriamine-functionalized carbon nanotubes dispersed in graphene oxide

colloids. Talanta. 146, 358–363 (2016).

55. Omer, A.M., Abd El-Monaem, E.M., Eltaweil, A.S.: Novel reusable amine-functionalized cellulose acetate beads impregnated aminated graphene oxide for adsorptive removal of hexavalent chromium ions. Int. J. Biol. Macromol. 208, 925–934 (2022).

56. Si, Y., Li, J., Cui, B., Tang, D., Yang, L., Murugadoss, V., Maganti, S., Huang, M., Guo, Z.: Janus phenol–formaldehyde resin and periodic mesoporous organic silica nanoadsorbent for the removal of heavy metal ions and organic dyes from polluted water. Adv. Compos. Hybrid Mater. 5, 1180–1195 (2022).

57. Alipour, A., Zarinabadi, S., Azimi, A., Mirzaei, M.: Adsorptive removal of Pb(II) ions from aqueous solutions by thiourea-functionalized magnetic ZnO/nanocellulose composite: Optimization by response surface methodology (RSM). Int. J. Biol. Macromol. 151, 124–135 (2020).

58. Yan, J., Li, R.: Science of the Total Environment Simple and low-cost production of magnetite / graphene nanocomposites for heavy metal ions adsorption. Sci. Total Environ. 813, 152604 (2022).

59. Khan, Z.U., Khan, W.U., Ullah, B., Ali, W., Ahmad, B., Yap, P.S.: Graphene oxide/PVC composite papers functionalized with p-Phenylenediamine as high-performance sorbent for the removal of heavy metal ions. J. Environ. Chem. Eng. 9, 105916 (2021).

60. Guo, T., Bulin, C., Ma, Z., Li, B., Zhang, Y., Zhang, B., Xing, R., Ge, X.: Mechanism of Cd(II) and Cu(II) Adsorption onto Few-Layered Magnetic Graphene Oxide as an Efficient Adsorbent. ACS Omega. (2021).

61. Samuel, M.S., Shah, S.S., Subramaniyan, V., Qureshi, T., Bhattacharya, J., Pradeep Singh, N.D.: Preparation of graphene oxide/chitosan/ferrite nanocomposite for

Chromium(VI) removal from aqueous solution. Int. J. Biol. Macromol. 119, 540–547 (2018).

62. Marques Neto, J. de O., Bellato, C.R., Silva, D. de C.: Iron oxide/carbon nanotubes/chitosan magnetic composite film for chromium species removal. Chemosphere. 218, 391–401 (2019).

63. Yan, Y., Chu, Y., Khan, M.A., Xia, M., Shi, M., Zhu, S., Lei, W., Wang, F.: Facile immobilization of ethylenediamine tetramethylene-phosphonic acid into UiO-66 for toxic divalent heavy metal ions removal: An experimental and theoretical exploration. Sci. Total Environ. 806, 150652 (2022).

64. Dayal, D., Mant, J., Srivastava, N., Hashem, A., Fathi, E., Allah, A., Shah, M., Bahadur, D.: Chemosphere Sustainable removal of arsenic from simulated wastewater using solid waste seed pods biosorbents of Cassia fistula L . Chemosphere. 287, 132308 (2022).

65. Tu, B., Wen, R., Wang, K., Cheng, Y., Deng, Y., Cao, W., Zhang, K., Tao, H.: Efficient removal of aqueous hexavalent chromium by activated carbon derived from Bermuda grass. J. Colloid Interface Sci. 560, 649–658 (2020).

66. Anush, S.M., Chandan, H.R., Gayathri, B.H., Asma, Manju, N., Vishalakshi, B., Kalluraya, B.: Graphene oxide functionalized chitosan-magnetite nanocomposite for removal of Cu(II) and Cr(VI) from waste water. Int. J. Biol. Macromol. 164, 4391–4402 (2020).

67. Zhao, J., Yu, L., Ma, H., Zhou, F., Yang, K., Wu, G.: Corn stalk-based activated carbon synthesized by a novel activation method for high-performance adsorption of hexavalent chromium in aqueous solutions. J. Colloid Interface Sci. 578, 650–659 (2020). https://doi.org/10.1016/j.jcis.2020.06.031

68. Abbar, B., Alem, A., Marcotte, S., Pantet, A., Ahfir, N.D., Bizet, L., Duriatti, D.:

Experimental investigation on removal of heavy metals (Cu2+, Pb2+, and Zn2+) from aqueous solution by flax fibres. Process Saf. Environ. Prot. 109, 639–647 (2017).

69. Hegazi, H.A.: Removal of heavy metals from wastewater using agricultural and industrial wastes as adsorbents. HBRC J. 9, 276–282 (2013).

70. Mnasri-Ghnimi, S., Frini-Srasra, N.: Removal of heavy metals from aqueous solutions by adsorption using single and mixed pillared clays. Appl. Clay Sci. 179, 105151 (2019).

71. Abdelfattah, I., Ismail, A.A., Sayed, F. Al, Almedolab, A., Aboelghait, K.M.: Biosorption of heavy metals ions in real industrial wastewater using peanut husk as efficient and cost effective adsorbent. Environ. Nanotechnology, Monit. Manag. 6, 176–183 (2016).

72. Liu, F., Zhou, K., Chen, Q., Wang, A., Chen, W.: Application of magnetic ferrite nanoparticles for removal of Cu(II) from copper-ammonia wastewater. J. Alloys Compd. 773, 140–149 (2019).

73. Zhou, G., Jia, X., Zhang, X., Li, L.: Multi-walled carbon nanotube-modified hydrothermal carbon: A potent carbon material for efficient remediation of cadmium-contaminated soil in coal gangue piling site. Chemosphere. 307, (2022).

74. Krishna, R.H., Chandraprabha, M.N., Samrat, K., Krishna Murthy, T.P., Manjunatha, C., Kumar, S.G.: Carbon nanotubes and graphene-based materials for adsorptive removal of metal ions – A review on surface functionalization and related adsorption mechanism. Appl. Surf. Sci. Adv. 16, 100431 (2023).

75. Iqbal, Z., Tanweer, M.S., Alam, M.: Recent advances in adsorptive removal of wastewater pollutants by chemically modified metal oxides: A review. J. Water Process Eng. 46, 102641 (2022).

76. Liu, S., Sun, J., Huang, Z.: Carbon spheres / activated carbon composite materials with high Cr (VI) adsorption capacity prepared by a hydrothermal method. 173, 377–

383 (2010).

77. Zhang, N., Zang, G.L., Shi, C., Yu, H.Q., Sheng, G.P.: A novel adsorbent TEMPO-mediated oxidized cellulose nanofibrils modified with PEI: Preparation, characterization, and application for Cu(II) removal. J. Hazard. Mater. 316, 11–18 (2016).

78. Nordin, A.H., Wong, S., Ngadi, N., Mohammad Zainol, M., Abd Latif, N.A.F., Nabgan, W.: Surface functionalization of cellulose with polyethyleneimine and magnetic nanoparticles for efficient removal of anionic dye in wastewater. J. Environ. Chem. Eng. 9, (2021).

79. Hu, D., Lian, Z., Xian, H., Jiang, R., Wang, N., Weng, Y., Peng, X., Wang, S., Ouyang, X. –K: Adsorption of Pb(II) from aqueous solution by polyacrylic acid grafted magnetic chitosan nanocomposite. Int. J. Biol. Macromol. 154, 1537–1547 (2020).

80. Yan, E., Cao, M., Jiang, J., Gao, J., Jiang, C., Ba, X., Yang, X., Zhang, D.: A novel adsorbent based on magnetic Fe3O4 contained polyvinyl alcohol/chitosan composite nanofibers for chromium (Ⅵ) removal. Solid State Sci. 72, 94–102 (2017).

81. Ahmad, S.Z.N., Wan Salleh, W.N., Ismail, A.F., Yusof, N., Mohd Yusop, M.Z., Aziz, F.: Adsorptive removal of heavy metal ions using graphene-based nanomaterials: Toxicity, roles of functional groups and mechanisms. Chemosphere. 248, 126008 (2020).

82. Wang, N., Ouyang, X.K., Yang, L.Y., Omer, A.M.: Fabrication of a Magnetic Cellulose Nanocrystal/Metal-Organic Framework Composite for Removal of Pb(II) from Water. ACS Sustain. Chem. Eng. 5, 10447–10458 (2017).

83. Mo, Z., Tai, D.Z., Zhang, H., Shahab, A.: A comprehensive review on the adsorption of heavy metals by zeolite imidazole framework (ZIF-8) based nanocomposite in water. Chem. Eng. J. 443, 136320 (2022).

84. Arya, K., Kumar, A., Mehra, S., Divya, Kumar, A., Kumar Mehta, S., Kataria, R.: Exploration and removal of multiple metal ions using mixed-linker-architected Zn-MOF in aqueous media. Sep. Purif. Technol. 307, 122551 (2023).

85. Ren, Y., Yang, Y., Qu, G., Ning, P., Ren, N., Wu, F., Chen, X., Wang, Z., Hu, Y.: Study on the mechanism of removing Pb (II) and Cd (II) from industrial wastewater by copper based MOF modified with ethylenediamine. Fuel Process. Technol. 247, 107798 (2023).

86. Wackerlig, J., Schirhagl, R.: Applications of Molecularly Imprinted Polymer Nanoparticles and Their Advances toward Industrial Use: A Review. Anal. Chem. 88, 250–261 (2016).

87. Liu, S.: Preparation of nanocellulose grafted molecularly imprinted polymer for selective adsorption Pb(II) and Hg(II). Chemosphere. 316, (2023).

88. Zhang, Z., Zhang, X., Niu, D., Li, Y., Shi, J.: Highly efficient and selective removal of trace lead from aqueous solutions by hollow mesoporous silica loaded with molecularly imprinted polymers. J. Hazard. Mater. 328, 160–169 (2017).

89. Branger, C., Meouche, W., Margaillan, A.: Recent advances on ion-imprinted polymers. React. Funct. Polym. 73, 859–875 (2013).

90. Lu, L., Li, Y., Liang, Y., Chen, Q., Lu, Q.: One-pot green synthesis of carboxylated cellulose nanocrystals through oxidative degradation of bamboo pulp. BioResources. 15, 49–61 (2020).

91. Elgarahy, A.M., Elwakeel, K.Z., Mohammad, S.H., Elshoubaky, G.A.: A critical review of biosorption of dyes, heavy metals and metalloids from wastewater as an efficient and green process. Clean. Eng. Technol. 4, 100209 (2021).

92. Boyrazlı, M., Güler, S.H.: Synthesis of carbon nanostructures from corn stalk using mechano-thermal method. J. Mol. Struct. 1199, (2020).

93. Hosseini, S.S., Hamadi, A., Foroutan, R., Peighambardoust, S.J., Ramavandi, B.: Decontamination of Cd2+ and Pb2+ from Wastewater Using a Magnetic Nanocomposite of Eggshell/Starch/Fe3o4. SSRN Electron. J. 1–25 (2022).

94. Nethaji, S., Sivasamy, A., Mandal, A.B.: Preparation and characterization of corn cob activated carbon coated with nano-sized magnetite particles for the removal of Cr(VI). Bioresour. Technol. 134, 94–100 (2013).

96. Vivian Abiaziem, C., Bassey Williams, A., Ibijoke Inegbenebor, A., Theresa Onwordi, C., Ehi-Eromosele, C.O., Felicia Petrik, L.: Adsorption of lead ion from aqueous solution unto cellulose nanocrystal from cassava peel. J. Phys. Conf. Ser. 1299, 0–16 (2019).

97. Shahnaz, T., S., M.M.F., V.C., P., Narayanasamy, S.: Surface modification of nanocellulose using polypyrrole for the adsorptive removal of Congo red dye and chromium in binary mixture. Int. J. Biol. Macromol. 151, 322–332 (2020).

98. Wang, Y., Li, L.L., Luo, C., Wang, X., Duan, H.: Removal of Pb2+ from water environment using a novel magnetic chitosan/graphene oxide imprinted Pb2+. Int. J. Biol. Macromol. 86, 505–511 (2016).

99. Hasan, I., Khan, R.A., Alharbi, W., Alharbi, K.H., Alsalme, A.: In situ copolymerized polyacrylamide cellulose supported Fe3O4 magnetic nanocomposites for adsorptive removal of Pb(II): Artificial neural network modeling and experimental studies. Nanomaterials. 9, (2019).

100. Khalid, A.M., Hossain, M.S., Khalil, N.A., Zulkifli, M., Arafath, M.A., Shaharun, M.S., Ayub, R., Ahmad Yahaya, A.N., Ismail, N.: Adsorptive Elimination of Heavy Metals from Aqueous Solution Using Magnetic Chitosan/Cellulose-Fe(III) Composite as a Bio-Sorbent. Nanomaterials. 13, 1–17 (2023).

101. Yu, X., Tong, S., Ge, M., Wu, L., Zuo, J., Cao, C., Song, W.: Adsorption of heavy

metal ions from aqueous solution by carboxylated cellulose nanocrystals. J. Environ. Sci. (China). 25, 933–943 (2013).

102. Wang, Z., Yao, M., Wang, X., Li, S., Liu, Y., Yang, G.: Influence of reaction media on synthesis of dialdehyde cellulose/GO composites and their adsorption performances on heavy metals. Carbohydr. Polym. 232, 115781 (2020).

103. Zhang, K., Li, H., Xu, X., Yu, H.: Synthesis of reduced graphene oxide/NiO nanocomposites for the removal of Cr(VI) from aqueous water by adsorption. Microporous Mesoporous Mater. 255, 7–14 (2018).

104. Pourmortazavi, S.M., Sahebi, H., Zandavar, H., Mirsadeghi, S.: Fabrication of Fe_3O_4 nanoparticles coated by extracted shrimp peels chitosan as sustainable adsorbents for removal of chromium contaminates from wastewater: The design of experiment. Compos. Part B Eng. 175, 107130 (2019).

105. Moges, A., Nkambule, T.T.I., Fito, J.: The application of GO-Fe_3O_4 nanocomposite for chromium adsorption from tannery industry wastewater. J. Environ. Manage. 305, 114369 (2022).

106. Mpelane, S., Mketo, N., Bingwa, N., Nomngongo, P.N.: Synthesis of mesoporous iron oxide nanoparticles for adsorptive removal of levofloxacin from aqueous solutions: Kinetics, isotherms, thermodynamics and mechanism. Alexandria Eng. J. 61, 8457–8468 (2022).

107. Largitte, L., Pasquier, R.: A review of the kinetics adsorption models and their application to the adsorption of lead by an activated carbon. Chem. Eng. Res. Des. 109, 495–504 (2016).

108. Pourmortazavi, S.M., Sahebi, H., Zandavar, H., Mirsadeghi, S.: Fabrication of Fe_3O_4 nanoparticles coated by extracted shrimp peels chitosan as sustainable adsorbents for

removal of chromium contaminates from wastewater: The design of experiment. Compos. Part B Eng. 175, 107130 (2019).

109. Banchhor, A.: Full-factorial design and mathematical models of fixed-bed column adsorption of hexavalent chromium by S . glauca. 1–16 (2023)

110. Abdel-Magied, A.F., Abdelhamid, H.N., Ashour, R.M., Fu, L., Dowaidar, M., Xia, W., Forsberg, K.: Magnetic metal-organic frameworks for efficient removal of cadmium(II), and lead(II) from aqueous solution. J. Environ. Chem. Eng. 10, 1–10 (2022).

CHAPTER (III): SYNTHESIS OF MAGNETIC CELLULOSE NANOCRYSTALS DERIVED FROM MAIZE WASTE FOR THE ADSORPTIVE REMOVAL OF LEAD FROM WASTEWATER SAMPLES

Abstract

Over the past few years, heavy metal ion (HMIs) pollution has become a crucial matter by threatening human health and the ecological system, owing to their toxic nature. It has been reported by various researchers that Pb (II) has the potential to transform clean water into a polluted and non-drinkable water. Thus, this study describes the synthesis and characterization of magnetic cellulose nanocrystal (MCNC) nanocomposite derived from maize stalk as an adsorbent for the removal of Pb (II) from wastewater. The synthesised MCNC using a co-precipitation method was confirmed and characterised using the Fourier-Transform Infrared Spectroscopy (FTIR), Powdered X-ray Diffraction (P-XRD), Transmission Electron Microscopy (TEM), Scanning Electron Microscopy (SEM) coupled with the Energy Dispersive X-ray Spectroscopy (EDX), Ultra-Violet Visible Spectroscopy (UV-Vis), Thermogravimetric Analysis (TGA), and the Brunauer–Emmett–Teller (BET). The FTIR spectrum analysis revealed the presence of C=O, COOH, CH, OH and the Fe-O stretching frequencies. The P-XRD diffractograms confirmed the monoclinic type 1 cellulose with 1β lattice and magnetite cubic spinel phases. The TEM confirmed the needle shape, rods and spherical or irregular shape and both rods, needle and irregular shapes for the CNC, magnetite and the MCNC, respectively. The Selected Area Electron Diffraction (SAED) confirmed the same crystallographic planes as the P-XRD and the particle average sizes obtained for all the three material was 31 nm, 14 nm and 21 nm for CNC, magnetite and MCNC, respectively. For the morphology, SEM indicated a smooth fibroid surface of CNC while the magnetite showed rod like and spherical structures indicating the presence of iron and oxygen. The UV-Vis spectra displayed the presence of both CNC and magnetite. Furthermore, the thermal stability studies indicated that MCNC was stable after 600 ºC. The BET displayed the surface area, pore size and pore volume of the MCNC as 56m^2/g, 98Å and 0,1465 cm^3/g.Å, respectively.

For the removal of Pb (II), the multivariate optimization tools were used. An average maximum adsorptive removal percentage of 97% for Pb (II) with acceptable precision (≤ 3%) and an adsorption capacity at 47 mg/g were obtained. The MCNC could still be reused for 4 consecutive cycles with the highest removal of 96%. Moreover, against real wastewater samples a removal of 53% was achieved. These results showed that the adsorption reaction followed Freundlich isotherm and Pseudo first order kinetic reaction with the exothermic and spontaneous thermodynamic reaction.

3.1 Background

The transition to modern life has accelerated the global expansion of developing countries through industrialization and urbanization. That act had a negative impact on many water streams, resulting in water pollution in wastewater [1]. The mining, agricultural, industrial, pharmaceutical, and many more industries are the ones in concern [1-2]. Heavy metal ions (HMIs), which are harmful, non-biodegradable, and carcinogenic. Moreover, the HMIs accumulates within the human system and interfere with the metabolic functions. Lead (Pb) is one of the most utilized and harmful HMIs among cationic ions found naturally in water [3]. Lead has been removed from wastewater over the years due to the health risks connected with drinking water usage. As such, many approaches were used in various studies to try to remove Pb (II) during wastewater treatment studies.

To effectively remove pollutants, the adsorption process is controlled by the mobility of the adsorbate from the adsorbent under optimal/experimental conditions such as pH, analyte concentration, adsorbent dosage, contact time, and temperature distribution [4]. Previously, most research employed univariate approaches, which optimized one parameter at a time [4]. This has resulted in setbacks such as increased time consumption and costs due to the need for more reagents [5]. Furthermore, using these approaches limits the interactions of other factors with both the adsorbent and the analyte. Furthermore, because it is an antique conventional method, few academics are actively pursuing multivariate applications of this analytical method [5]. This approach optimizes numerous parameters simultaneously while

utilizing high adsorption capacity, a larger surface area, be porous, and crystalline adsorbents [5-6].

Reverse osmosis, solvent extraction, photocatalysis, leaching, membrane filtering, ion exchange resins, electro-kinetic, and many more methods have been employed in the past, but their limitations have been demonstrated [6-7]. These include the production of secondary pollutants, the use of severe conditions, expensive methods, and, in some cases, the need for regular maintenance, as well as higher energy intensive maintenance [6-7]. Alternatively, the adsorption process has emerged as a viable option since it is cost-effective, requires little energy, and creates fewer hazardous byproducts [7-8].

Adsorbents like graphene, carbon and silica-based material have been on the forefront due to their physicochemical properties such as good mechanical strength, thermostability and adequate functional groups which provide the capacity to adsorb HMIs due to the potential of a higher crystallinity and good surface area [5-7]. Yet, these adsorbents are limited in terms of selectivity, low adsorption capacity, poor dispersion and are costly [8-9]. Researchers are currently running away from expensive adsorbents and are opting to focus on adsorbents derived from natural materials like agricultural waste. Maize stalk from agricultural waste contains a higher content of cellulose [10-11]. Cellulose is a natural organic polymer that provides similar traits as the commercial ones, although, it comes with added advantages of biodegradability, recyclable and abundantly available [10-11]. Its advantages also include a higher crystallinity and surface area though, it also has setbacks like selectivity and low adsorption capacity.

Various researchers have modified the cellulose surface to enhance the adsorption capacity and also selectivity [10]. Through the use of different reagents, various authors have introduced ligands, while others have modified the surface by attaching different functional groups like amine, carboxylic, hydroxyl and sulphates [12]. In other studies, Soliman *et al* [13], Hosseinzadeh *et al* [7] functionalized the nano adsorbent with magnetite (Fe_3O_4) due to its super magnetism property, for enhanced separation and easy operation that does not require

tedious methods like centrifuging and filtration [7,13]. Ba-abbad *et al* [14] developed and optimised their synthetic method to prepare magnetite nanoparticles with controlled properties such as particle size, morphological structures, monodispersed surface area and biocompatibility to ensure there is a higher removal efficiency for HMIs [14].

These studies achieved their desired results using a variation of synthetic methods which includes solvothermal, hydrothermal and sol-gel, co-precipitation, physical combustion, thermal decomposition methods [1-3]. Amongst these synthetic methods, the co-precipitation method has proven to be the most preferred method for producing crystalline Fe_3O_4 nanoparticles while taking into consideration the oxidation states of each element within the material [14].

In as much as the magnetite nanoparticles are preferred for adsorptive removal of HMIs [14-15], they have also shown limitations in exhibiting agglomeration during synthesis but that can be overcome by adding a stable polymeric material like cellulose for support and allow ease of dispersity of iron during synthesis [7,15]. According to the authors' knowledge, it is the first time reporting the synthesis of the MCNC derived from maize waste (stalk) for the adsorptive removal of Pb (II) from wastewater.

3.2 Experimental procedure

3.2.1 Materials and chemicals

Maize stalks were harvested locally in Mankweng, Polokwane, South Africa. The chemicals and reagents used, were purchased from Sigma Aldrich, South Africa. Sulphuric acid (H_2SO_4), Iron II sulphate $Fe(SO_4)_2.7H_2O$, Ferric chloride hexahydrate ($FeCl_3.6H_2O$), 25 % diluted Ammonium hydroxide solution (NH_4OH), Sodium hydroxide (NaOH), 1.7 % diluted Hydrogen peroxide (H_2O_2), Glacial acetic acid (CH_3COOH), Nitric acid (HNO_3) 65 %, Certified single elemental standard reference material for Lead (Pb) at 1 000 ppm with 2% nitric acid were purchased from De Bruyn Spectroscopic Solutions cc, (South Africa). Refrigerated centrifuge (Dupont Co., Wilmington, DE, Model RC-5) South Africa, Nitrogen gas (N_2) cylinder was collected from Afrox, Limpopo, South Africa. Milli-Q® IQ water purification system for

producing 2.8 µm ultra-pure deionised water was purchased from Merck-Millipore, Germany. Sep Sci Lab Tech Shaker purchased from Daihan Labtec, South Korea, 400 L digital oven purchased from Labotec (South Africa). The Sintered Neodymium Iron Boron (NdFeB) 100mmx50mmx40mm and Membrane filter pore size 0,45 µm and 47 mm diameter were both purchased from Merck (South Africa). Micropipette and the 0,45 µm micro filters, centrifuge tubes (50 mL and 15 mL), filter papers 150 cm diameter, were purchased from CC Imelmaan, South Africa.

3.3 Methods

3.3.1 Extraction methods

The maize stalks were harvested, collected, and washed with deionised water. They were later cut into smaller pieces and dried at 40 °C in an air-dry oven according to a method by Silvéro *et al* [16] with minor modifications. Thereafter, the small pieces of the corn stalk were then placed inside a blender. They were crushed into a fine powder and sieved to 300-400 µm before use. About 60 g of fine maize powder was weighed and transferred into a 1 L Erlenmeyer flask as shown in **Fig. 3.1**. The 2 % wt. solution of NaOH was transferred into a 1L volumetric flask, thereafter 800 mL of the solution was poured into the maize powder for the alkaline hydrolysis process to occur. The mixture was heated at 80 ℃ while under magnetic stirring for 4 hrs to break the lignin and hemicellulose bond. Initially when the hydrolysis solution was added, the mixture turned yellow and after 4 hrs the presence of cellulose was observed when a dark brownish product was formed.

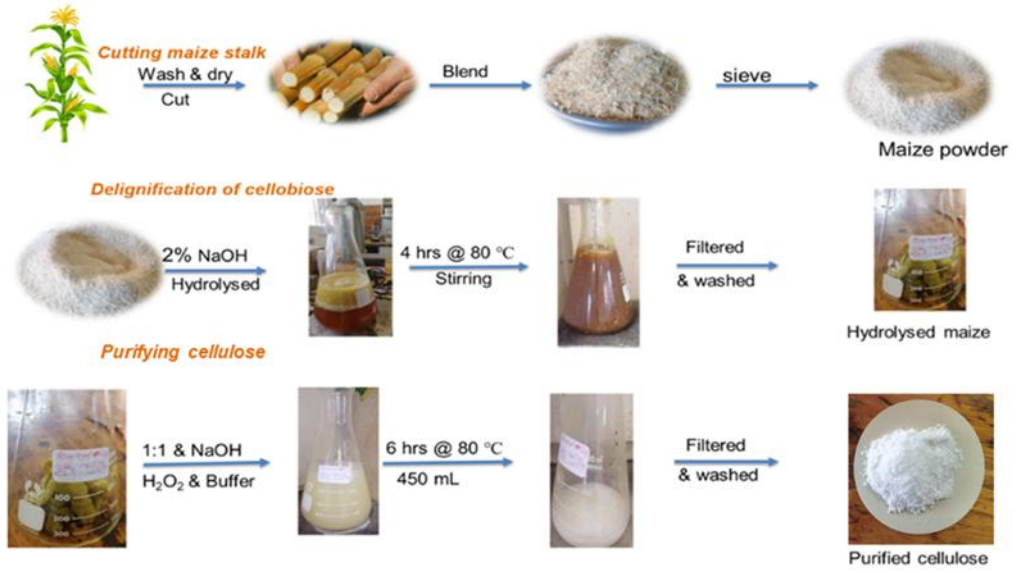

Figure 3.1: The extraction process of cellulose nanocrystals

The cellulose was left to cool, then filtered with gravity filtration and washed several times to remove impurities. After filtration, the residue was kept, and the filtrate was discarded [16].

3.3.2 The purification method of Cellulose Nano Crystals (CNC)

For the purification process, a bleaching solution was prepared by weighing 27 g of NaOH and poured into a 1 L volumetric flask and 500 mL of deionised water was added to the flask. In a different flask, a buffer solution containing 75 mL of glacial acetic acid and 75 mL of hydrogen peroxide with a ratio of 1:1 was prepared in a 250 mL volumetric flask and deionised water was added to the mark. The buffer solution was shaken for a minute and then transferred into a NaOH solution, where an additional 250 mL of deionised water was further added. For bleaching, 35 g of the hydrolysed cellulose was placed in an empty 1 L Erlenmeyer flask and 900 mL of the bleaching reagent was added. The bleaching occurred for 6 hrs at 80 ℃ while stirring, to purify the cellulose fibres and until a white gel was observed. The mixture was allowed to cool for an hr then it was filtered and washed with deionised water multiple times. The residue was collected and later dried in an oven at 40 ℃ for 24 hrs. The crystalline product was then blended into fine particles of powder and sieved as displayed in **Fig. 3.1**.

The sieved particles were collected as purified CNC (cellulose nanocrystals) for further synthesis of the magnetic cellulose nanocrystal (MCNC) and characterization [16].

3.3.3 Synthesis of the Magnetic Cellulose Nano Crystals (MCNC)

The in-situ co-precipitation method was used to prepare the MCNC (magnetic cellulose nanocrystals) according to a method by Ba-abbard *et al* [14]. An amount of 2.25 g of $FeSO_4.7H_2O$ and 8.48g of $FeCl_3.6H_20$ were added into a 250 mL Erlenmeyer flask. Then, about 20 mL of de-ionized water was added to the flask to dissolve the ferrous salt ($FeSO_4.7H_2O$) as the Fe^{2+} source and ferrite salt ($FeCl_3.6H_20$) as the Fe^{3+} source with a ratio of 2:1 and an orange colour was observed. Thereafter, 4 g of the purified CNC was further added to the iron solution as exhibited in **Fig. 3.2**.

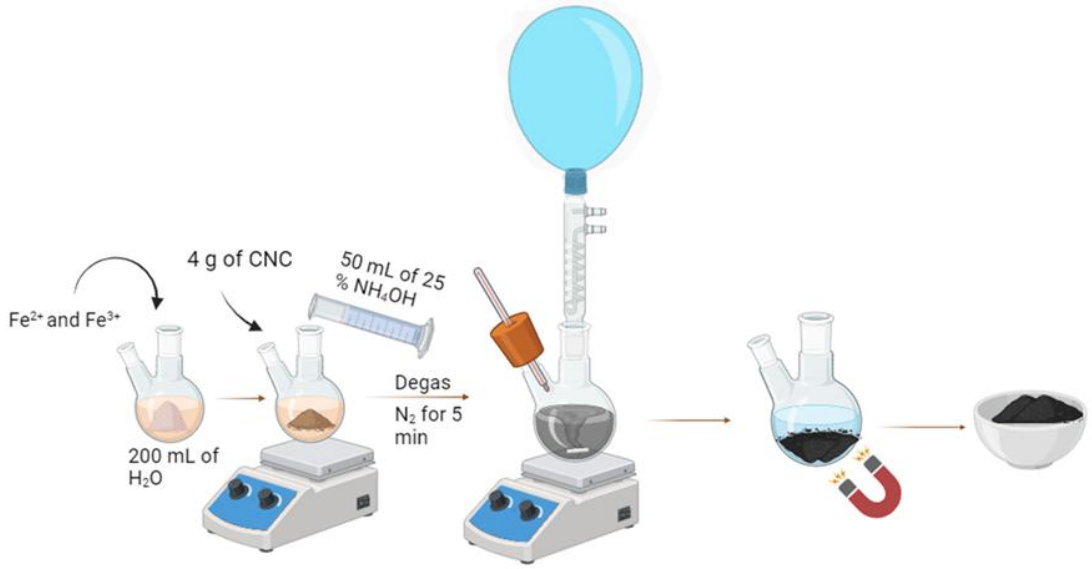

Figure 3.2: Synthetic process of the MCNC nanocomposite adsorbent

An aliquot of 180 mL of deionised water was further added to the mixture. The mixture was then transferred into a 250 mL 2-necked round bottom flask. For pH adjustment of pH=11, 40 mL of ammonia solution (NH_4OH) of 25 wt.% was slowly added while stirring. The mixture was degassed with N_2 gas for 5 min to remove the noxious fumes. In the presence of a waterless condenser under nitrogen gas atmosphere, the mixture was vigorously stirred at 1000 rpm and heated to 80°C in a reactor. Immediately a black precipitate was formed, and the reaction was allowed to proceed for 2 hrs. The precipitate was collected using an external

magnet and the supernatant was removed by decanting. The MCNC was filtered using a vacuum filtration and washed with deionized water several times and later placed in an oven at 40 ℃ for 24 hrs to remove the remaining moisture. The MCNC was later crushed, sieved and collected for characterization and the adsorption process was applied [14].

3.3.4 Characterization methods

The FTIR analysis was conducted for functional group identification and confirmation of the formation of the three materials. The TL-8000 FTIR equipment from PerkinElmer (South Africa) was used with the transmittance running from 400 to 4000 cm^{-1} with a resolution of 10 nm, and the scans were maintained at 32 scans per min. The materials were further confirmed and quantified by the UV-Vis {SP-UV 500VDB variable slit (colour touch)} operated between 200-800 nm. An aliquot of 3 mL of the sample was transferred into glass cuvettes and sample analysis was obtained at a specific wavelength depending on the analyte. The data containing the absorbance at a certain wavelength was collected and converted into a CVS format for further plotting. The crystallinity, particle size distribution and the phase identification of these nanomaterials were investigated using the P-XRD. The (P-XRD) analysis was performed on a 2 theta range from 10-90º. A sample of about 100 mg was placed into a sample holder using a spatula to make the surface even and introduced into the P-XRD. The phase identification was performed by searching and matching the obtained diffraction patterns with the powder diffraction file database with the help of EVA software. The SEM coupled with EDS was used to identify the morphology and composition of these materials. For SEM, a 500 VP microscope coupled with EDS was used for morphological and elemental composition analysis. For sample preparation, the carbon tape was placed on the stub and a tip of a spatula of the sample was placed on the carbon tape. The sample was then coated with carbon and grounded. This process helps to eliminate sample charging and electrons accumulating. The stub was then placed on the equipment with an acceleration voltage-operated on 10 KV. The detector used was the secondary electron detector with a working distance of about 6.9 nm and the aperture set at 30 µm. Images were then taken at various magnifications between

(1µm – 200 nm). The TEM (Phillip Technai, G2 F20 X-Twin MAT) was used to confirm the morphology, particle size, selective area diffraction pattern (SAED) and the lattice plane of the material. An amount of 100 mg of the sample was placed on the sample 200 mesh size Cu-grid and the analysis of the materials was measured at 200 Kv, with a current of 48 µA at an angle of 15°. The TGA was used to evaluate the stability and the decomposition of the materials using a TGA (Perkin Elmer, South Africa). The measurements were evaluated between 35 °- 700 °C, heated at rate of 10 °C/min using a thermal analyser from an inert environment maintained at 20 mL/min of N_2 gas. The surface area and porous measurements were evaluated by N_2 adsorption–desorption at 77K using the Brunauer–Emmett–Teller (BET) method. The materials were analysed between 80-100 °C for 8hrs. Then later for the quantification analysis, the adsorbate was measured using the ICP-OES (Agilent 700 series) under Ar gas at 800 Kpa and plasma flow rate of 22,5 L/min using an ICP expert 2 software. The wavelength was carried out at 220 nm for the adsorption data.

3.4 Application methods

3.4.1 Sampling of wastewater

Sampling was conducted in one of the wastewater treatment plants (WWTP's) in Gauteng, South Africa. On the day of sampling, the weather was sunny. Sampling was prepared from the wastewater influents where random selection of samples was collected, in the morning of 12 December 2023 around 10 am. The sampling collection was done randomly from Epis River, wastewater influent, wastewater effluent and the samples were placed in 500 mL brown, amber bottles. The bottles were previously washed with aqua regia solution. The samples were then placed in a cooler bag containing crushed ice and rushed to the laboratory. In the laboratory, it was then filtered to remove solid impurities and the as prepared of 2 % HNO_3 was immediately poured to minimize HMIs adsorption from the container and to preserve the HMIs. The samples were centrifuged at 10,000 rpm for 10 min to further remove the solid particles and filtered using a 0,45 micro filters. Then later preserved according to the procedure that followed the standard methods for the examination of water and wastewater.

The samples were immediately placed in a refrigerator at 4 ºC for further analysis. Thereafter, a 10 times dilution factor was used to reduce the concentration and the adsorption process was applied using the verified conditions for too concentrated samples.

3.4.2 Adsorption batch experimental process

The removal of Pb(II) was conducted using the adsorption process and the parameters such as were investigated based on the optimal conditions reported in various studies [33, 34]. These include pH (3-6), Dosage (2-50 mg), concentration of the analyte (2-10 ppm), contact time (10-60 minutes), temperature (25-60 ℃) and at the ramping speed of 160 rpm. These batch experiments were prepared according to the half factorial design method set by Minitab 18 software and were followed sequentially. After adjusting the pH and adding the analytes and their concentrations, the dosages were also included in 15 mL centrifuge tubes, with an aliquot of 10 mL aqueous mixtures. They were placed in a lab shaker at the required speed and the temperature set according to the half factorial method on Minitab. After adsorption, magnetic solid phase extraction was used to isolate the adsorbate from the adsorbent with the aid of an external magnet. After adsorption, 15 mL centrifuge tubes were placed in between the three external magnets for about a minute to allow the adsorbent to attach itself to an external magnet. The adsorbate was collected from the centrifuge tubes and poured via decanting into a 5 mL syringe with a 0, 45 µm micro filtered into another 15 mL centrifuge tube, to add an aliquot of 10 mL volume of the adsorbate. **Equation 3.1** was used to calculate the % removal of Pb (II) for all the adsorbed samples after the quantification analysis. To further understand the material, the most influential parameters were further validated, optimised and the surface response methodology (RSM) of the nano adsorbents was further investigated.

3.4.3 Multivariate optimization of the adsorption procedure

3.4.3.1 *Half factorial design (HFD)*

The screening process involves setting up the factorial design according to the required parameters including the number of experiments performed within the multivariate analysis.

This can be obtained by calculating the factorial design using the equation of 2^{n-1} where n represents the number of parameters used for designing the experiments. For an example, if the method used half factorial and requires 5 parameters, it will be noted as $2^{5-1} = 2^4 = 16$. This resulted in performing 16 experiments, later subjected to the adsorption process. The results were analysed using ICP-OES and the % removal was then obtained. The calculation was achieved using the following formula:

% removal = (Ci-Cf/Ci) *100 *3.1*

Where the Ci and Cf and the initial and final concentration of the analyte.

3.4.3.2 Response surface methodology (RSM)

Once the percentage removal of the analyte was calculated, it was then used for determining the significant and non-significant figures using the standardised effects displayed by the pareto chart. The central composite design (CCD) was further used for the optimization of the significant parameters whereby 20 trials with similar parameters were optimised according to the CCD design. The ANOVA was further used to further investigate the non-significant parameters. The validation process was also conducted by validating the optimal conditions over 6 trials performed for intra and inter day within a 2hr gap range. The surface response, surface response optimizer and the contour plots were employed while observing the factorial regression summary, R^2 value, R-sq. and the standard deviation. The isotherms, kinetics and thermodynamic studies were also investigated.

3.4.3.3 The adsorption isotherms, kinetics and thermodynamic studies

Six experiments were conducted using the constant validated optimal parameters of temperature (60 ºC) and time (5 minutes) while varying concentrations within a range of 50 – 500 ppb (50, 100, 150, 200, 300 and 500) ppb. The kinetics, concentration (100 ppb) and temperature (60 ºC) remained constant, while varying time from 0 – 30 minutes (0, 5, 10, 15, 20, 25 and 30 minutes). Lastly for the thermodynamic adsorption studies of temperature were

evaluated from 25 until 70 ºC (25, 30, 40, 50, 60 and 70 ºC). The results were analysed and the plotted using equation formulas listed below.

$$\mathrm{qmax} = \frac{(\mathrm{Ci}-\mathrm{Ce})}{W} * \mathrm{V} \qquad 3.2$$

where q_{max} is the maximum adsorption capacity at equilibrium, measured by (mg/g), Ci is the initial concentration before adsorption (mg/L), Ce is the equilibrium concentration after adsorption (mg/L), W is the adsorbent mass used and V is the solvent volume measured in L. The recoveries and re-usability studies were also investigated.

3.4.3.4 Reusability studies of the adsorbent

The reusability studies were conducted using the validated optimal conditions of Pb (II), where the method is described **in Section 3.2.2.6.2** with validated parameters. Then to retrieve the adsorbent, a 2 % HNO_3 acid solution was added to the adsorbent and was centrifuged for 5 min. The filtrate as an eluent, was collected and the residue was dried in an air-dry oven at 40 ºC for 6 hrs. The dried material was further used for multiple times and the results obtained were then recorded. With the same optimal parameters, the material was further used to investigate the capability of removing Pb (II) ions form wastewater analysis.

3.5 Results and discussion

3.5.1 Characterization

After the synthesis, three materials were obtained, the cellulose nano crystal (CNC), magnetite (M) nanoparticles and the Magnetic cellulose nano crystal (MCNC). To confirm the synthesis of the materials, the following techniques FTIR, P-XRD, TEM, SEMEDS, UV-Vis, TGA, and BET were utilised.

3.5.1.1 FTIR analysis

To confirm the formation of the materials and the functional groups present within the materials, FTIR was conducted as demonstrated in **Fig. 3.3.** On the CNC spectra, it can be observed that 3 peaks are shown, where there is a major broad band located between 3 000 cm^{-1} and 3 350 cm^{-1}. It was attributed to the stretching vibrational bond of OH, the presence

of COOH and CH. Furthermore, two additional minor peaks are observed at 1 700 cm^{-1} and 500 cm^{-1} indicating the presence of C=O, and the aromatic ring, respectively. The M spectrum displays a peak at 700 cm^{-1} which represents the formation of Fe_3O_4 nanoparticles. This also correlates with various reports where Fe_3O_4 was formed within the fingerprint region that is between 700-750 cm^{-1}[14-15].

The final spectrum of MCNC confirms the formation of the magnetic cellulose nano crystal because it has all the peaks observed by the magnetite and the cellulose nano crystal spectrums. From literature, it was noted that the MCNC also obtained similar peaks exhibiting the presence of Fe-O stretching bond within the fingerprint region and the presence of CNC exhibiting similar peaks [14-15]. Since the material were confirmed by the FTIR, these materials were further characterized using P-XRD analysis.

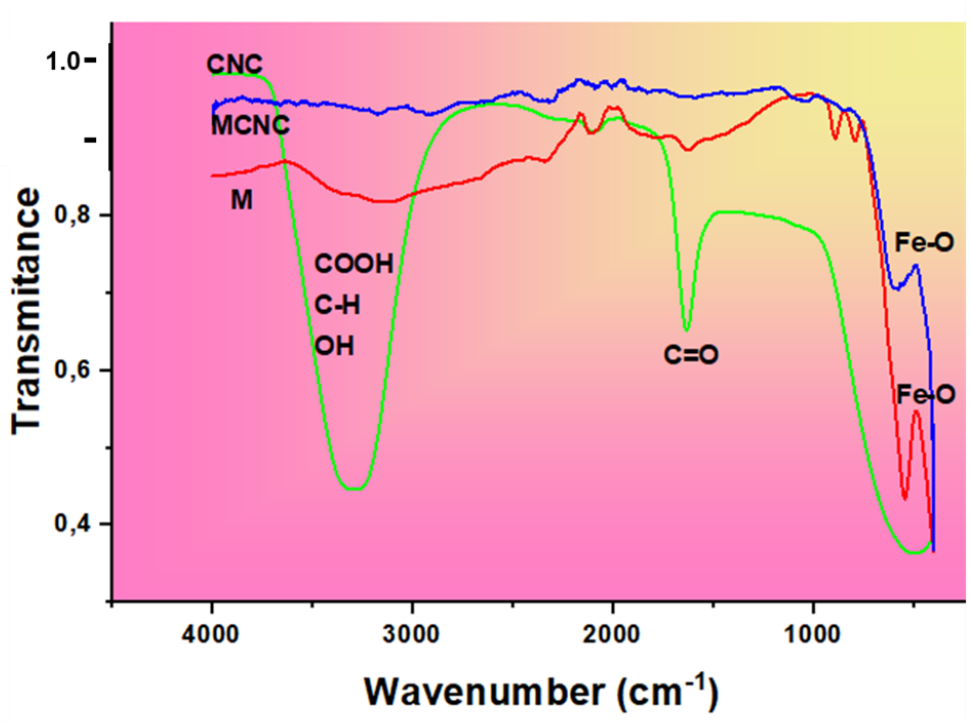

Figure 3.3: FTIR analysis of CNC, Magnetite (M) and MCNC

3.5.1.2 P-XRD analysis

The crystallinity and the phase identification of the three materials (CNC, magnetite and MCNC) were investigated using the P-XRD as depicted in **Fig. 3.4**. From the CNC spectra, seven distinct characteristic diffraction peaks were observed at 2θ= 11,5º; 16,7º; 19,1º; 22,5º; 25,8º; 29,8º and 36,7º which could be attributed to the lattice diffraction planes of (-110), (110), (002), (220), (021), (004) and (040). These results indicate that the phase formation is monoclinic type 1 cellulose with 1β lattice planes [17]. This also corroborates with the various reports [17-19]. Furthermore, our results confirm that CNC indeed exhibited a crystalline structure and could have an effective impact on the % removal and the enhanced adsorption capacity later when applying the adsorption process. This is due to the removal of the amorphous phase during the bleaching stage. The magnetite nanoparticles exhibited six diffraction peaks at 2θ = 22,18º, 30,0º; 35,6º; 43,0º; 57,2º, 62,8º and these were attributed to the crystallographic planes of (002), (220), (311), (400), (422) and (440) which also agree with the literature [18,20]. These results also indicate the cubic spinel phase of the crystal structure of M nanoparticles. This was also confirmed by the joint committee on powder diffraction standards (JCPDS) card 88-0315.

,

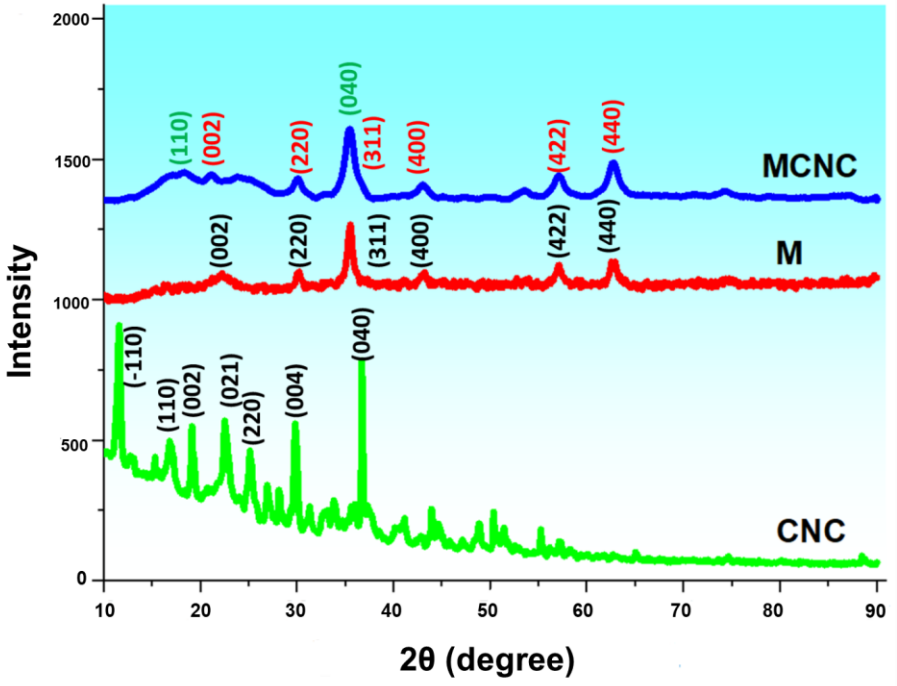

Figure 3.4: the XRD analysis of CNC, Magnetite (M) and MCNC

The MCNC exhibited 6 peaks, where two peaks confirm the formation of MCNC, these peaks are the (010) and the (040) at 2θ= 22,4º and 38,0º. Four crystallographic peaks of (311), (400), (422) and (440) from the Magnetite nanoparticle spectrum at an angle of 35,4º; 43,2º; 57,3º and 62,7º were identified. Furthermore, amongst these peaks one peak confirmed both the presence of Magnetite and CNC at displaying two crystallographic planes of (040) representing CNC and (311) for the Magnetite nanoparticles. This indicated that the presence of both CNC and the Magnetite also confirmed the formation of MCNC within the MCNC diffractogram.

The particle size of these materials was calculated using the debye Scherrer equation:

$$D = \frac{k\lambda}{\beta Cos\theta} \qquad 3.3$$

Where D is the average crystalline size and measured in nm, k stands for the shape factor of the material and measured at 0,9, the half width at half maximum (HWHM) is represented by the β values and an angle θ [18-20]. All the peak position, β=FWHM of these three materials

were measured and exhibited on the supplementary **Table S1**. The particles sizes of CNC, M and MCNC were calculated to be 9 nm: 5 nm and 7 nm, respectively. Moreover, the intensity of sharp CNC peaks, depicts that the CNC is indeed crystalline. However, it is observed that after the deposition of M, the MCNC peaks became broader and yet still exhibited sharp peaks, which suggests that MCNC is not amorphous but semi crystalline. Thus, these results confirm the formation of the three materials (CNC, M and MCNC) and verify that they are indeed nano materials. The MCNC is therefore expected to obtain a higher removal of Pb (II) due to its crystal nature and its smaller particle size. Moreover, the results also corroborate with various studies for the formation, the crystallinity, and the phase identification of the materials [6-20-21]. These materials were further taken for the morphological analysis as exhibited in **Fig. 3.5**

3.5.1.3 The TEM analysis

The three materials, the CNC, M and the MCNC were further characterized with TEM to confirm the formation and the diffraction patterns of these materials, and the results are presented in **Fig. 3.5 (a-l)**. From the presented results in **Fig.3.5 (a),** evenly distributed needle like morphology of the CNC as specified by the dotted rod-like shapes and the irregular shapes were observed. These results corroborate what has been reported in literature, where CNC displays the rod-like shape and the smooth surface [22-23]. The SAED confirmed the CNC is crystalline with 4 distinctive patterns as exhibited in **Fig. 3.5 (b)** which could confirm the crystallographic planes observed from the P-XRD analysis. The particle size distribution was calculated using Image J software, where the average distribution particle size of the CNC was calculated to be 31 nm. The P-XRD analysis confirms that the CNC particle size was the largest amongst the other two materials (MCNC and magnetite) and TEM also confirmed the same finding. These results are corroborated with studies where the average particle size for the CNC ranges between 20-50 nm [24-25].

Fig. 3.5 (d-f) represents the morphological, diffraction patterns and the particle sizes of the Magnetite nanoparticles. In **Fig. 3.5 (d)**, two morphological shapes, rod like or cubic shape and the irregular or partially spherical shapes showing a bit of agglomeration were observed.

These results concur with studies from literature, where rod like and spherical shapes were identified [13,26]. The SAED results displayed in **Fig. 3.5 (e)** indicated the material is polycrystalline with various diffraction patterns which could also be confirmed by the P-XRD results where 6 diffraction planes were discovered. The average particle size distribution of Magnetite was calculated to be 14,82 nm and most sizes were ranging between 15-20 nm as exhibited in **Fig. 3.5 (f)**. The Magnetite particle size results differ slightly from the P-XRD analysis where the average size was calculated to be 4.98 nm. This could be due to the agglomeration that was noted in the morphological analysis, which shows a lot of clustering and aggregation of the nanoparticles resulting in a higher particle size analysis comparing to the individual crystallite sizes from XRD.

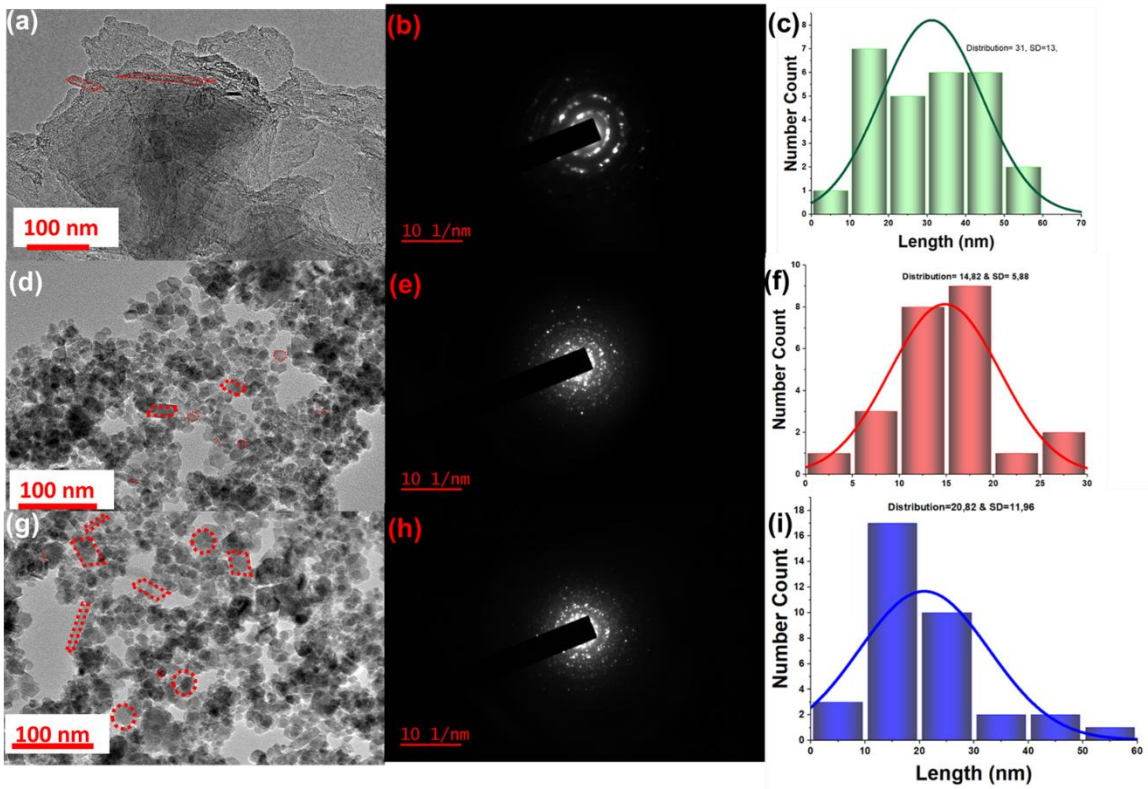

Figure 3.5 (a-i): The morphological, SAED and particle size distribution of CNC, Magnetite and MCNC

For the MCNC morphological analysis (see **Fig. 3.5 g**), three shapes; the rod like or cubic shape, irregular or spherical and the long needle like shapes were observed. The long tube indicates the presence of CNC, the rod like and the spherical or irregular shapes indicated

the presence of magnetite. Moreover, the grains as exhibited by the single dotted line in **Fig.3.5 (g**) shows that they are oriented at different directions which confirms that the material is polycrystalline. The SAED results **Fig. 3.5(h),** also confirmed the polycrystallinity nature of the material, which had an average particle size distribution of 20,82 nm. These results confirm the formation of a crystalline material composed of both the Magnetite and the CNC nanoparticles.

3.5.1.4 The SEM/EDS analysis

The morphology of the CNC, M and MCNC were investigated using the SEM coupled with the EDS for elemental composition. In **Fig. 3.6 (a),** a smooth surface of CNC was observed. The results are similar to the morphology obtained in a study by Liu *et al* [27]. They indicated that the smoothness comes from the crystallinity of the material [27]. In **Fig. 3.6(b)**, two shapes were observed, the rod-like and the cubic or spherical morphology and these are corroborated by the TEM results. This could be due to the presence of iron and oxygen molecules that were confirmed previously by the Fe-O bond from FTIR. Literature has reported various morphologies of Fe_3O_4 nanoparticles in different studies [14]. Most of the optimised synthetic methods vary in terms of parameters like precursors, solvents, and calcination temperatures to control the particle size and the morphology. Studies that used the co-precipitation method while using Ferric chloride tetrahydrate ($FeCl_3.4H_2O$) as a precursor mostly obtained spherical structures for the Fe_3O_4 nanoparticles [23,26]. When Ferric Chloride hexahydrate ($FeCl_3.6H_2O$) was used mostly, rod like morphologies were formed [26]. This could be due to the excess oxygen molecules that transformed the spherical Fe_3O_4 to a rod-like structure of Fe_3O_4. Furthermore, in one of the studies, Ba-abbad *et al* [14] also optimized their synthetic parameters when using the co-precipitation method [14]. They formed cubic structures when they used a precursor of $FeCl_3.6H_20$ and added 25 (wt.) % of ammonium hydroxide solution during synthesis and they attained a mixture of rods and cubic structures. This was confirmed by a balanced chemical reaction product of

$$Fe_3O_4.\ Fe^{2+} + 2\ Fe^{3+} = 8OH^- \rightarrow Fe_3O_4 + 4H_2O \quad [14,28]$$

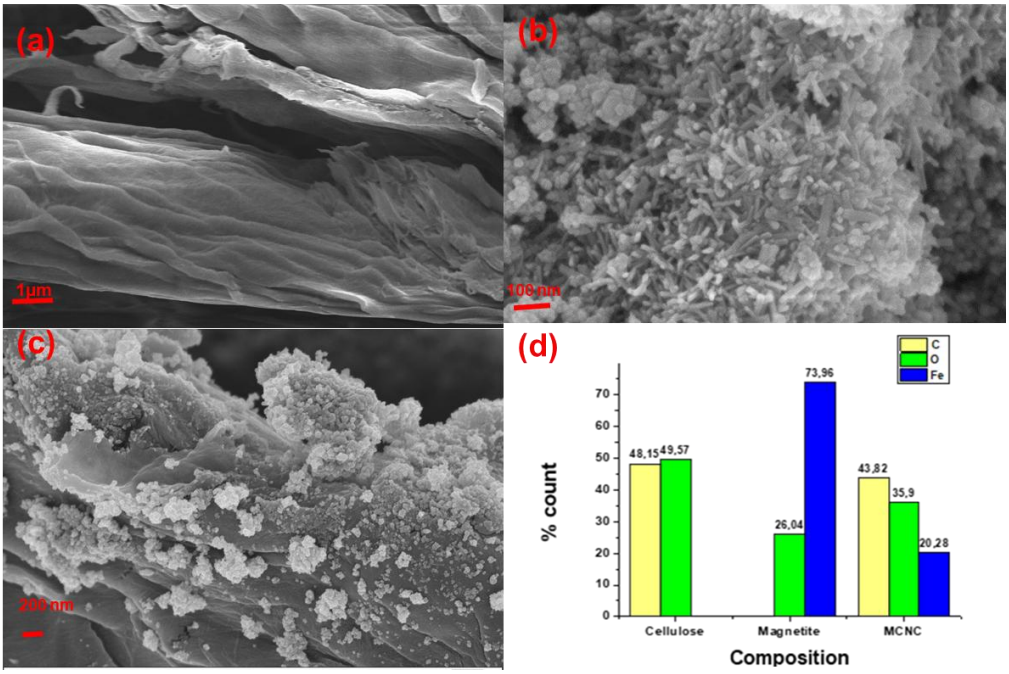

Figure 3.6(a-d): SEM and EDS analysis of CNC, Magnetite and MCNC

These results were also corroborated by Kulkarni *et al* [28] where the co-precipitation method was used under similar conditions but drying at 100 ℃ instead of 40 ℃ and obtained only cubic morphology for the Fe_3O_4 nanoparticles.

The MCNC displayed in **Fig. 3.6(c)** also showcased the formation of Fe_3O_4 nanoparticles by exhibiting similar morphologies of Magnetite and CNC nanoparticles prompting the presence of Fe_3O_4 and cellulose nanocrystal within the formation of MCNC. The MCNC morphology confirmed by the presence of the fibroid structures and sitting as a support and a stabilizer for the Magnetite nanoparticles. Moreover, this indicated that it allowed the dispersity of Magnetite molecules on to its surface to prevent Magnetite from agglomerating. Furthermore, the results confirm the combination of CNC and Magnetite nanoparticles and the formation of the MCNC composite.

The elemental composition of these three materials is also displayed in Fig. **3.6(d)** where carbon (49 %) and oxygen (48 %) are present in CNC bar and the carbon molecules are slightly dominant to the oxygen groups. The presence of Iron (74%) and oxygen (26%) is also observed in the Magnetite nanoparticle material bar, with iron molecules more dominant.

Finally, with the MCNC material bar, the presence of carbon (43 %), oxygen (35 %) and iron (20 %) were noted, where carbon is the dominant and key element of the material. This confirmed the formation of MCNC material, where the Magnetite nanoparticles and CNC materials are present within the MCNC bar. These results correlate with the FTIR, XRD and SEM data, confirming that all our materials have been formed as anticipated. To further confirm the optical properties of these materials, they were further characterized by the UV-Vis spectroscopy.

3.5.1.5 UV-Vis analysis

The CNC, M and the MCNC materials were further evaluated for the optical properties as shown in **Fig. 3.7**. For the CNC results denotes an absorption peak was at 320 nm. This gives an idea that the CNC is expected to absorb at lower wavelength. This can also be confirmed by reports where it was visible within the range of 200 – 350 nm [26-27]. In the magnetite nanoparticle spectra, the absorption peak at 264 nm was noted. Wang *et al* [27] and Khalid *et al* [26] also observed the absorption peaks at 276 nm and 230 nm, respectively [26-27]. According to their findings, this peak resulted from the effect of oxygen-charged molecules when transitioning [26]. It can be explained by a chemical reaction which follows:

$O_2^- \rightarrow Fe^{2+} + O^{2-} \rightarrow Fe^{3+}$ [26].

Kulkarni *et al* [28] also reported the same adsorption peak at 400 nm using the same co-precipitation method [28]. Their justification for this absorption peak was due to the combustion of oxygen [28]. Therefore, this then can confirm and corroborates with literature that Fe_3O_4 absorbs within the range of 200 – 400 nm [23,26]. The MCNC spectra confirmed the formation of MCNC material by indicating an absorption peak at 320 nm which confirmed the presence of CNC. Moreover, the tiny peak also displayed at 250 nm also confirmed the presence of iron within the MCNC material.

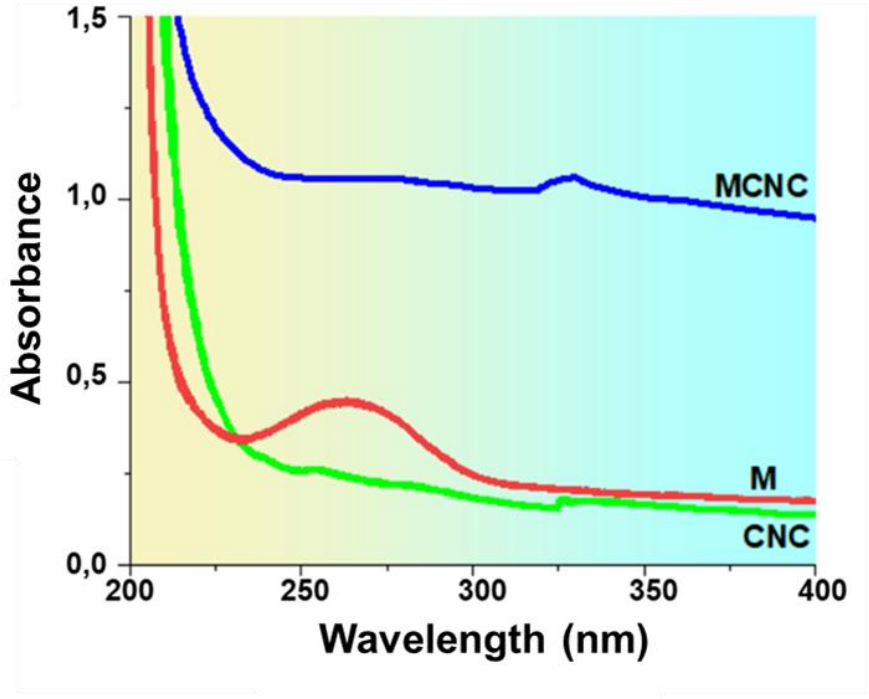

Figure 3.7: UV-Vis analysis of CNC, M and MCNC nanoparticles.

3.5.1.6 The TGA and DTG analysis

The TGA was conducted to investigate the thermal stability of CNC, M and MCNC materials as exhibited in **Fig.3.8 (a)**. All the materials displayed three thermal curves. Starting with the CNC nanoparticles, the first minor thermal decomposition curve was observed between 33 – 800 ℃ and that amounts to a weight loss of 5,16 % of CNC also listed in **Table 3.1**. This could be attributed to the evaporation of moisture heated at 100 ℃.

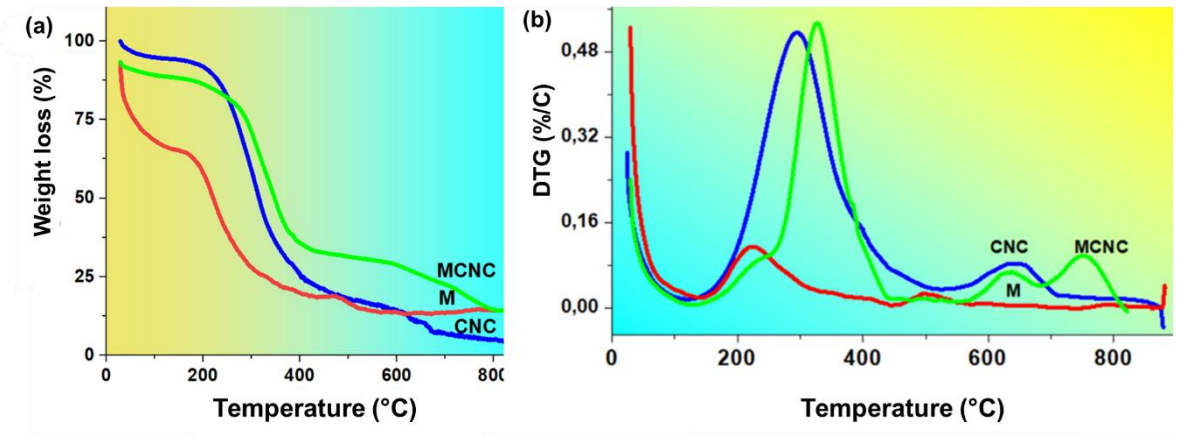

Figure 3.8: (a)TGA and (b) DTG analysis of CNC, M and MCNC nanoparticles

The second major decomposition curve was observed between 235 and 441 ℃ at a percentage loss of 67,87 %. This could be attributed to the decomposition of the amorphous phase during the hydrolysis process that occurred during the treatment method, which broke the glycosidic bond from the natural fibres for the formation of crystalline CNC and reports by Lu *et al* [29] and Silvero [16] *et al* corroborate these findings [16, 29]. The last decomposition curve for CNC was observed above 400 ℃, this could be accredited to the bleaching process that has removed the hemicellulose and the lignin. Furthermore, the leftover carbon after bleaching treatment was transformed and compelled CNC to decompose above 400 ℃, even though it might have also been slightly stable at that temperature [17]. Moreover, the CNC showed a higher weight loss of 28% amongst the other materials which could be due to the presence of carbon with a rapid decomposition between the temperature range of 235 and 441 ºC. This was also confirmed by the DTG thermogram where the CNC showed the higher decomposition peak around 296 ºC as exhibited in **Fig. 3.8 (b)**.

The magnetite thermogram also indicated three decomposition peaks as displayed in **Fig. 3.8 (a),** where the first decomposition occurred when M was heated from 33 and 197 ºC with 24,14 % weight loss. This could be attributed to the loss of moisture. The second weight loss peak was observed from 206 until 310 ºC with a major weight loss of 37 %. Moreover, in the DTG thermogram exhibited in **Fig, 3.8 (b),** a major peak was observed at 225 ºC which is also in agreement with the TGA. This weight loss could be attributed to the decomposition of oxygen. The last peak representing a weight loss, was found between 503 and 725 ºC with a minor loss of 2,79 %. In comparison to the CNC thermogram, it could be highlighted that the M thermogram was more stable than the CNC due to the decomposition of carbon.

Lastly, the MCNC thermogram also exhibited three decomposition peaks. A 7,15 % weight loss occurred during the removal of moisture between 33 - 216 ºC as depicted in **Table 3.1**. Thereafter, a 40% weight loss between 288 and 384 was observed. This was also confirmed by the DTG thermogram of MCNC in **Fig. 3.8(b**) at 329 ℃. Moreover, the MCNC, exhibited a similar degradation peak from that of the CNC as displayed in **Fig. 3.8(b)**. This

could be due to the thermal degradation of the magnetic nanocomposite [20,24]. Furthermore, this confirmed the presence of iron which also compelled peak shifting and exhibited less stability from CNC. In comparison, the MCNC was more thermally stable compared to magnetite nanoparticles and CNC, respectively.

Table 3.1: The thermal decomposition percentage of our material

	Initial weight Loss (%)	Major loss (%)	Final weight loss (%)	Maximum decomposition temperature (℃)
CNC	5,16	67,87	11,28	235
M	24,14	37.41	2.79	191
MCNC	7,15	40,35	4,75	288

3.5.1.7 The BET analysis

The CNC, M and MCNC materials were taken for BET analysis (**Fig.3.9)** for investigation of the surface area and porosity. The N_2 adsorption-desorption curves are represented by a star for CNC in **Fig. 3.9(a),** spherical curve for Magnetite and diamonds for MCNC. All these curves, each have an inlet of a pore size distribution plot. The last image is the surface area plot of all the materials represented in **Fig. 3.8(d)**.

For the CNC material, the specific surface area, pore size and volume were measured to be 3,44 m^2/g, 0,037 cm^3/g.Å and 107,96 Å, respectively. The CNC BET curve indicates a type 2 adsorption isotherm starting with micro porous layers with a possible low adsorption rate particularly at low relative pressures. This can suggest that during adsorption, the interaction between the analyte and the adsorbent might be weak. However, it was also observed that a rapid adsorption which is increasing also suggests that the material has a monolayer surface, allowing an effective adsorption.

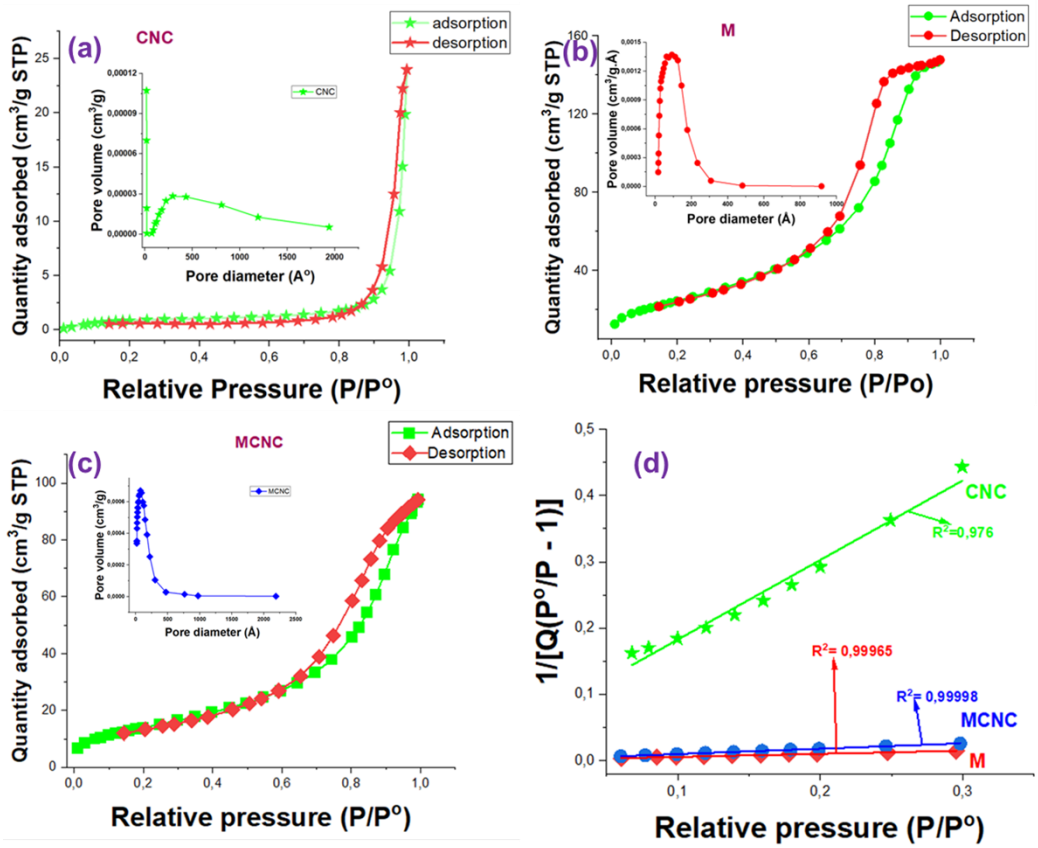

Figure 3.9: The N_2 adsorption-desorption isotherms and the BJH pores sizes distribution plot type of (a) CNC, (b), Magnetite and the (c) MCNC materials with their relative surface area plots.

These low surface area results concur with data reported in literature using extracted cellulose from the agricultural waste. Sun *et al* [30] and Karim *et al* [31] obtained less surface are of 1,90 and 3,10 m^2/g, respectively [30-31]. However, in other reports the surface areas ranged between 8 m^2/g to a maximum of 13 m^2/g and that could be attributed to subjecting their CNC to freeze drying method [22,32].

Table 3.2: The specific surface area, pore size, pore volume and the R^2 value of the surface area plot

Material	Surface area M^2/g	Pore size Å	Pore volume $cm^3/g.$ Å	R^2 value
CNC	3,444	107,96	0,037	0,976
M	92,15	96,64	0,229	0,9996
MCNC	52,65	98,93	0,1465	0,9998

The magnetite nanoparticles reported a higher surface area of 92 m^2/g and an increased pore volume of 0,229 $cm^3/g.$ Å. A type 4 adsorption curve was noted, and it also showed multilayers of micro and mesoporous surface at low pressure, and assuming to increase at higher pressures filling the monolayer surface. Moreover, the desorption isotherm exhibited similar behaviour when starting with a saturated multilayer surface at higher relative pressure and desorbing rapidly with decreasing pressure. This suggested that adsorption would be assumed to be caused by its porous surface property.

The MCNC noted an increase in the surface area from 3, 44(CNC) to 52,65 m^2/g (MCNC) as shown in **Table 3.2.** The pore volume and the pore diameter of MCNC also improved from 0, 037 to 0,1465 $cm^3/g.$Å and 12,5 to 25,5 nm, respectively. The increase in surface area and pore volume might have minimised aggregation of the cellulose when functionalizing it with magnetite nanoparticles [30]. The N_2 adsorption-desorption also exhibited a type 4 isotherm caused by the presence of magnetite nanoparticles with similar traits to the magnetite curve. A gradual increase in adsorption caused by mesoporous surface and an increased adsorption with increasing relative pressure was noted. This continued with a rapid increase caused by a monolayer surface and finishing with a microporous surface. These results can assume that the surface material contains two layers (mono and multilayers) constituting of the mesoporous and microporous surface. These results predict that, the higher surface area and porosity of MCNC could be conducive for the adsorptive removal of Pb from water [30]. In comparison with the reported studies, it can be safely reported that with the

improved properties, the surface area of MCNC is higher than most of the reported MCNC from agricultural waste. A surface area of 1,33 m^2/g was obtained from Nordin *et al* [33], 13,96 m^2/g by Ariaeenejad *et al* [34] and the 56,50 m^2/g obtained from the study reported by Sun *et al* [30] which are less than the surface area obtained from this study (56,65 m^2/g) [30,33,34]. After confirming the formation and properties of the MCNC adsorbent, it was further investigated for the adsorptive removal of Pb (II).

3.5.2 Application results

3.5.2.1 Screening

The MCNC nanocomposite adsorbent was used to adsorb the Pb (II) based on the lowest and highest optimal conditions reported by various reports from literature and the parameters are captured in **Table 3.3**.

Table 3.3: Minimum and maximum optimal parameters from various studies

Parameters	Minimum	Maximum
Dosage (mg)	2	50
Concentration (ppm)	2	8
Contact time (min)	10	60
Temperature (ºC)	25	60
pH	3	6

3.5.2.2 Half factorial design (HFD)

The 16 experiments were conducted and the pareto chart as exhibited in **Fig. 3.10** was measured showcasing the significant parameters obtained after the half factorial design (HFD) during the screening process. The half factorial screening results are presented on the supplementary information as **Fig. S.1.** Data extrapolated from those results was used to

generate the standardised pareto chart results, as represented in **Fig. 3.10.** The pareto chart signifies three parameters that include time, concentration and dosage as the most effective parameters within the adsorption reactions. This is shown by the standardised dotted line across the result, the parameters appearing on the right hand are the significant parameters. The ones appearing on the left of the dotted line indicates the non-significant parameters. So, the non-significant parameters according to the results presented in **Fig. 3.10** are the pH and the contact time. This can also be verified by the analysis of variance (ANOVA) graph which indicated that the p-values of pH and time as 0,629 and 0,713 as shown in **Fig. S.2.** The results stipulated by the ANOVA rule stating that any factor that is below 0,5 is significant and more than 0,5 is not significant, hence the significant and non-significant parameters were clearly obtained. During the experimental procedure when the % removal of Pb (II) was calculated, a higher dosage seemed to have had a positive effect on the experiments.

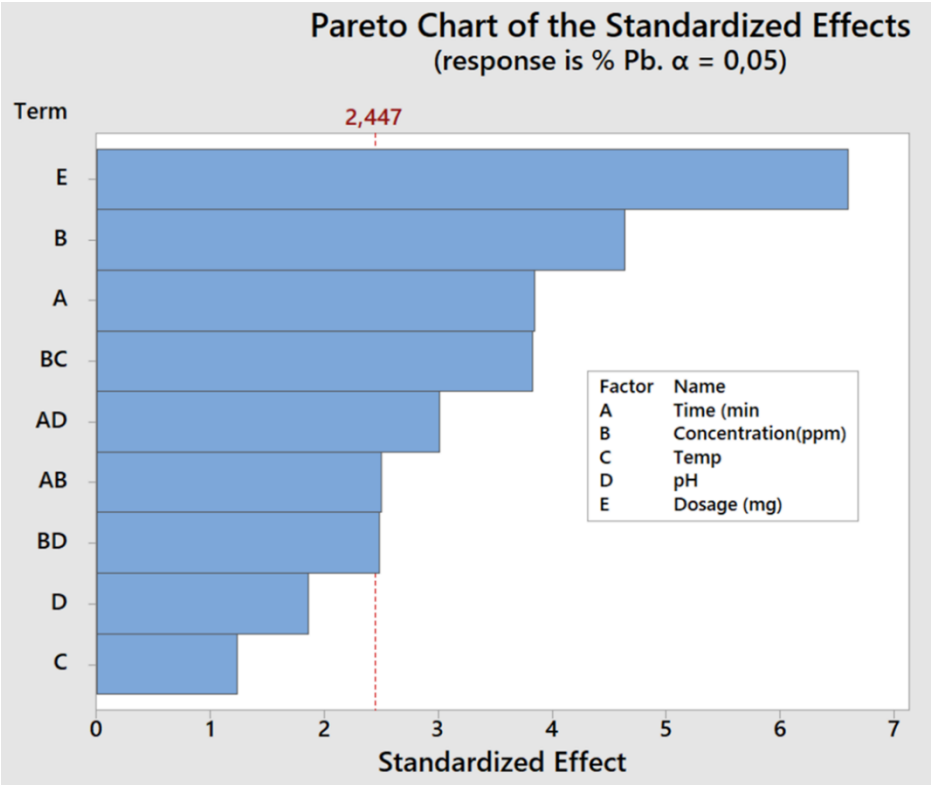

Figure 3.10: Pareto chart of the standardised effects for Pb (II)

The dosage has a significant effect on the active sites of the adsorbent carries, according to another research that has already been conducted [10,13]. It was also noted that adding

more dose to reach equilibrium saturation of the adsorbent could not help the reaction; hence, the effective dosage is required when conducting experiments [13]. Considering that when the adsorbent has enough porosity and has also acquired a large surface area, it can easily trap the Pb (II) ions within these pores allowing for enhanced adsorption capacity [15-32]. This is also verifying to BET results presented in **Fig. 3.9 (c)**. It anticipated for the physical adsorption caused by the multilayer surface. Moreover, MCNC showed an enhanced surface area with the adequate pore size which allowed the analyte to be trapped within the pores [35]. Furthermore, it can also be noted that by virtue of having magnetic properties which also contributed to the adsorption, the analyte as the metal ions, were attracted to the magnetic adsorbent via the electromagnetic field. At higher concentrations of 50 mg, less removal was observed. The pH and time did not give much of a difference and literature also stipulated that electrostatic interaction of the cationic analytes like Pb (II) when they interact with the adsorbent, particularly at acidic conditions, they tend to also increase the removal percentage of the analyte [36]. This was reported by different reports since pH was reported the most effective where these indicated that the cationic analytes are easily attracted by the electrostatic reaction created when the proton from the acid binding to the analyte and for the alkaline solution tend to precipitate the Pb (II). Hence, it is mostly active within the less acidic environment [4,24], However, in this study, that was not the case, the interaction confirms dosage to be the leading parameter as already stipulated with an adequate surface capacity. On the same note, the significant parameters were later optimised and validated to attain the optimal conditions following the CCD method which designed 20 more experiments for optimization.

3.5.2.3 Response surface methodology (RSM)

3.5.2.3.1 Multivariate optimization of the adsorption procedure

The CCD optimization procedure was utilised to investigate the interaction between the Pb (II) and the MCNC surface. Thus, a representation of results composed of these parameters (time, dosage and concentration) is represented in **Fig. 3.11.** The contour plot

quantifies the parameters against each other. The best percentage removal against Pb (II) using the three parameters was when it showed a dark green colour outside the plot. It shows that these olive colour can only be observed when the percentage removal is over 95 %. So, based on the results appearing in **Fig. 3.11**, for the contour plot results, the optimal value for contact time was less than 10 min, dosage more than 60 mg and concentration less than 1 ppm. The surface plot showed the highest removal occurred when the dosage was more than 60 mg, and the concentration was around 1 ppm. These results are also corroborated by the surface plot and the surface optimizer where these parameters were confirmed.

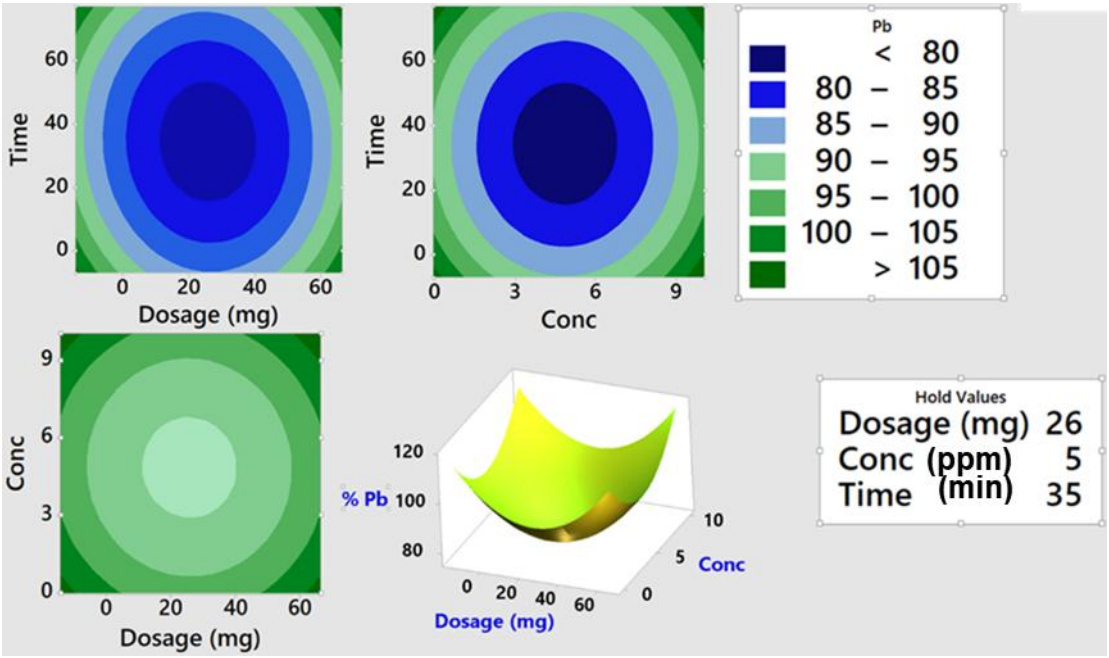

Figure 3.11: Contour plots and the surface plot results of MCNC against Pb (II)

The surface optimiser is a tool that optimises the surface of the adsorbent and is also used to confirm the parameters obtained from the contour plot and the surface plot. From the analysis, it was noted that contact time was best at 5 min and dosage 66,30 mg. This predicted that the desired values for the removal of Pb (II) will be based on these parameters as exhibited in **Fig. 3.12**. The results are shown and written in red on the middle of the higher and lower conditions.

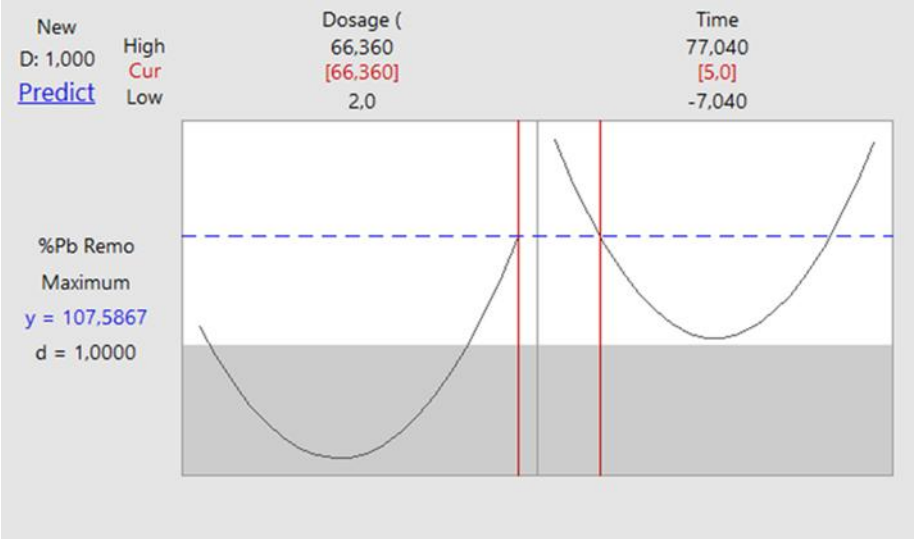

Figure 3.12: The surface optimizer of MCNC against Pb (II) ion removal

In addition to the results presented in **Fig. 3.12** from the surface optimiser, the pH and time was also included, amongst the optimised parameters. Since they were not significant during the screening process. So, the selected value of these parameters was guided by following the majority of reported articles that states their efficient values. Thus, the pH was kept at 6 and contact time at 5 min. Using similar conditions, the other adsorbent material such as CNC and magnetite were also validated together with the MCNC. This was conducted to monitor and to compare the efficiency of these adsorbents. Each analysis for the various adsorbents was conducted three times using inter day experiments that were later presented in **Fig. 3.13**.

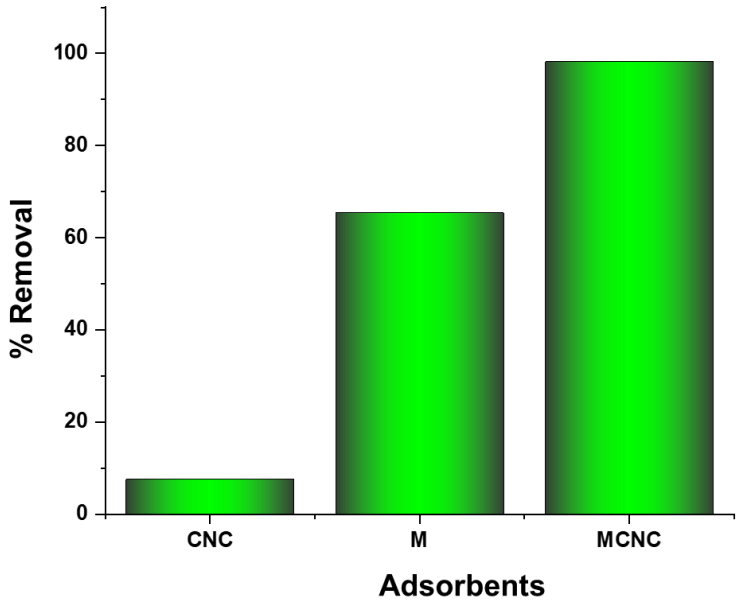

Figure 3.13: Validating three adsorbents against Pb (II)

According to the results, the CNC was the least effective adsorbent with the highest % removal of 7.5 %. This could have been due to the hydroxyl groups that are not efficient for heavy metal removal in water [32-35]. Magnetite had a better removal than CNC (65%) but less than the MCNC (98%). This could have been due to the magnetic properties, they possess. The results confirms that the MCNC had a better efficiency than the rest of the adsorbents, which could be that the iron enhanced the MCNC giving the best removal efficiency. This could be caused by the better affinity and the efficient rate of adsorption, particularly required from the adsorbents for water treatment [4].

To further understand the interaction between the MCNC and the Pb (II), an investigation of the isotherms, kinetics and thermodynamics studies were conducted and analysed and the adsorption capacity of MCNC was further calculated.

3.5.2.4 Adsorption isotherms

Two adsorption isotherms models (Langmuir and Freundlich isotherms) were evaluated to investigate the relation interaction of MCNC adsorbent and Pb (II). The results obtained from that investigation are captured in the supplementary information presented as **Table S2.**

Based on the adsorption isotherm governing the interaction between Pb (II) and the MCNC as an adsorbent. It has undergone the evaluation of two adsorption isotherms as presented in **Fig. 3.14 (a) and (b**). Which exhibits the investigated results of Langmuir and Freundlich adsorption isotherms and displays decided which interaction occurred between the chemisorption and the physisorption the reaction followed. The results demonstrated that the reaction can be physical also chemical. When comparing the two, it is observed that the reaction best fits the Freundlich isotherm with a R^2 value of 0,9889 since it is more than the adsorption Langmuir (0,98468) isotherm. The results confirm a Freundlich isotherm governed by the physical interaction corroborated with the BET results that confirmed the multilayer surface appropriate for the heterogeneous adsorption process. Anticipating on the physisorption isotherms as confirmed by the relative coefficient according to the results exhibited in **Fig. 3.14 (b).** This confirms the that the MCNC had multilayered active sites and a large pore volume which allowed an efficient interaction between the Pb (II) and MCNC.

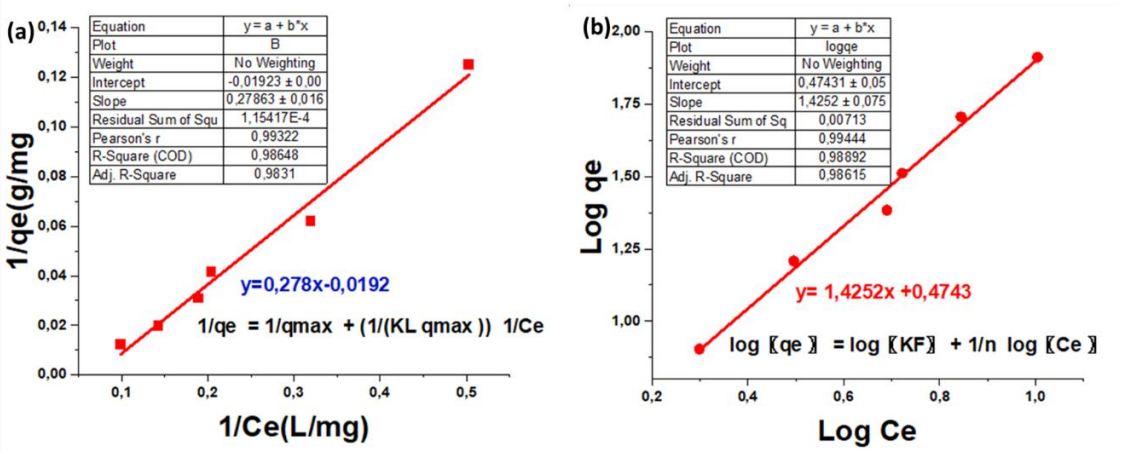

Figure 3.14: (a) Langmuir isotherm and (b) Freundlich isotherm

The physisorption mechanism between the adsorbate and magnetic cellulose nanocomposite in their aqueous solution is caused by weak van der Waals forces as it occurs on the adsorbent's crystal surfaces as described in **Figure 3.15**.

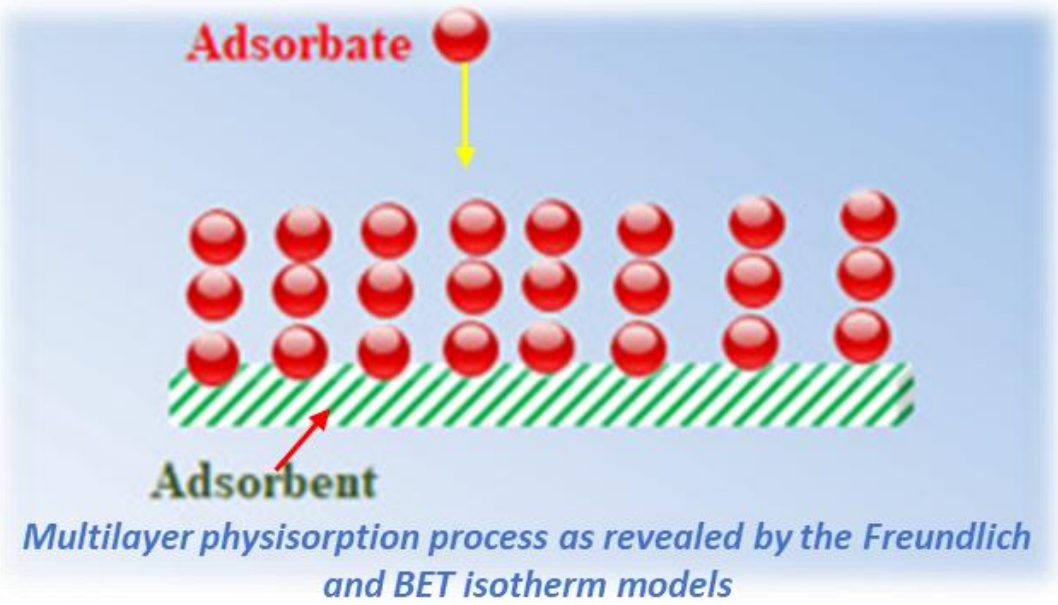

Figure 3.15: Physisorption mechanism between the Pb (II) and MCNC

The results further confirmed that the chemisorption reaction was not favoured and can be corroborated by the insignificant factor of pH where the electrostatic attraction was supposed to be active. This could suggest that an interaction caused by a covalent bond on these studies which was governed by the chemisorption during the Langmuir adsorption

isotherms did not occur in this study. Therefore, these results do not corroborate with those studies [36]. To understand how the interaction between Pb (II) and MCNC occurred, an investigation on kinetics studies was further conducted.

3.5.2.4.1 Adsorption kinetics reaction models

The following results were obtained from the adsorption kinetic studies conducted between 5-30 minutes, while other optimal parameters were kept constant. To obtain the linear regression coefficient, equation **2.4** and **2.5** were used which assumes the PFO or the PSO models. These models are exhibited in **Fig. 3.16.**

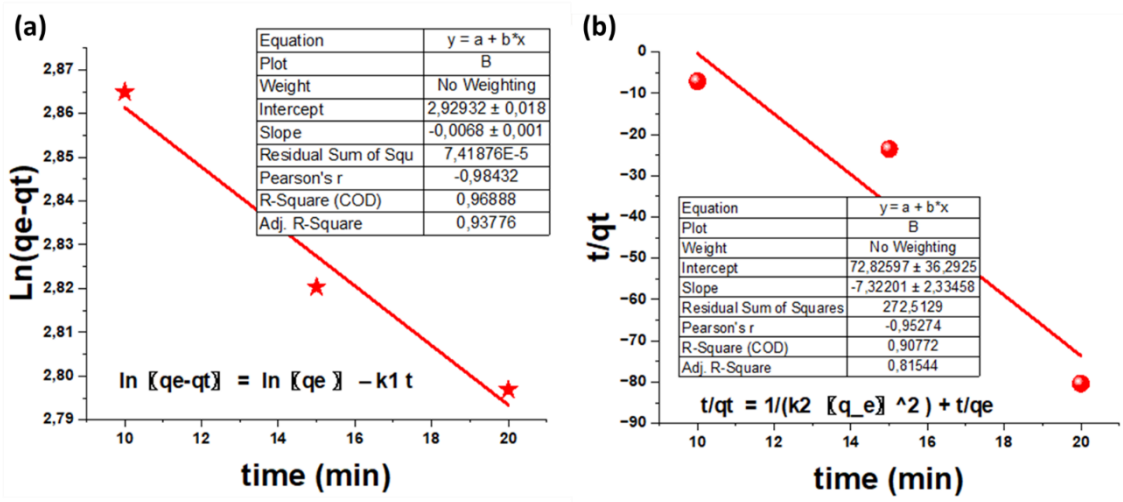

Figure 3.16: (a) PFO model and (b) PSO model

According to the results presented in **Fig. 3.16**, the correlation coefficient indicated that the reaction best fitted for PFO with the value of 0,97 and did not follow the PSO which says 0,91. The PFO confirms the two active sites of the MCNC which has the ability to bind one adsorbate molecule. This indicates that one active site of the adsorbent binds to one adsorbate molecule. Furthermore, the kinetics interaction did not fit the PSO kinetics which could have been due to the over saturation of the adsorbent affected by two reactants [36]. This could have been due to the addition of magnetite on to the surface material that also had a positive effect and attracted more Pb (II) as a cationic metal ion [36]. These results do not agree with

literature presented in **Table 2.3** from the previous chapter where the kinetics reaction followed the PSO kinetic model.

Table 3.5: The adsorption isotherms, kinetics and thermodynamics studies

a) Isotherms Parameters		
Type of Isotherm	Parameter	Results
Langmuir	Q_{max} (mg/g)	47,70
	K_L (L/mg)	0,07
	R_L	0,21
	R^2	0,98
	Intercept	0,02096
	Slope	0,28271
Freundlich	K_F	2,83
	1/n	-1,48
	R^2	0,96
	Intercept	0,45253
	Slope	-1,48466
Type of Kinetic models		
PFO	$q_{e\ exp}$ (mg/g)	8,293649
	K_1 (min)	0,070516
PSO	R^2	0,04133
	Intercept	19,66
	Slope	4,62
	qe (mg/g)	0,21
	qe^2	0,04
	K_2 (g/(mg.min)	1,08
	R^2	0,58
	Intercept	0,0015
c)Thermodynamic	Slope	0,0010
	ΔH (KJ/mol)	0,0084
	ΔS (J/K.mol)	0,00018
	ΔG (J)	-0,0622

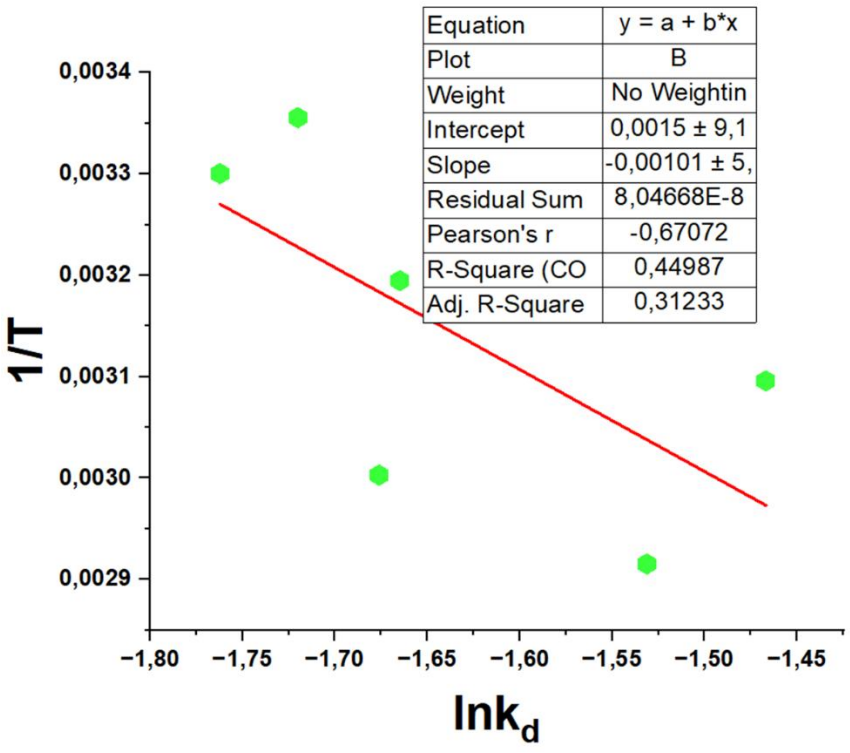

Figure 3.17: Thermodynamic studies of MCNC against Pb (II)

The thermodynamic studies were conducted from 25-40 ºC and the results obtained were used to plot a thermodynamic graph as displayed in **Fig. 3.17.** According to the results (ΔG= -0,06 J, ΔH= -0,08 KJ/mol and ΔS= 0,0018 J/K.mol), the reaction was exothermic and spontaneous with an increased entropy reaction. To investigate the stability of the MCNC adsorbent, the re-usability studies were investigated.

3.5.2.4.2 The reusability of MCNC nano-adsorbent

The same optimal conditions were used to conduct the re-usability and the results of the reusability and the FTIR are exhibited in **Fig. 3.18 (a)** and **(b)**. According to the results, the removal of Pb (II) using MCNC was 97% with the first cycle and was stable and re-usable until the 4th cycle with the removal of 94 %. A minimal reduction in the degradation efficiency was noted till the 4th cycle as the nano adsorbent still had a removal of 94%. This suggests that the material was highly efficient and cost effective. Moreover, the material was still intact and did not degrade as shown in the FTIR analysis.

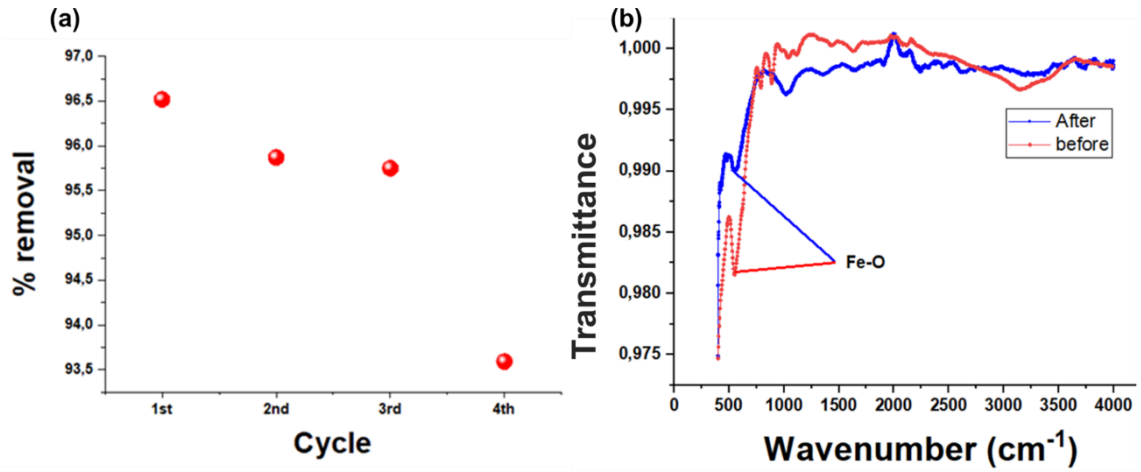

Figure 3.18 (a) re-usability studies and (b) the FTIR analysis

3.5.3 Conclusion

The MCNC was synthesized from the combination of magnetite and cellulose that was previously derived from the agricultural waste. FTIR, XRD, SEM, EDS, UV-Vis, TGA and BET techniques confirmed the physical, morphological, optical, and surface properties of the MCNC, M and CNC. The MCNC nanocomposite proved to be stable and crystalline, owing to

XRD, TGA and DTG. The MCNC nanocomposite surface area, pore volume and diameter were improved by the functionalizing it with M nanoparticles. The MCNC was able to remove over 97 % Pb (II) from the aqueous water with the maximum adsorption capacity of 47 mg/g at optimal conditions of 60 mg, 5 min, 10 ppm, pH=6 and 60 ºC. The MCNC material could be reused for up to 4 cycles. From the linear isotherm and kinetic plots generated in this work, a correlation value of R^2 = 0.9889 was noted and it can be concluded that the adsorption process is physisorption and a heterogenous multilayer interaction as the Freundlich model. The thermodynamic studies showed an increase in entropy with a spontaneous endothermic reaction.

References

1. Sivaranjanee, R., Kumar, P.S.: Treatment of textile wastewater using biochar produced from agricultural waste. Elsevier Ltd. (2021)

2. Qiao, A., Cui, M., Huang, R., Ding, G., Qi, W., He, Z., Klemeš, J.J., Su, R.: Advances in nanocellulose-based materials as adsorbents of heavy metals and dyes. Carbohydr. Polym. 272, (2021).

3. Obasi, P.N., Akudinobi, B.B.: Potential health risk and levels of heavy metals in water resources of lead–zinc mining communities of Abakaliki, southeast Nigeria. Appl. Water Sci. 10, 1–23 (2020).

4. Iqbal, Z., Tanweer, M.S., Alam, M.: Reduced Graphene Oxide-Modified Spinel Cobalt Ferrite Nanocomposite: Synthesis, Characterization, and Its Superior Adsorption Performance for Dyes and Heavy Metals. ACS Omega. 8, 6376–6390 (2023).

5. Elumalai, V., Brindha, K., Lakshmanan, E.: Human exposure risk assessment due to heavy metals in groundwater by pollution index and multivariate statistical methods: A case study from South Africa. Water (Switzerland). 9, (2017).

6. Abujaber, F., Zougagh, M., Jodeh, S., Ríos, Á., Guzmán Bernardo, F.J., Rodríguez Martín-Doimeadios, R.C.: Magnetic cellulose nanoparticles coated with ionic liquid as a new material for the simple and fast monitoring of emerging pollutants in waters by magnetic solid phase extraction. Microchem. J. 137, 490–495 (2018).

7. Hosseinzadeh, H., Ramin, S.: Effective removal of copper from aqueous solutions by modified magnetic chitosan/graphene oxide nanocomposites. Int. J. Biol. Macromol. 113, 859–868 (2018).

8. Vincent, S., Kandasubramanian, B.: Cellulose nanocrystals from agricultural resources: Extraction and functionalisation. Eur. Polym. J. 160, 110789 (2021).

9. Ahmed-Haras, M.R., Kao, N., Ward, L.: Single-step heterogeneous catalysis

production of highly monodisperse spherical nanocrystalline cellulose. Int. J. Biol. Macromol. 154, 246–255 (2020).

10. Shojaeiarani, J., Bajwa, D.S., Chanda, S.: Cellulose nanocrystal based composites: A review. Compos. Part C Open Access. 5, 100164 (2021).

11. Liu, Z., He, M., Ma, G., Yang, G., Chen, J.: Preparation and characterization of cellulose nanocrystals from wheat straw and corn stalk. Palpu Chongi Gisul/Journal Korea Tech. Assoc. Pulp Pap. Ind. 51, 40–48 (2019).

12. Singh, R., Singh, J., Sonika, Singh, H.: Green synthesis of carboxymethyl cellulose from agricultural waste its characterization. J. Phys. Conf. Ser. 2267, (2022).

13. Soliman, A.I.A., Díaz Baca, J.A., Fatehi, P.: One-pot synthesis of magnetic cellulose nanocrystal and its post-functionalization for doxycycline adsorption. Carbohydr. Polym. 308, 120619 (2023).

14. Ba-abbad, M.M., Benamour, A., Ewis, D., Mohammad, A.W.: Synthesis of Fe 3 O 4 Nanoparticles with Different Shapes Through a Co-Precipitation Method and Their Application. JOM. 74, 3531–3539 (2022).

15. Zhu, X., Tong, J., Lan, H., Pan, D.: Fabrication of Polyethyleneimine-Functionalized Magnetic Cellulose Nanocrystals for the Adsorption of Diclofenac Sodium from Aqueous Solutions. Polymers (Basel). 14, (2022).

16. Silvério, H.A., Flauzino Neto, W.P., Dantas, N.O., Pasquini, D.: Extraction and characterization of cellulose nanocrystals from corncob for application as reinforcing agent in nanocomposites. Ind. Crops Prod. 44, 427–436 (2013).

17. Singh, S., Bhardwaj, S., Meda, R.S., Verma, C., Chhajed, M., Ghosh, K., Maji, P.K.: Insights into thermal degradation kinetics and liquid crystalline behavior of cellulose nanocrystals from the waste of Cajanus cajan (pigeon pea). Int. J. Biol. Macromol. 242, (2023).

18. Huang, S., Zhou, L., Li, M.-C., Wu, Q., Zhou, D.: materials Cellulose Nanocrystals (CNCs) from Corn Stalk: Activation Energy Analysis.

19. Zhang, F., Pang, Z., Dong, C., Liu, Z.: Preparing cationic cotton linter cellulose with high substitution degree by ultrasonic treatment. Carbohydr. Polym. 132, 214–220 (2015).

20. Etemadifar, R., Kianvash, A., Arsalani, N., Abouzari-Lotf, E., Hajalilou, A.: Green synthesis of superparamagnetic magnetite nanoparticles: effect of natural surfactant and heat treatment on the magnetic properties. J. Mater. Sci. Mater. Electron. 29, 17144–17153 (2018).

21. Soliman, A.I.A., Díaz Baca, J.A., Fatehi, P.: One-pot synthesis of magnetic cellulose nanocrystal and its post-functionalization for doxycycline adsorption. Carbohydr. Polym. 308, 120619 (2023).

22. Lu, P., Hsieh, Y. Lo: Preparation and properties of cellulose nanocrystals: Rods, spheres, and network. Carbohydr. Polym. 82, 329–336 (2010).

23. Lu, S., Ma, T., Hu, X., Zhou, Y., Wang, T., Song, Y.: Synthesis and characterization of cellulose nanocrystal-Fe composite nanoparticles and their digestion behavior in simulated gastric fluid. Int. J. Biol. Macromol. 225, 198–206 (2023).

24. El Nemr, A., El-Assal, A.A.M., El Sikaily, A., Mahmoud, M.E., Amira, M.F., Ragab, S.: New magnetic cellulose nanobiocomposites for Cu(II), Cd(II) and Pb(II) ions removal: kinetics, thermodynamics and analytical evaluation. Nanotechnol. Environ. Eng. 6, 1–20 (2021).

25. Brinkmann, A., Chen, M., Couillard, M., Jakubek, Z.J., Leng, T., Johnston, L.J.: Correlating Cellulose Nanocrystal Particle Size and Surface Area. Langmuir. 32, 6105–6114 (2016).

26. Khalid, A., Ahmed, R.M., Taha, M., Soliman, T.S.: Fe_3O_4 nanoparticles and Fe_3O_4

@SiO_2 core-shell_ synthesize, structural, morphological, linear, and nonlinear optical properties. J. Alloys Compd. 947, 169639 (2023).

27. Liu, C., Jin, R.N., Ouyang, X. kun, Wang, Y.G.: Adsorption behavior of carboxylated cellulose nanocrystal—polyethyleneimine composite for removal of Cr(VI) ions. Appl. Surf. Sci. 408, 77–87 (2017).

28. Kulkarni, S.S., Sawarkar Mahavidyalaya, S., Shirsat, M.D.: Optical and Structural Properties of Zinc Oxide Nanoparticles. Int. J. Adv. Res. Phys. Sci. 2, 14–18 (2015)

29. Lu, L., Li, Y., Liang, Y., Chen, Q., Lu, Q.: One-pot green synthesis of carboxylated cellulose nanocrystals through oxidative degradation of bamboo pulp. BioResources. 15, 49–61 (2020).

30. Sun, J., Cui, L., Gao, Y., He, Y., Liu, H., Huang, Z.: Environmental application of magnetic cellulose derived from Pennisetum sinese Roxb for efficient tetracycline removal. Carbohydr. Polym. 251, (2021).

31. Karim, Z., Mathew, A.P., Grahn, M., Mouzon, J., Oksman, K.: Nanoporous membranes with cellulose nanocrystals as functional entity in chitosan: Removal of dyes from water. Carbohydr. Polym. 112, 668–676 (2014).

32. Abu-Danso, E., Srivastava, V., Sillanpää, M., Bhatnagar, A.: Pretreatment assisted synthesis and characterization of cellulose nanocrystals and cellulose nanofibers from absorbent cotton. Int. J. Biol. Macromol. 102, 248–257 (2017).

33. Nordin, A.H., Wong, S., Ngadi, N., Mohammad Zainol, M., Abd Latif, N.A.F., Nabgan, W.: Surface functionalization of cellulose with polyethyleneimine and magnetic nanoparticles for efficient removal of anionic dye in wastewater. J. Environ. Chem. Eng. 9, 104639 (2021).

34. Ariaeenejad, S., Motamedi, E., Hosseini Salekdeh, G.: Immobilization of enzyme cocktails on dopamine functionalized magnetic cellulose nanocrystals to enhance

sugar bioconversion: A biomass reusing loop. Carbohydr. Polym. 256, 117511 (2021).

35. Lu, J., Jin, R.N., Liu, C., Wang, Y.F., Ouyang, X. kun: Magnetic carboxylated cellulose nanocrystals as adsorbent for the removal of Pb(II) from aqueous solution. Int. J. Biol. Macromol. 93, 547–556 (2016).

36. Bai, C., Wang, L., Zhu, Z.: Adsorption of Cr(III) and Pb(II) by graphene oxide/alginate hydrogel membrane: Characterization, adsorption kinetics, isotherm and thermodynamics studies. Int. J. Biol. Macromol. 147, 898–910 (2020).

CHAPTER (IV): FABRICATION OF POLYETHYLENEIMINE-FUNCTIONALIZED MAGNETIC CELLULOSE NANOCRYSTALS FOR SELECTIVE ADSORPTION OF CHROMIUM FROM AQUEOUS SOLUTIONS

ABSTRACT

Heavy metal pollution, including hexavalent chromium ion, Cr (VI), possess health threats to the environment [1]. Therefore, this calls for researchers to fabricate low-cost adsorbents that can rapidly and effectively remove Cr (VI) from contaminated wastewater. The current study describes the synthesis and modification of the cellulose nanocrystal crosslinked with TEMPO and grafted with polyethyleneimine and magnetite (MCNC-TEMPO-PEI) derived from maize stalk. The crosslinking with polyethyleneimine (PEI) was conducted by using 2,2,6,6-tetramethylpiperidinyloxy (TEMPO) to enhance the selectivity of the MCNC-TEMPO-PEI towards Cr (VI) ions. The final nanocomposite (MCNC-TEMPO-PEI) was characterised using FTIR, P-XRD, TEM and SEM coupled with EDS. The FTIR analysis confirmed a successful formation and the presence of carboxylic acid, amine groups and the incorporation of the Fe-O bond on the final nano composite (MCNC-TEMPO-PEI). The P-XRD confirmed the crystal structure for CNC-TEMPO and the amorphous nature for both the CNC-TEMPO-PEI and the MCNC-TEMPO-PEIMCNC-TEMPO-PEI. The analysis from TEM confirmed a smooth and oval surface for TEMPO-CNC and an irregular morphology for the CNC-TEMPO-PEI. Furthermore, the MCNC-TEMPO-PEI exhibited four morphologies, the smooth surface, needle like, an irregular and oval morphological shape from the TEM analysis to confirm the formation and incorporation of TEMPO and PEI. The adsorption performance of MCNC-TEMPO-PEI on Cr (VI) was investigated by using univariate optimization tools. The optimal parameters of MCNC-TEMPO-PEI were dosage = 30 mg, concentration = 5 ppm, temperature = 25 ºC, contact time = 15 min and the pH = 2. The 5 adsorbent materials were evaluated against each other, and the results indicated that the MCNC-TEMPO-PEI showed the highest adsorption capacity of 4,4 mg/g with a 98 % removal. The interaction between the adsorbent and the adsorbate indicated that the reaction best fitted the Langmuir adsorption isotherm with the correlation coefficients of 0,93378 following the PSO kinetic model confirming the chemisorption of the

electrostatic interaction with Cr (VI) ions in addition to the magnetic and ionic exchange forces. The thermodynamic interaction indicated a non-spontaneous endothermic reaction with a favourable reaction. The adsorbent could be reused at least 8 times with a removal efficiency above 75 %. The results revealed that the real wastewater sample that was analysed from this study did not contain Cr (VI) ion.

4.1 Background

Chromium (Cr) is regarded as one of the most poisonous heavy metal ions (HMIs) and has unfortunately become notorious in the field of study [1-2]. It is a metalloid that can be found in natural and man-made contexts [3-4]. Natural sources of Cr include water, air, soil, and minerals created by anthropogenic activities such as metallurgy, electro-plastics, leather, battery manufacture, insecticides, and others [1-2]. Chromium exists in several oxidation states, ranging from (II) to (VI), with (III) and (VI) being stable in natural water [2]. It is known to be the seventh most plentiful element on Earth, although it is also known to be more poisonous than Cr III [3-4]. Thus, researchers have attempted to remediate Cr (VI) ions due to their toxicity as they were undetectable at quantities of less than 1 ppb in a sample [5]. Cr (VI) may now be identified at lower quantities thanks to a complexing compound known as 1,5-diphenylcarbazide (DPC), making quantification easier when attempting to eliminate it [4,6].

In addition to its toxicity, it has been shown to be carcinogenic, extremely oxidative in nature, bio-accumulative, and very reactive [8-9]. Thus, the Environmental Protection Agency (EPA) and the International Agency for Research on Cancer (IARC) have named Cr (VI) ions as the number one carcinogen [5]. Its maximum containment level (MCL) in water must not exceed 50 ppb, hence quantities of no more than 20 ppb are permitted in drinking water. It has grown to be more dangerous to humans when taken at concentrations higher than those permitted in drinking water. Meanwhile, it invades human organs and easily infiltrates the human cell wall, releasing its toxicity within the human cell [5-9]. As a result, increasing health concerns including cardiovascular effects, kidney, bladder failure and immunological disorders [5-7]. It is therefore very crucial to obtain access to clean water without fear of toxins in drinking water.

Researchers have studied a variety of remediation strategies to treat wastewater and remove Cr (VI) from water in recent years, including ion exchange, flocculation, electrochemical, reverse osmosis, and chemical precipitation [10]. However, several

disadvantages have been found, including the use of harmful chemicals, the need for multiple treatments, more maintenance, and more energy-intensive procedures [10,11]. Consequently, the adsorption process has several advantages over conventional approaches, including its simplicity, high adsorption effectiveness, suitability for industrial applications, low energy consumption, and many others [11-12]. The adsorption is a removal process in which the adsorbate interacts with the surface of an adsorbent material via the attraction forces that regulate physisorption or chemisorption.

These governing factors for physisorption include weak Van Der Waals interactions, hydrogen bonding, and ion exchange, with the latter occasionally involving electrostatic attraction between the adsorbent and the adsorbate [13–14]. This works flawlessly in a setup with porous or mesoporous adsorbents. In contrast, chemical adsorption (chemisorption) is a process driven by factors such as chelation, covalent, ion exchange, and coordination bonds [13-14]. Chemical interaction bonding, which is activated by functional groups on the adsorbent surface, holds the adsorbate molecules to its surface [15]. The technique is well-known for its cost-effectiveness, increased adsorption capacity, and economic value [13-15]. Thus, researchers prefer adsorbents that must have a larger capacity for effective removal of Cr (VI). The commercial adsorbents are effective but tend to also show limitations of low adsorptivity, selectivity and expensive.

Biosorbents derived from agricultural waste are the hotspot and have sparked interest in recent years due to potential widespread availability, biocompatibility, effectivity and cost efficiency [16]. A number of investigations have used agricultural waste adsorbents to eliminate HMIs. Furthermore, agricultural-based adsorbents are selected by several researchers because they have a high concentration of carbon and cellulose, which are commonly employed for stability and dispersion [16]. These agricultural-based adsorbents are derived from corn, rice husk, newspaper, seed shells, and other sources [16–17]. Zhao *et al* [18] produced activated carbon from maize stalk to remove Cr (VI) and achieved an adsorption capacity of 90 mg/g [18].

Cellulose nanocrystal (CNC) is a biopolymer with several OH functional groups, yet these OH groups reduce the selectivity of the targeted analytes [19]. This is feasible when the reaction occurs when carried out in the presence of NaBr and NaClO as the principal oxidant and catalyst for the production of sodium carboxylates [22]. The use of TEMPO has additional benefits, such as selectively converting the major OH groups, particularly at the C6 position of the CNC surface, to COOH groups without altering the original CNC crystal [22-24]. This drives it to create functionalized CNC with reduced particle sizes and diameters [22–24]. As a result, the number of carboxylic groups increases, as does the specific surface area, crystallinity, and specific strength [24]. Furthermore, it introduces strong amino groups that are useful for increased adsorption capacity due to the addition of another polymer like polyethyleneimine.

Polyethyleneimine (PEI) is a branched or linear type polymer with abundantly available amino groups in primary, secondary, and tertiary amines, permitting the availability of positive protonation and anionic adsorbents which could target both cationic and anionic analytes, using electrostatic interaction during adsorption [19,24]. In the presence of glutaraldehyde (GLA), it permits the PEI functionalization with carboxylic groups as a bridge by a Shiff base structure reaction to form a carbon and a nitrogen bond through dehydration condensation [24-25]. This ensures there is a strong photophilic property, which allows for mechanical strength and a formation of strong hydrogen bonds with the proton donors [24-25]. In this case, permitting the carboxylic group to easily attach to the amine groups targeting Cr (VI) [24-26]. Furthermore, enhancing the selectivity and the adsorption capacity of our nanocomposite [26]. In addition to the simplicity of easy separation, the magnetic properties with the help of an external magnetic to enhance the adsorption capacity. The authors' according to their knowledge are reporting for the first time the synthesis of the magnetic cellulose nanocrystal crosslinked with TEMPO and grafted with polyethyleneimine (MCNC-TEMPO-PEI) derived from maize stalk for the adsorptive removal of Cr (VI) from wastewater.

4.2 Experimental procedure

4.2.1 Materials and reagents

All the reagents, 2,2,6,6-tetramethylpyperidine (TEMPO), sodium hypochlorite (NaClO), sodium bromide (NaBr), sodium hydroxide (NaOH), 37 % diluted hydrochloric acid (HCl), branched polyethyleneimine (PEI), dilute solution of 25 % glutaraldehyde (GLA), ferric chloride hexahydrate ($FeCl_3.6H_2O$), iron II sulphate $Fe(SO_4)_2.7H_2O$, 25 % dilute solution of ammonium hydroxide solution (NH_4OH), 1.7 % diluted hydrogen peroxide (H_2O_2), glacial acetic acid (CH_3COOH), 65 % diluted nitric acid (HNO_3), 1,5 Diphenyl carbazide (DPC) reagent and 99 % ethanol were bought from Merck suppliers, South Africa. Certified single elemental standard reference material for Chromium Cr (VI) at 1 000 ppm with 2 % nitric acid was purchased from De Bruyn Spectroscopic Solutions cc, (South Africa). Refrigerated centrifuge (Dupont Co., Wilmington, DE, Model RC-5) South Africa, Nitrogen gas (N_2) cylinder was collected from Afrox, Limpopo, South Africa. Milli-Q® IQ Water Purification System for producing 2.8 µm ultra-pure deionised water was purchased from Merck-Millipore, Germany. Sep Sci Lab Tech Shaker was purchased from Daihan Labtech, (South Korea). The membrane filter with pore size of 0,45 µm and 47 mm diameter was purchased from Merck (South Africa). Micropipette (10 ppb -1000 ppb), the 6-digit analytical balance and bench top pH meter were all purchased from Separations (South Africa). The 0,45 µm micro filters, centrifuge tubes (50 mL and 15 mL), 5mL and 10 mL plastic syringe, 0,45 µm membrane filters, filter papers 150 cm diameter, sterilised 1 mL plastic pipette tips were purchased from Cc Immelmann, South Africa. The maize stalk was harvested in Limpopo, (South Africa).

4.3 Methods

4.3.1 Synthesis of the adsorbent (MCNC-TEMPO-PEI)

4.3.1.1 Modification of CNC surface using TEMPO via crosslinking process

The synthesis of TEMPO-CNCs was performed according to the method by Zhao *et al* [26] with some minor modifications. The as-prepared CNC material was obtained by the synthetic method reported in **Section 3.2.2.2.** The synthesized CNC was further weighed to

make a solution of 8 wt. % in a 1L Glass bottle while sonicating with 200 ml deionised water and allowed to disperse. The colloidal mixture was soaked with 20 mg of TEMPO and 200 mg of NaBr for 2 hrs at room temperature. A solution of 15 wt. % NaClO was prepared separately and from that solution, 80 mL of the NaClO solution was added into the colloidal mixture. Another solution of 0,1 M NaOH was also prepared where 0,4 g of NaOH pellets were added into 100 mL of deionised water. To adjust the pH measurement of the colloidal suspension to pH = 10,5 the NaOH solution was added dropwise while monitoring the pH meter. After the adjusted pH, the mixture was placed on the magnetic stirrer plate for 8 hrs, for slow and intense oxidation of the CNC with additional carboxylic groups (COOH). An additional 8 mL of ethanol was added to terminate the oxidation process after 8 hrs. Then later, the mixture was adjusted to neutral by adding the 0,1 M HCl resulting in a pale yellowish product. The product was allowed to freeze at -25 ºC for 24 hrs. Then, the frozen product was later subjected to freeze drying for 7 days to remove the remaining moisture and leave a powdered product [26].

4.3.1.2 Crosslinking CNC-TEMPO with PEI

Grafting of PEI on TEMPO CNC was conducted through the use of a glutaraldehyde (GLA) crosslinker following the methods by Xing *et al* [25] and Zhang *et al* [27] with minor modifications [25,27]. In a 1 L glass bottle, 100 mL of deionised water was poured, an amount of 1 g of CNC-TEMPO was transferred into the same glass bottle to make a 1 % solution. The CNC-TEMPO was allowed to disperse in water by placing the bottle in an ultra-sonicate at room temperature for an hour at maximum speed. Then, the magnetic stove was adjusted to 60 ^{o}C and the colloidal mixture was removed after the ultrasonication onto the hot plate. An amount of 5,2 g of PEI branched gel was weighed and transferred onto the mixture and the reaction was then heated at 60 ^{o}C for an hour. Thereafter, 4 mL of 25% dilute glutaraldehyde was poured dropwise into the mixture while stirring, the mixture precipitated with bigger white pellets with some yellowish and light pink colour. The reaction continued at 60 ^{o}C for another 2 hrs. The pH measurements were taken and adjusted to pH = 8 using 0,1 HCl or 0,4 M NaOH solutions. Then, the product was washed and purified by ethanol and de-ionised water while

filtration took place. Then, it was freeze-dried for 7 days and collected for further characterization [25,27].

4.3.2 The incorporation of magnetite on MCNC-TEMPO-PEI

The synthesis of the MCNC-TEMPO-PEI was conducted by functionalising CNC-TEMPO-PEI with the magnetite using a co-precipitation method following a method reported by Nording *et al* [20] with a few modifications. A ratio of 3:1,3, 75 g of the prepared CNC-TEMPO-PEI with 1,25 g of the as-prepared Fe_3O_4 was transferred into a 250 mL glass beaker and 200 mL deionised water was added to the mixture. The glass beaker was then placed in a hot water bath at 65 ºC for an hr. An amount of 5 mL of the dilute 25 % GLA was added dropwise into the mixture while heating under vigorous stirring for another 1 hr. To allow a smooth crosslinking process of TEMPO and PEI and for purification, a solution of 90 mL of methanol and 10 mL of glacial acetic acid was also added to the mixture. For the impregnation process of PEI onto the MCNC nanoparticles to occur, the mixture was left heated at 65 ºC for 24 hrs. To remove solvents from the mixture, the mixture was subjected to a distillation process at 140 ºC connected to an ice and chiller to maintain the conditions. The dried product was then collected and used for further characterization [20].

4.3.3 Characterization

The materials were characterised following the method described in **Section 3.2.3.** The formation of the materials and the functional groups obtained from the nanocomposites were analysed using FTIR (TL-8000 FTIR equipment). An amount of 100 mg of the analyte was poured on to the equipment for analysis. The transmittance was run from 400 to 4000 cm^{-1} with a resolution of 10 nm. The crystallinity, particle size distribution and the phase identification of these nanomaterials were investigated using the P-XRD. The (P-XRD) analysis was performed on a 2 theta range from 10-90º. The powder sample of 100 mg was placed into a sample holder using a spatula to make the surface even and introduced into the P-X-ray diffractometer. The phase identification was performed by searching and matching the obtained diffraction patterns with the powder diffraction file database with the help of EVA

software. The SEM coupled with EDS was used to identify the morphology and composition of these materials. For SEM, a 500 VP microscope coupled with EDS was used for morphological and elemental composition analysis. The sample was then coated with carbon and grounded. This process helps to eliminate sample charging and electrons accumulating. The stub was then placed on the equipment with an acceleration voltage-operated on 10 Kv. The detector used was the secondary electron detector with a working distance of about 6.9 nm and the aperture set at 30 µm. Images were taken at various magnifications between (1µm – 200 nm). TEM was used to confirm the morphology, particle size, selective area diffraction pattern (SAED) and the lattice plane of the materials, using a JEM 2100 (FEI XL40 ESEM) equipped with two detectors, the EDAX Sapphire Si (Li) and EDS detectors. These were operated at a voltage of 200 Kv, current at 48 µA at an angle of 15 ° and with a resolution of 0.24 nm. An amount of about 100 mg of the sample was placed on the sample 200 mesh size Cu-grid and the analysis of the materials were measured. For the adsorption analysis, the MCNC-TEMPO-PEI were further detected by the Spectrum-SP-UV- 500VDB and operated at 547 nm in the presence of a DPC reagent. An aliquot of 3 mL of the sample was transferred into glass cuvettes and the calibration curve was obtained with the linear regression equation. The obtained data were used to calculate the adsorption capacity and the removal percentage.

4.3.4 Application methods

The sampling methods were carried out according to the methods described in **Section 3.2.4.** The samples were prepared, and the MCNC-TEMPO-PEI was added during the adsorption process.

4.3.4.1 Batch adsorption process.

The experiments were conducted using the univariate method where 5 parameters were evaluated and optimised against the removal of Cr (VI) ion. These parameters include the concentration (1-50) ppm, dosage (5-50) mg, pH (2-7), time (5-180) min and temperature (20-40) ºC following different reports [28-29]. These experiments were conducted in triplicates and were analysed using the UV-Vis spectrophotometer in the presence of the 1,5-diphenyl

carbazide (DPC) reagent. The adsorption capacity (qe) of the adsorbent and the percentage removal of Cr (VI) was calculated using **equation 3.1** and **3.2**. The results were used to select the best efficiency within these parameters whilst optimising the MCNC-TEMPO-PEI against the Cr (VI) ions.

4.3.4.2 The adsorption isotherms, kinetics and thermodynamic studies

Isotherm, kinetics and thermodynamic studies were conducted following the validated optimal conditions, where the other parameters were kept constant while investigating the concentration pattern of (1, 3, 5, 7 and 9) for adsorption isotherms studies. **Equations 2.2 and 2.4** were used to plot the adsorption isotherms plot for both the Langmuir and Freundlich isotherms. The monolayer adsorption capacity (q_{max}), the adsorption equilibrium constant (K_L), Freundlich constants (KF and 1/n), the slope, intercept and the correlation coefficient were extrapolated from the same plot. The Pseudo first order (PFO) and pseudo second order kinetic (PSO) were also evaluated between 5 – 30 min using **equations 2.6** and **2.8**. The thermodynamics interaction reactions were also investigated between 20-40 ºC. The same validated conditions were further used to evaluate the other adsorbents efficiency.

4.3.4.3 The validation process after optimization

The adsorbents were used to validate the optimised parameters for the concentration of 5 ppm with the dosage of 30 mg at pH of 2 with a temperature of 25 ºC within 15 min by conducting the same experimental conditions on the Magnetite, MCNC, CNC-TEMPO, CNC-TEMPO-PEI and the MCNC-TEMPO-PEI.

4.3.4.4 The reusability studies and real water analysis.

The same validated conditions obtained during optimizations were further used to investigate the stability and reusability of the MCNC-TEMPO-PEI for a multiple cycle. During the procedure, after the adsorption was conducted following the same procedure reported in **Section 4.3.4.1**, the adsorbate was removed using an external magnet, then filtered using the 0,45 µm filters and the DPC solution was added while waiting for a few minutes. The adsorbate

was analysed using the UV-Vis spectrophotometer at 547 nm. After the first cycle, the release and reuse of the MCNC-TEMPO-PEI materials was achieved by introducing HNO_3 (2.0%) for an hr while shaking at 300 rpm speed to recover the adsorbent after each cycle. Then the material was filtered and washed several times using the same HNO_3 solution, heated for 2 hr to remove moisture. Similar parameters at optimal conditions were used to carry out analysis using the MCNC-TEMPO-PEI for the removal of Cr (VI) ions. The Cr (VI) ions are not easily detectable within the UV-Vis spectrophotometer; however, it can only be detectable at a wavelength of 547 nm once complexed.

4.3.4.5 The complexation of Cr (VI) ions using the DPC

The Cr (VI) ions have undergone a complexation process where DPC reagent was used to complex Cr (VI) ions to form a Cr-DPCA complex. This is also presented in **Fig. 4.1**, exhibiting the bonding mechanism of Cr (VI) ions and the bidentate DPC ligand.

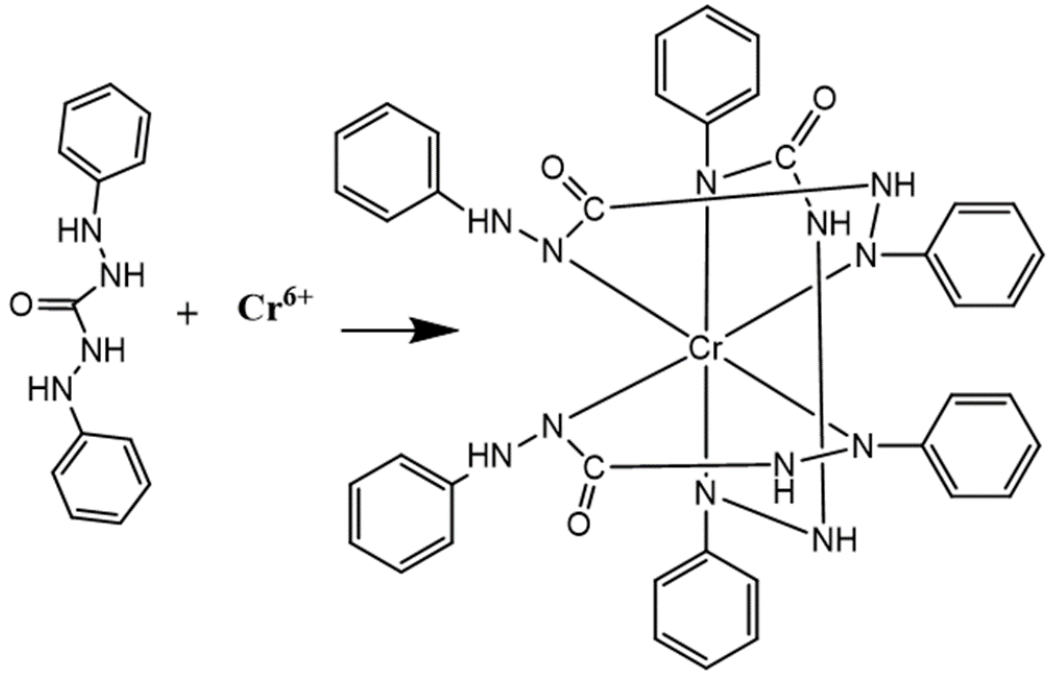

Figure 4.1: The bidentate DPC ligand bonding mechanism with Cr (VI) ions

Three bidentate ligands from the DPC reacted with the hexavalent ions under complexation process to fill the octet rule and form a Cr-DPCA complex. This has the ability

change the Cr (VI) ions from its original orange colour to a purple colour when the reaction reaches equilibrium. This is done by targeting and removing only the Cr (VI) ions from the adsorbate at 547 nm using UV-Vis spectrophotometer as also presented in **Fig. 4.2** [28-29].

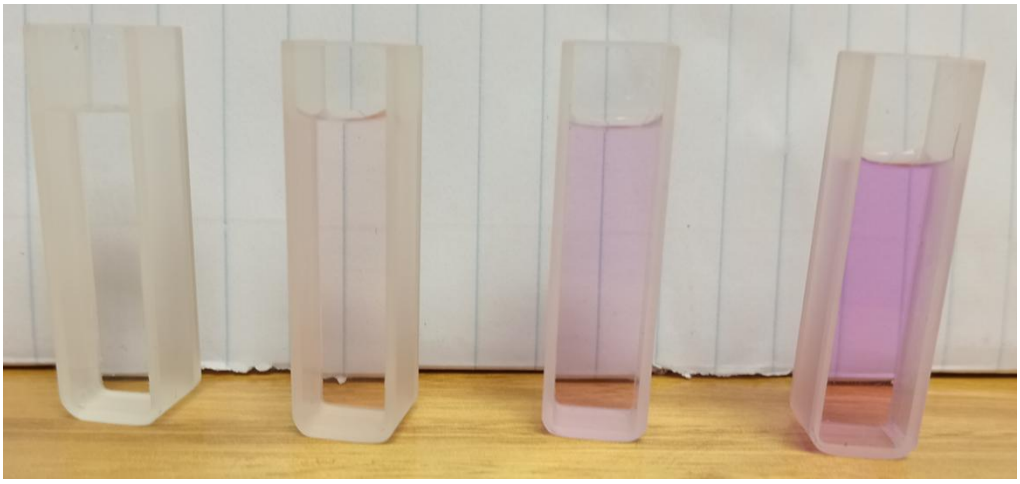

Figure 4.2: The complexed Cr (VI)ions detected by the DPC reagent

This reagent after complexation, only targets the Cr (VI) until they are completely transformed after reaching equilibrium. The principles are similar to that of an indicator, where more or less Cr (VI) ions detected are represented by a faint colour change. It was discovered that the more the Cr (VI) ions are present in the solution, the darker and persisting pink colour was observed when the interaction has reached equilibrium.

4.4 Results and discussion

4.4.1FTIR ANALYSIS

The three materials, the CNC-TEMPO, CNC-TEMPO-PEI and the MCNC-TEMPO-PEI were examined for the formation and the functional groups that are found within these materials. The results are shown in **Fig. 4.3.** From the FTIR analysis (**Fig. 4.3**), of the crosslinked CNC with TEMPO spectra, small bands at 416 cm^{-1} and 699 cm^{-1} representing an aromatic compound and a mono aromatic material, respectively were identified. Peaks at 2011 cm^{-1} and a vibrational band at 2187 cm^{-1} representing the COO- for both the asymmetric and the symmetric of the carboxylic group [23] and the CH band were also noted. A broad band at 2900 cm^{-1} was also observed, which could be ascribed to the C=O, CH and the OH band,

confirming the successful crosslinking of the TEMPO to form the carboxylic group on the surface of CNC material. Lastly, a band at 3400 cm^{-1} was observed, representing the OH and the C=O bonds. These results are also corroborated with various reports where the carboxylic group indicates the presence of TEMPO particularly at these two peaks (2900 and 3400 cm^{-1}) [23,26].

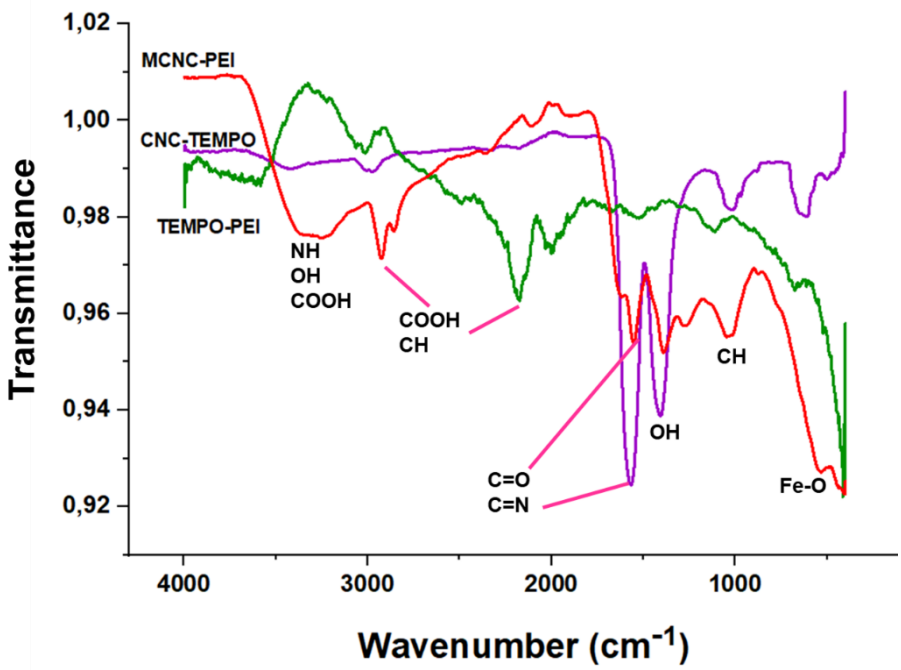

Figure 4.3: FTIR spectra of CNC-TEMPO, CNC-TEMPO-PEI and MCNC PEI

To confirm the formation of the CNC-TEMPO-PEI and the surface modification of depositing PEI to the surface material of CNC-TEMPO, two major stretching bands at 1418 and 1573 cm^{-1} were identified. These were ascribed to the carbonyl stretching vibrations, the asymmetric vibrations of C≡N, and the stretching band of OH confirming the deposition of PEI by exhibiting the NH_2 groups [30-31]. Furthermore, a small broad peak observed at 2900 cm^{-1} representing the OH and the NH bonds confirmed the presence of amine groups. The added peaks displayed at 480 and 614 cm^{-1} confirmed the aromatic ring.

Lastly, from the MCNC-TEMPO-PEI spectra, two stretching bands similar from the TEMPO-PEI were also exhibited on the MCNC-TEMPO-PEI indicating the presence of C≡N, OH, C=C [30-31]. In addition to these two peaks, another broadband also verifying the

presence of amine groups from 3400 cm^{-1} was noted. The results confirmed the presence of the amine group coming from the grafting of the PEI. The first two vibrational peaks, representing the aromatic ring and the Fe-O bond were identified at 424 and 558 cm^{-1}, respectively. This confirmed the presence of iron within the material in the fingerprint region and that the material is aromatic. Moreover, all the other peaks observed on the CNC-TEMPO were also visible on the MCNC-TEMPO-PEI for CH, OH and COOH vibrational bands at 1072, 1277, 2137 and 2963 cm^{-1}, respectively. These results confirmed the successful synthesis of the magnetic cellulose nanocrystal modified by the polyethyleneimine polymer after the crosslinking process, for introducing the amine groups. This will assist with the selectivity for the adsorptive removal of Cr (VI). For crystallinity, these materials were further analyzed using P-XRD analysis.

4.4.2P-XRD ANALYSIS

The materials (CNC-TEMPO, CNC-TEMPO-PEI and the MCNC-TEMPO-PEI) were further investigated for formation, phase identification, crystallinity and crystallite size distribution using the P-XRD analysis. The results obtained from the examination are displayed in **Fig. 4.4.**

The CNC-TEMPO diffractogram shows 7 diffraction planes that appear on CNC material as exhibited from the previous chapter, namely the (-110), (110), (002), (220), (021), (004) and (040) observed at angle 2θ of 9,08º; 19,16º; 27,37º; 31,97º; 45,82º and 56,41º confirming the presence of CNC. Abou-zeid *et al* [22] and Huang *et al* [26] identified the presence of TEMPO and confirmed its formation by the three diffractograms represented by these diffraction planes, the (-110), (002) and the (200), particularly for (200) from which they observed at 22,5º [22-26]. Also in this study, TEMPO was also observed at 22.98 º at a diffraction plane of (200). Moreover, the crystallinity of the material was confirmed by the higher intensity, the width base, and the sharp peaks, also it has been maintained from the former CNC nanoparticles from our previous results. The particle size distribution was calculated using equation 3.4 as the debye Scherrer equation The crystallite size was

calculated to be 12,29 nm and the results are presented on the supplementary information under **Table. S.4**.

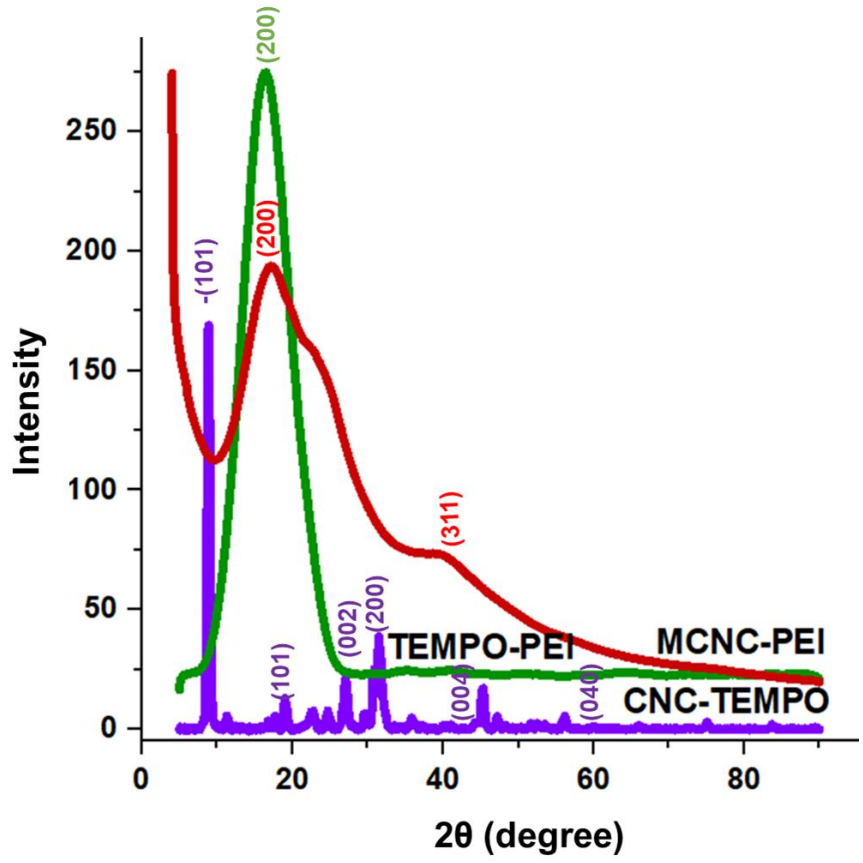

Figure 4.4: XRD analysis of CNC-TEMPO, CNC-TEMPO-PEI and MCNC PEI

The CNC-TEMPO-PEI diffractogram only exhibited a broad peak at 17,62º of (200) confirming the deposition of PEI on to the carboxylic group from the surface of the CNC. The broad peak suggests the amorphous nature of the material owing to the addition of two polymers (CNC and PEI) during the synthesis method. The crystallite size for this particular peak was calculated using the debye Scherrer equation and was found to be 1 nm according to the calculated results presented in **Table. S.4**. These results are similar to the study done by Buchman *et al* [24] where the particle size of PEI was recorded as 1,4 nm [24]. The magnetic nanocomposite also showed two peaks, the PEI and the Fe planes observed as (200) and (311) at 17,10º and 36,59º, respectively. These results were verified by literature

where PEI was observed at 17,62 º and Fe at 43,2º, respectively and the shifting could have been due to the incorporation of Fe [32]. These results also indicate that the material is amorphous, and the calculated average particles size distribution was 0,432 nm as displayed in **Table S.4**.

4.4.3 TEM Analysis

The morphology of the three materials were investigated using TEM analysis and the results are displayed in **Fig. 4.5**. In **Fig. 4.5 (a)**, the CNC material had a smooth sheet like morphology with needle/rods also observed. For the CNC-TEMPO-PEI (**Fig. 4.5 (c))**, two distinct morphologies, the oval morphology and the smooth big surface underneath the oval shape were identified. The spherical or oval shape could be attributed to the presence of PEI whereas the smooth surface could be due to the presence of CNC as a base material.

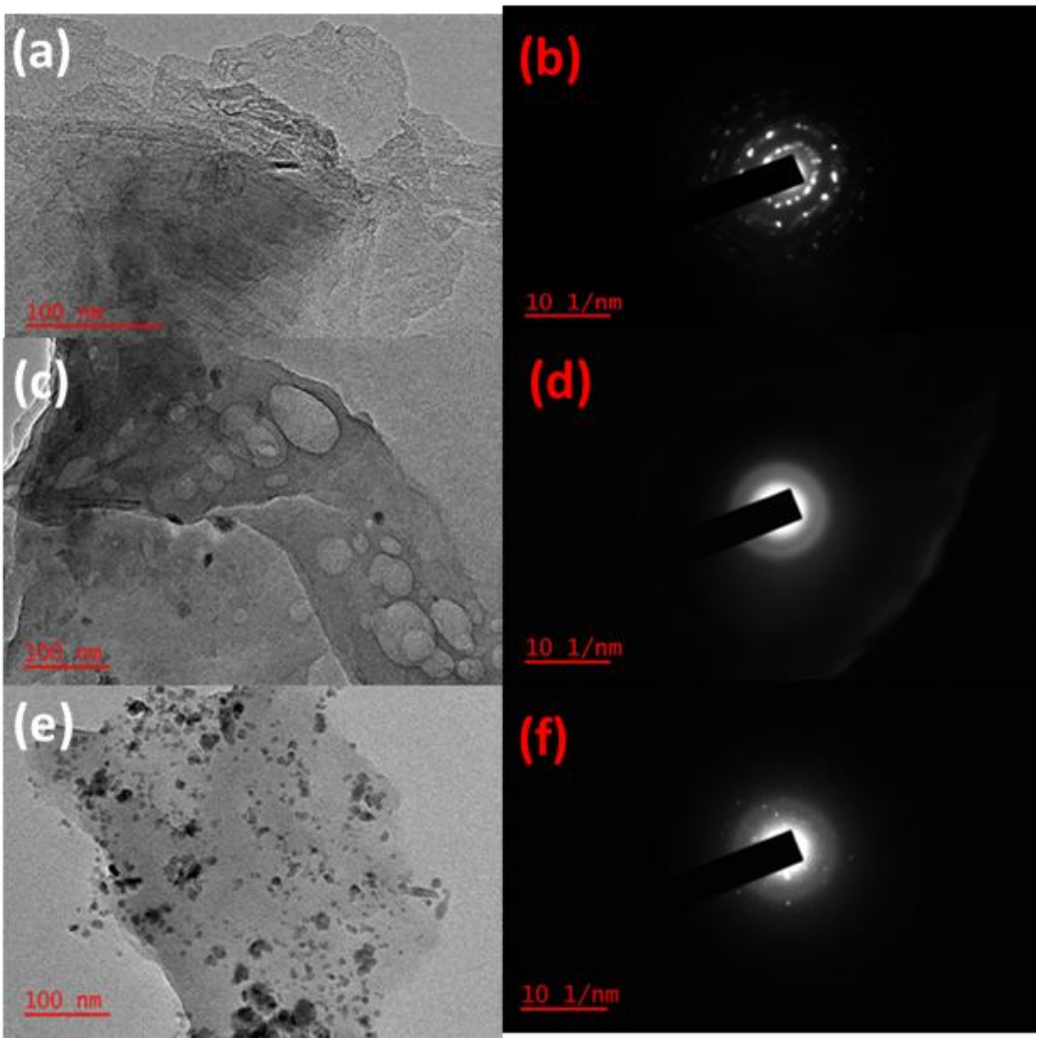

Figure 4.5: The morphology and SAED analysis of the CNC-TEMPO, CNCTEMPO-PEI and MCNC-TEMPO-PEI)

The MCNC-TEMPO-PEI had three morphologies, irregularly shaped, spherical and needle-like structures. The oval or spherical shape which could be credited to the presence of PEI and the needle like shape representing the presence of CNC was also observed [6-27]. These morphologies confirmed the formation of the MCNC-TEMPO-PEI [11]. The SAED of the CNC confirmed the crystallinity of the material as also elaborated in the P-XRD analysis from the previous section. The CNC-TEMPO-PEI and the MCNC-TEMPO-PEI showed a bright light around the planes which could be attributed to the amorphous nature of these materials as exhibited in **Fig. 4.4**.

4.4.4SEM ANALYSIS

The materials (CNC-TEMPO, CNC-TEMPO-PEI and MCNC-TEMPO-PEI) were further investigated for morphology and their results are exhibited in **Fig. 4.6**.

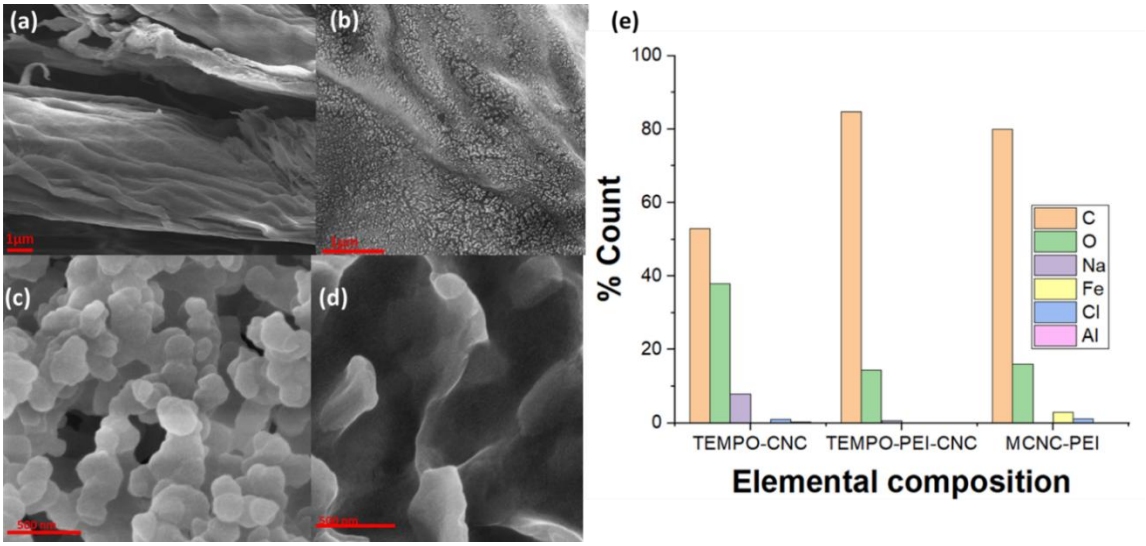

Figure 4.6: SEM ANALYSIS of (a) CNC, (b) TEMPO-CNC, (c) CNC-TEMPO-PEI, (d) MCNC-TEMPO-PEI and (e) EDS elemental composition of the materials

From the analysis of these results, it can be observed that the bare CNC (**Fig 4.6(a))**, showcased a smooth and needle like morphology. The CNC-TEMPO {**Fig 4.6(b}** indicated a morphology of tiny rods at µm level, which can only be visible once zoomed in. The CNC-TEMPO-PEI (**Fig 4.6 c**) confirmed an irregular structure which could be identified as a clustered cubic morphology. A similar morphology of the cubic structure of TEMPO-PEI was also observed at the tip of the surface as exhibited in **Fig 4.6(d)** representing the MCNC-TEMPO-PEI. The base looks smooth representing the higher presence of PEI and confirming a successful impregnation. The EDS analysis of these materials is exhibited in **Fig. 4.6(e)** where carbon holds a major percentage of 52 %, 84 % and 80 % in CNC-TEMPO, CNC-TEMPO-PEI and MCNC-TEMPO-PEI, respectively. This shows an increase in carbon when introducing COOH by adding TEMPO during the crosslinking of CNC and that also caused an increase in carbon when it was further functionalized with PEI polymer. The presence of Na is displayed by the addition of NaBr and NaClO during the cross-linking process. Also, it confirms

the successful formation of the carboxylic group when bonding the COONa during the crosslinking. This makes it easier for the impregnation of PEI at a later stage. Similar traits were also observed on the CNC-TEMPO-PEI, however as the PEI was added, it was anticipated that the NH groups would then dominate which was not the case.

Lastly, the formation of MCNC-TEMPO-PEI was confirmed by the carbon, iron and oxygen molecules. It has been reported that TEMPO/NaClO or NaBr molecules tend to easily penetrate to the CNC surface as indicated in **Fig. 4.6(b)** [33]. Moreover, due to the swelling, which might have been caused by the oxidation of the TEMPO leading to the carboxylic acid sodium salt on the surface material of the CNC [8,26]. This indicates and confirms the presence of the intended carboxylic acid on the surface material of the CNC. These results corroborate with literature where the carboxylic groups from TEMPO onto CNC surface are shown by the rods [23]. After all the obtained characterization results were analyzed and confirmed, the synthesis and the formation of these three materials. Including the cooperation of TEMPO and PEI on to the MCNC. Then the MCNC-TEMPO-PEI was further optimized, validated and compared against the other derivatives for adsorption efficiency.

4.5 Application

The nanocomposite (MCNC-TEMPO-PEI) was used for the adsorptive removal of Cr (VI) ions using the method elaborated under **Section 4.3.4.1.**

4.5.1 Adsorption process against Cr (VI) ions

The MCNC-TEMPO-PEI was further optimized with 5 different parameters for the adsorptive removal of Cr (VI) ions. Starting with the concentration effect from 1-5 ppm, were conducted following a few other studies that reported adsorption of Cr (VI) in the presence of DPC reagent and quantifying using UV-Vis analysis [28-29]. A calibration standard curve was generated using similar concentration for the standards of 1-5 ppm. The calibration curve results are displayed in **Fig.4.7**.

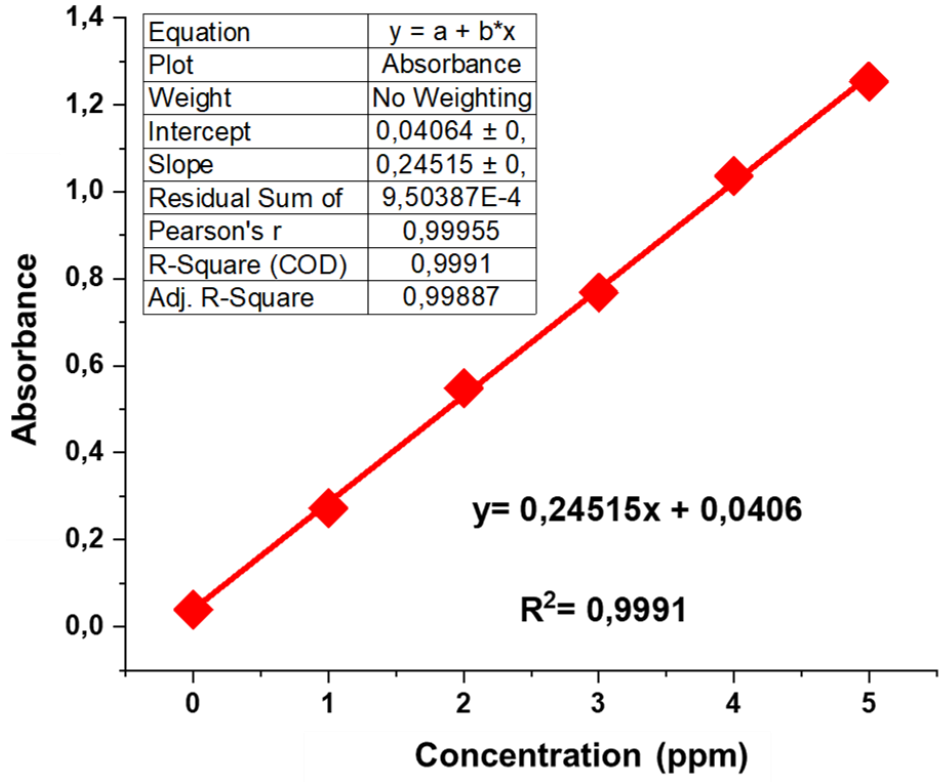

Figure 4.7: Calibration curve obtained for Cr (VI) ions.

The equation followed Beers lambert law in that it states that y = mx +c where the highest peak was noted at 547 nm and all the absorbance within the same wavelength were obtained and used to calculate and measure the calibration curve which will assist with identifying the concentrations of these points. According to the Beers law, y represents the absorbance, m the gradient/slope, x the concentration and c the intercept. Giving a linear regression formula of y = 0,24515x + 0,0406 with a correlation coefficient (R^2) value of 0,9991 with a positive slope of 0,24515 and an intercept of 0,0406 was obtained and displayed in **Fig. 4.7.** This linear standard regression curve formula was further used to calculate the concentrations from the results, which were further used for the adsorption capacity and removal percentage during the adsorption process.

4.5.2 Optimization

The five (5) parameters (concentration, dosage, pH, temperature and contact time) were each optimized according to the method described in **Section 4.3.4.3**

4.5.2.1 Effect of concentration

When optimizing the concentration, the range was stretched from 1-50 ppm to allow an interaction of the MCNC-TEMPO-PEI within a variety of concentration in triplicates and the obtained results are presented in **Fig. 4.7.** The accuracy, consistency and reliability of these ranges were only possible with lower concentration (1-5 ppm) ranges as also shown in **Fig. 4.8**. At higher concentrations (6-50 ppm), inconsistency and inaccuracy from these concentrations during analysis were observed. The saturation of the binding sites was displayed on the surface of the MCNC-TEMPO-PEI adsorbent and this suggests the possible monolayer coverage of Cr (VI) ions on the adsorbent surface between 6 ppm to 50 ppm [46]. Furthermore, at a concentration above 6 ppm, the access concentration of Cr (VI) ions did not allow sufficient removal with the depleting sites from the surface and thus leaving the complexed Cr-DPCA unabsorbed. The % removal of Cr (VI) was calculated using the standard linear curve formula (y = 0,24515x + 0,0406) and the percentage removal was noted in **equation 3.1**. The results revealed the following percentage removals as 94 % at 1 ppm; 94 % at 2 ppm; 95 % at 3 ppm; 95 % at 4 ppm and 97 % at 5 ppm, respectively as exhibited in **Fig. 4.8**. These results show that the best removal was recorded at 5 ppm. Moreover, it is generally expected that as the concentration of the adsorbate increases the metals removed should increase. The increase in concentration of adsorbate brings about increase in competition of adsorbate molecules in solution for a few available binding sites on the surface of the adsorbent increasing the amount of metal ions removed [28-29].

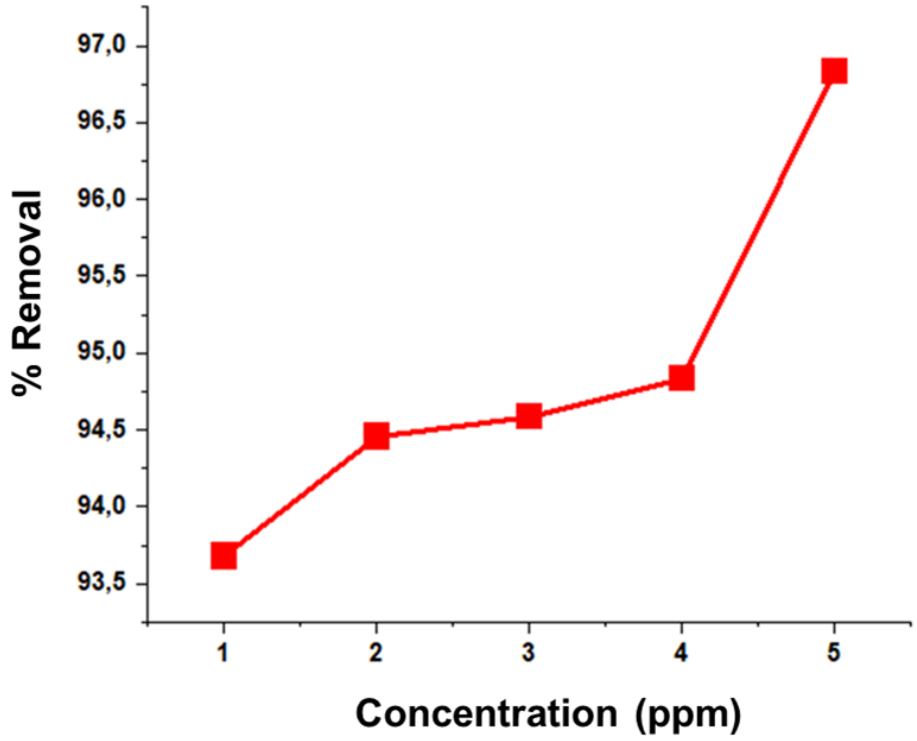

Figure 4.8: The effect of concentration of the removal of Cr (VI) ions

These results agree with work done by Qhubu *et al* [28] where a higher removal was achieved at a lower concentration range of less than 5 ppm and giving a lower adsorption capacity [28].

4.5.2.2 Effect of the MCNC-TEMPO-PEI dosage

The variation of dosage was conducted from 5 mg and stretched towards 50 mg in triplicates to optimize dosage while keeping concentration at 5 ppm. Since the accessibility and availability of adsorption sites is determined by the dosage of the adsorbent. The results obtained from these experiments were further calculated using the same linear regression formula. Furthermore, the adsorption capacity (qe) at equilibrium was calculated according to **equation 3.2** and the results obtained was plotted versus dosage as exhibited in **Fig. 4.9**.

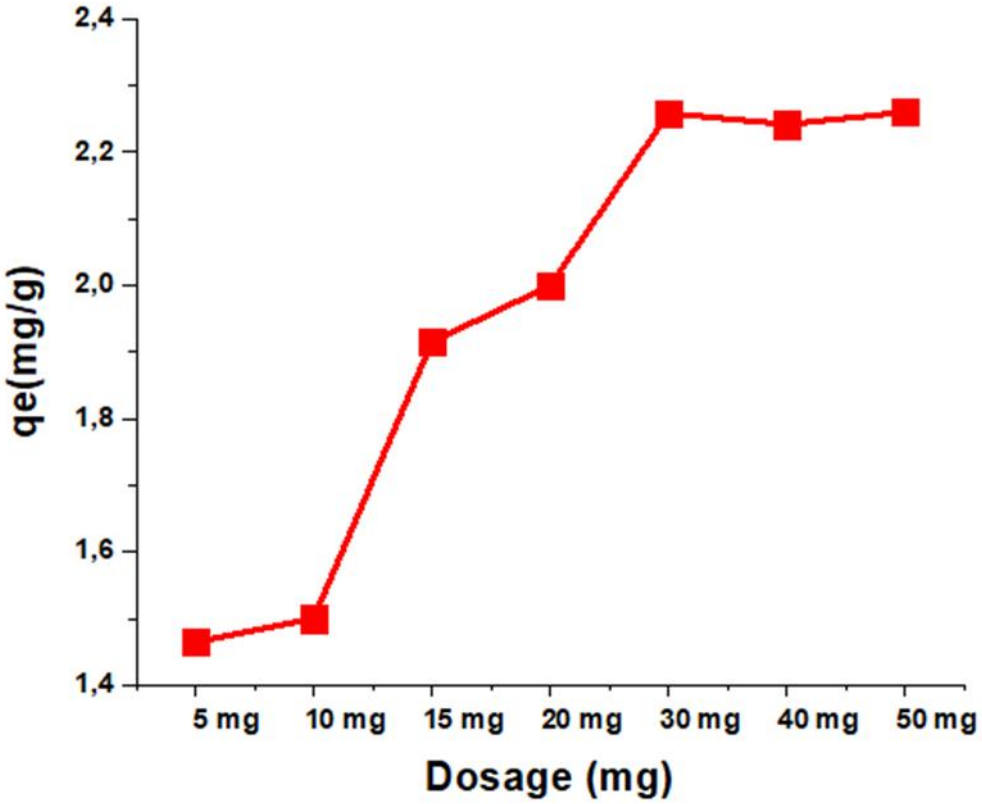

Figure 4.9: The effect of dosage conducted between 5 – 50 mg.

The results revealed that with increasing dosage, the capacity was also increased and were captured as follows: 1,46 mg/g at 5 mg, 1,5 mg/g at 10 mg, 1,92 mg/g at 15 mg, 1,99 mg/g at 20 mg, 2,26 mg/g at 30 mg, 2,24 mg/g at 40 mg and 2,26 mg/g at 50 mg. The increase in qe increased with a higher adsorbent dosage, this could be due to the excess availability of exchangeable sites at higher dose of the adsorbent [27]. This indicates the best qe was achieved at 30 mg, suggesting that the reaction reached equilibrium and optimised at 30 mg. Moreover, it could also have been due to the availability of the adsorption active sites as the dosage increased from the surface material of the MCNC-TEMPO-PEI against Cr (VI) ions [32]. To confirm these findings the % removal was also calculated according to **equation 3.1**. The results showed that at 5 mg the % removal was captured as 62 %, whilst increasing to 64 % at 10 mg, then 81 % at 15 mg, 85 % at 20 mg, 96 % at 30 mg, 95 % at 40 mg and 96 % at 50 mg. This confirmed a gradual increase from 5 mg to 30 mg and making 30 mg the optimal dosage. It is also worth noting that from 30 mg until 50 mg, the removal efficiency seemed to

be constant with minor differences indicating that the reaction has reached equilibrium and the plots have reached plateau which can also be verified by the image taken after adsorption from optimizing dosage effect and as exhibited in **Fig. 4.10**.

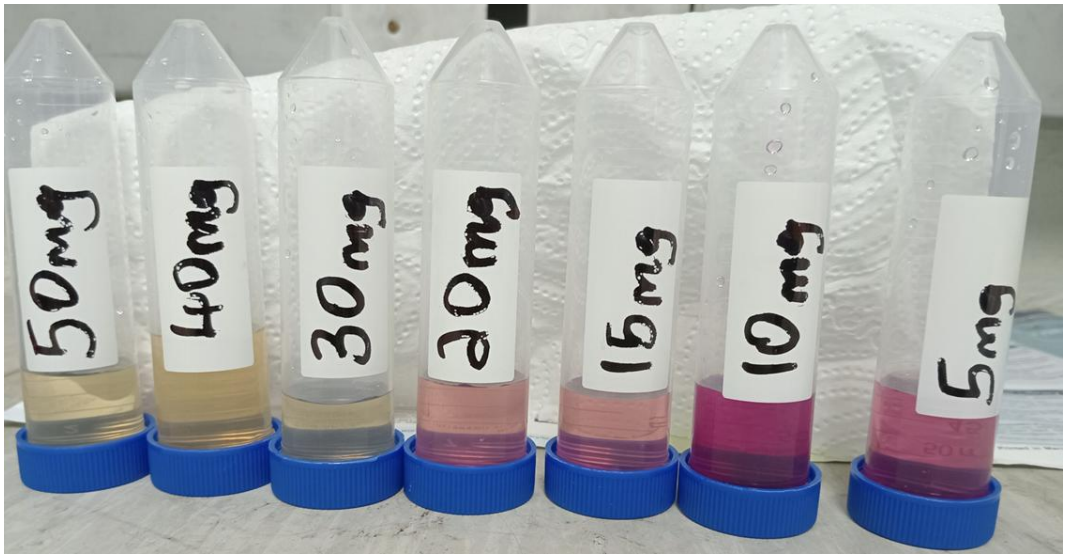

Figure 4.10: The effect of DPC reagent after adsorption when optimizing dosage

From **Fig. 4.10**, it is observed that the colour change was clearer at 30 mg than the rest of the samples and confirmed the best removal efficiency was obtained at 30 mg with the percentage ≈ 96 %. This suggests that the MCNC-TEMPO-PEI might have obtained a larger surface area with vacant sites and leading to effective removal of Cr (VI) ions and providing the qe of 2,26 mg/g [4]. These results corroborate with work done by Bagheri *et al* [5], where in their study, they reported an adsorption capacity of 0,75 mg/g against Cr (VI) ion adsorption [5]. Upon optimizing the concentration and dosage, the pH parameter was further optimised.

4.5.2.3 The effect of pH during optimization

The pH measurements were carried out between 2-7 and the results from these experiments are exhibited in **Fig. 4.11**. According to these results, the adsorption was efficient within the acidic medium, whereas a low efficiency within the alkaline environment was recorded. This could be due to the variation of Cr (VI) ionic forms, from a class of oxyanions such as hydrogen chromate ($HCrO_4^-$), chromate (CrO_4^{2-}) and dichromate ion (Cr_2O_7) that exist within different pH levels [47, 48]. This is evident when the highest adsorption capacity and

the percentage removal were observed at pH=2, giving a qe of 1,99 mg/g and the % removal of 92 %. This could have been due to the protonation (NH_3^+) of amine groups (NH^-_2) from the surface material of MCNC-TEMPO-PEI within the strongly acidic medium. Allowing electrostatic interaction between the negative anions ($HCrO^{4-}$) from the Cr (VI) ions and protonation, thus attacking the hydrogen chromate and providing an efficient adsorption at pH=2 [29].

Since hydrogen chromate ($HCrO^{4-}$) is predominant at acidic conditions and because of that, making it vulnerable within this environment. Hence, it is also observed that even between pH=4-pH=6, at higher percentage removal, the adsorption capacities were also observed. The results are as follows: at pH=4, at qe was calculated to be 1,96 mg/g with the removal of 92 %, meanwhile at pH=5, the qe was 1,83 mg/g with the % removal of 92 % and at pH=6 an adsorption capacity of 1,80 mg/g was observed with the % removal of 90 %. This also suggest that as the pH increases the adsorption capacity decreases [13-15].

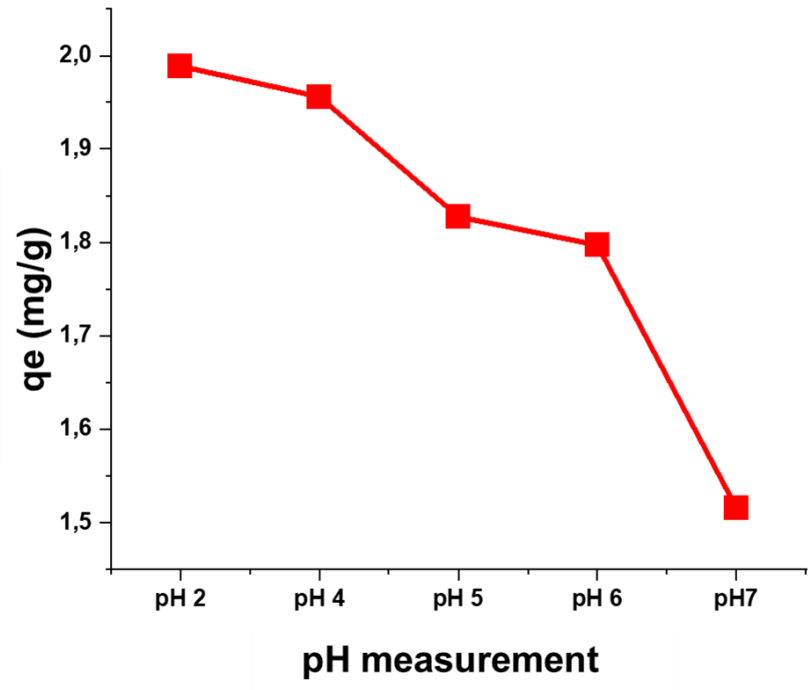

Figure 4.11: the effect of pH during optimization

This could mean that deprotonation reaction occurred when the hydrogen chromate was converted to chromate ions (CrO_4^{2-}) at weak acidic conditions as the pH is slightly approaching neutral medium [35-36]. This is also confirmed when the qe at pH = 7 was 1,52 mg/g and the % removal was 91 %. It is also observed that at alkaline environment, the adsorption capacity and the % removal further decreased, whereby the qe was 0,48 mg/g and the % removal was 80 %, respectively at pH = 9. This could suggest that the excessive hydroxyl anions (OH^-) from the surface material of MCNC-TEMPO-PEI are competing and opposing with the dichromate ions from the Cr (VI) ions within the alkaline medium, resulting in a decrease in qe [13,15]. Furthermore, these hydroxyl radicals can further disassociate the hydrogen bonds keeping the analyte intact and resulting in a decrease in the qe [15]. Moreover, this could also be due to the conversion of dichromate ions to chromate ions in basic conditions which repelled the negatively charged surface against the negative ions, thus leading to less efficiency [15].

These results agree with reports where the acidic conditions provided efficient capacity and removal against Cr (VI) ions [28-29]. Similar observations were made by Anirudhan *et al* [36], when between pH = 2 and pH = 5 the adsorption efficiency for Cr (VI) was higher due to electrostatic interactions between the Cr (VI) anions and the surface of the CNCs. Furthermore, the decrease in the adsorption of Cr (VI) ions at pH = 7 and above, can be explained by the progressive increase in the competition of the –OH- groups from the solution and the Cr (VI) ions leading to the decrease in the adsorption efficiency of the adsorbate [15,31].

4.5.3The effect of temperature

The effect of temperature was conducted and investigated between the range of 20 – 40 ºC to optimize the MCNC-TEMPO-PEI against the Cr (VI) ions. The results were calculated and plotted as qe versus temperature and are presented in **Fig. 4.12**. From the analysis shown in **Fig. 4.12**, the adsorption capacities were obtained as follows: at 20 ºC the qe was 1,76 mg/g, 25 ºC - 1,77 mg/g, at 30 ºC - 1,77 mg/g, at 35 ºC - 1,77 mg/g and at 40 ºC - 1,76 mg/g.

The same findings were also confirmed by the % removal conducted within similar temperature range.

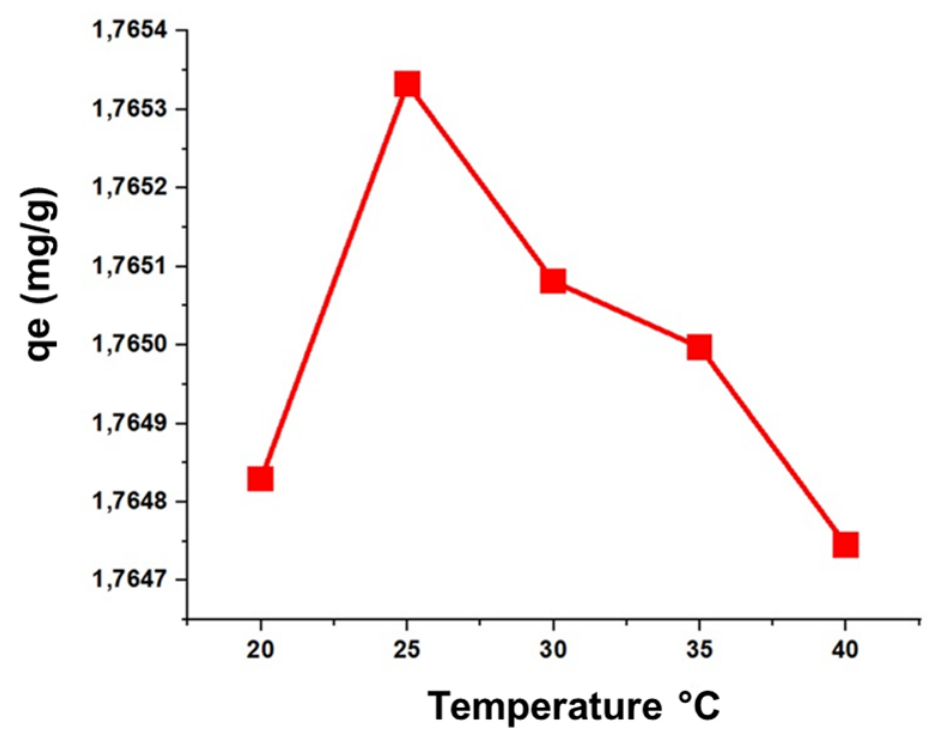

Figure 4.12: The effect of temperature

The outcomes were captured as follows: 92 % across all the temperature ranges. According to these results, temperature did not play a significant role because at all the temperatures, a 92 % removal and 1,77 mg/g adsorption capacity was reported. This suggests that these reactions did not require a lot of heat energy to reach equilibrium.

4.5.4 The effect of contact time

In this study, the effect of contact time on the adsorption capacity of Cr (VI) ions by MCNC-TEMPO-PEI was investigated from 5-180 min. Other optimised parameters remained constant at 5 ppm, 30 mg, pH = 2 and at 25 ºC and the results obtained from these experiments are presented in **Fig. 4.13**. The percentage removal and the adsorption capacities using MCNC-TEMPO-PEI against Cr (VI) ions were calculated and the obtained results were recorded as 90 % and 1,36 mg/g at 5 min, 92 % and 1,56 mg/g at 10 min, 99 % and 2,27 mg/g at 15 min. From the results in **Fig. 4.13**, the reaction reached equilibrium and the qe was rapid

within the 15 min. The results indicate that the equilibrium contact time is dependent on the optimized reaction conditions for the optimum removal and capacity of the Cr (VI) ions in the solution. Thus, suggesting that the effect is due to the plentiful active sites available within the surface of the MCNC-TEMPO-PEI material [28-29].

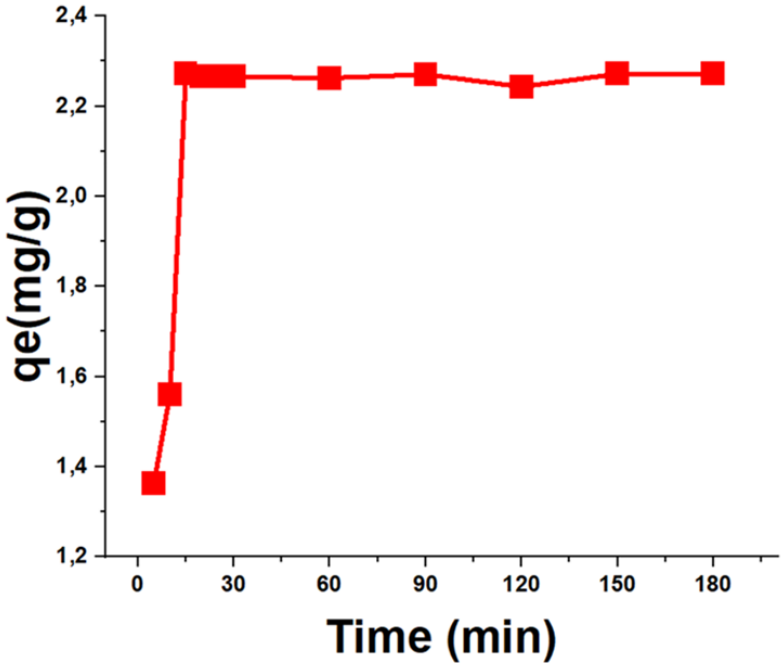

Figure 4.13: The effect of contact time of MCNC-TEMPO-PEI against Cr (VI)

Moreover, the chances of the MCNC-TEMPO-PEI possessing a large pore would have also added to the fast adsorption of Cr (VI) ion. These results are corroborated with similar reports where this type of an adsorbent produced rapid removal within the first few minutes [28-29]. The optimization process showed that the MCNC-TEMPO-PEI was efficient at these parameters, concentration of 5 ppm, 30 mg of dosage, at pH = 2 and 25 ºC within 15 min contact time. Thus, validation of these parameters was required on the same material, also to evaluate the contributing factor amongst the rest of the adsorbent's materials functionalised, crosslinked, and grafted for the formation of the MCNC-TEMPO-PEI.

4.5.5Validating MCNC-TEMPO-PEI and comparing it with other adsorbents

To investigate the functional groups responsible for contributing to an effective removal. Five various adsorbents were used to validate these optimal conditions and to also assess the

performance of the MCNC-TEMPO-PEI against the Cr (VI) ions. These adsorbents are Magnetite, MCNC, CNC-TEMPO, and the CNC-TEMPO-PEI which were functionalized until the final product of MCNC-TEMPO-PEI was formed. The results obtained after the adsorption of Cr (VI) ions using the optimal conditions are exhibited in **Fig. 4.14**. The average adsorption capacity of the five materials were calculated and the results revealed that 3,04 mg/g; 3,05 mg/g, 1,98 mg/g, 3,05 mg/g and 4,41 mg/g were achieved for the Magnetite, MCNC, CNC-TEMPO, CNC-TEMPO-PEI and the MCNC-TEMPO-PEI, respectively. Furthermore, the average removal percentages of these five materials were also calculated and recorded as 62 % for CNC-TEMPO, 98 % for the MCNC-TEMPO-PEI, 96 % for magnetite, MCNC and CNC-TEMPO-PEI, respectively. This indicates that MCNC-TEMPO-PEI had the highest adsorption capacity of 4,41 mg/g with the highest % removal of 98 %.

According to these results, Fe_3O_4 played a vital role in enhancing the efficiency of these adsorbents materials. This is observed that the adsorbents that contained Fe_3O_4 were effective and produced adsorption capacities of over 3 mg/g with the removal of 96 %. The attraction from the magnetic field of the adsorbents materials is more enhanced when the analyte is a metallic pollutant, making it an easier target. It can be confirmed by looking at CNC-TEMPO without iron coating, performing less than the other magnetic coated materials and displaying qe of approximately 2 mg/g and removal of 62 %. This gives the impression that TEMPO on its own, has the ability to open pores for further modification. It is therefore suspected to not been sufficient enough due to the presence of carboxylic groups that might require additional modification to compete with Fe_3O_4 for the efficient removal [16]. However, with additional functional groups like amines, it can therefore become more active as exhibited in **Fig. 4.14,** where in the presence of amine groups from PEI, it was as effective as magnetic adsorbents both with the removal and the reported adsorption capacity.

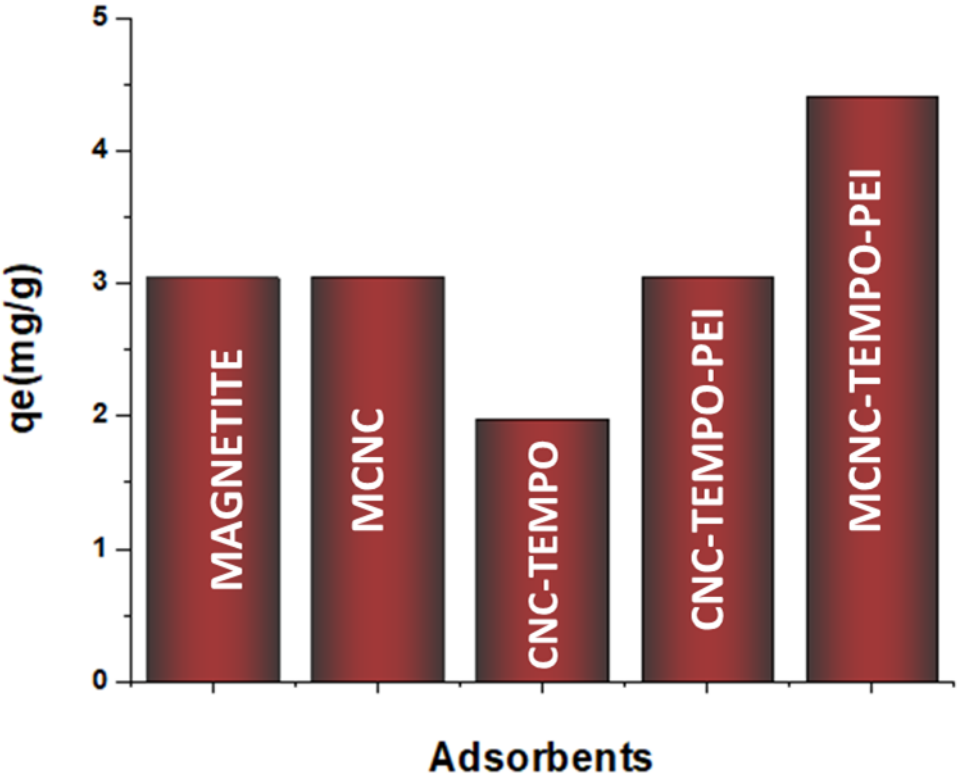

Figure 4.14: The comparison of other adsorbents against the MCNC-TEMPO-PEI

The efficiency of the MCNC-TEMPO-PEI could have been due to the strong surface modification on the surface of the MCNC-TEMPO-PEI adsorbent. Thus, it can therefore be more active in the presence of additional functional groups attached to the surface material [16,20]. The combination of the carboxylic and amine, like in case with PEI produced a 96 % removal that is similar to magnetic adsorbents. Moreover, the presence of PEI has an added advantage of possessing the magnetic response from which the magnetic properties from within the surface adsorbent are enhanced and giving the highest efficiency [16,20]. These results were also corroborated with various studies providing an efficient percentage removal [16-32]. The MCNC-TEMPO-PEI was further investigated for the adsorption isotherms studies and the interaction reaction with the Cr (VI) during the adsorption process.

4.5.6 The adsorption isotherms studies

To understand the interaction between the adsorbate and the adsorbent in this study, the Langmuir and Freundlich adsorption isotherms were further investigated. The equilibrium

adsorption studies were conducted where the concentration range of 1 ppm, 3 ppm, 5 ppm, 7 ppm and 9 ppm were studied, whilst other experimental parameter conditions were kept at their optimum conditions. The data plots that were generated from the experimental data calculated using the non-linear **equations** of **2.2** and **2.4** are presented in the supplementary information in **Table S5.** The maximum adsorption capacity, slope, intercept, relative coefficients, Langmuir and Freundlich adsorption constants were also presented in **Table S5**. The results for the adsorption isotherms are exhibited in **Fig. 15 (a),** representing the Langmuir plot and **(b)** the Freundlich plot. The calculated experimental adsorption capacities at a particular concentration were recorded as follows 0,41 mg/g for 1ppm, 0,99 mg/g for 3 ppm, 1,60 mg/g for 5 ppm, 2,04 mg/g for 7 ppm and 3,14 mg/g for 9 ppm, respectively. According to the experimental data presented in **Fig. 15**, it appears as though none of the isotherm plots displayed a good fit with the experimental data and a non-linear curve. However, when comparing between the two plots against each other, it can be noted that the interaction between the MCNC-TEMPO-PEI and Cr (VI) ions best fitted the Langmuir adsorption isotherm. The regression coefficient (R^2) was 0,93378 for the Langmuir as compared to 0,76965 for the Freundlich regression coefficient. This suggests that there was a chemisorption reaction interaction with a homogeneous coating of the MCNC-TEMPO-PEI on a monolayer surface material [5]. Thus, represented by a non-linear outcome from the Langmuir adsorption isotherm theory exhibited in **Fig. 4.15**.

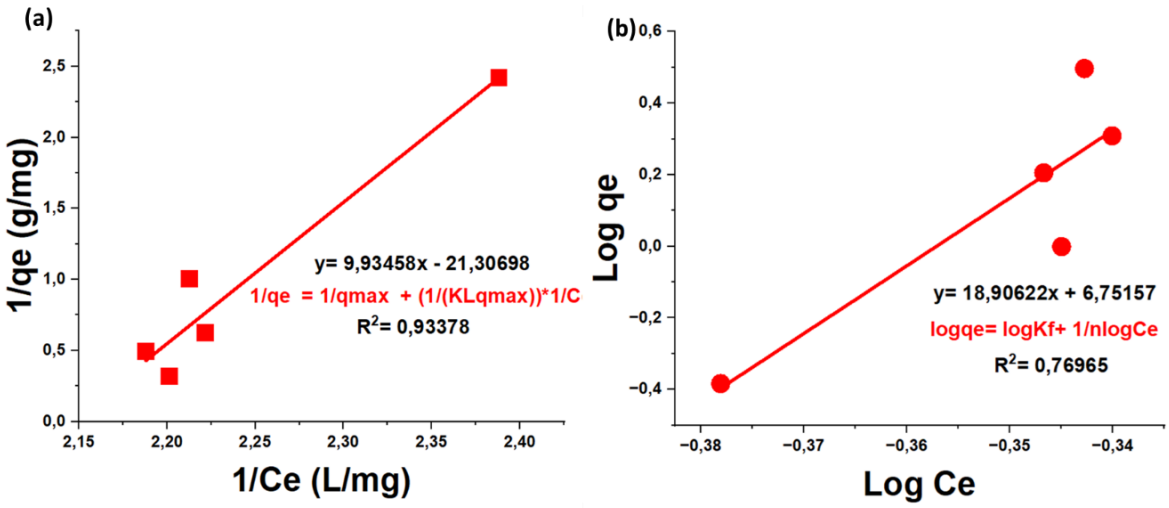

Figure 4.15: (a) Langmuir and (b) Freundlich adsorption study plots

It is assumed that the active sites were responsible when the adsorption was occurring [1-2]. The results propose a Langmuir isotherm model indicating the monolayer distribution on the surface of the MCNC-TEMPO-PEI nanocomposites [12,27]. These findings are in agreement with the findings observed with the plot of pH optimization, where the pH value of 2 provided the highest adsorption efficiency This confirms the adsorption mechanism that there is an ionic chemisorption between the adsorbent surface and the adsorbate [21,26]. However, after filling the surface area, the monolayer was therefore not sufficient to release enough active sites binding the Cr (VI) ions from the surface.

From the Langmuir plots, a maximum adsorption capacity (q_{max}) and the Langmuir separation factor (R_L) were calculated using the slope and intercept as exhibited in **Fig. 15 (a)**, where the q_{max} and R_L were 0,04693 mg/g and 0,10284, respectively. This demonstrates a favorable adsorption based on the reports that when R_L=0, it suggests that the adsorption type is irreversible, but unfavorable when it is more than one (1) and favorable when less than one (1) [1,29]. Moreover, it also followed a chemical interaction assumed and observed when the electrostatic interaction occurred during adsorption within the acidic conditions that protonated the amine groups to target the anionic Cr (VI) ions. So, in this study, the Langmuir separation factor (R_L) was calculated to be 0,10284 confirming a favorable reaction since is

less than one (1). These results can confirm what has already been reported by different studies where a variety of adsorbents were used for the removal Cr (VI) while following the Langmuir isotherms [11]. Utilizing the data and calculations as displayed under the supplementary information in **Table S2**, the adsorption kinetics were also obtained and plotted to also confirm the interaction between MCNC-TEMPO-PEI and Cr (VI) and to evaluate the binding capacity of MCNC-TEMPO-PEI on Cr (VI).

4.5.7The adsorption kinetics studies

To understand the adsorption mechanism, the rate of adsorption was evaluated using two kinetics models, namely the pseudo first order (PFO) and the pseudo second order (PSO). The triplicate experiments were conducted from 5-30 min for both the PFO and the PSO with kinetics studies calculated according to **equation 2.6** and **2.8**. The results obtained from these experiments were also presented in **Table S5** and the plotted results of ln(qe-qt) versus time in min for PFO and the t/qt against time for PSO graphs were also presented in **Fig. 4.16**. The corresponding data and calculation for the kinetics are exhibited under the supplementary information as **Table S5** and a summary information is displayed in **Table 4.1**.

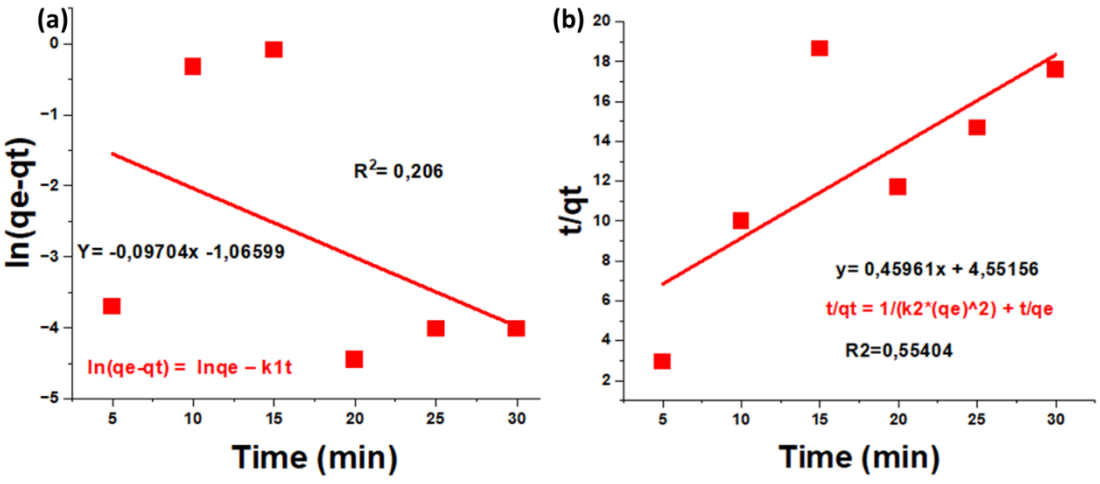

Figure 4.16: PFO and PSO for the removal of Cr (VI) ions

According to the results presented in **Fig. 4.16,** the results favored the PSO model with a non-linear regression curve that showcased the R^2 of 0,554. The results give an indication that the mechanism could be from the heterogenous surface comprised of multiple functional

groups like hydroxyl, amine, carboxylic and iron which strengthens the binding sites on the surface of MCNC-TEMPO-PEI. Moreover, predicting the interaction to be chemisorption and confirming what the Langmuir isotherms were also predicted. Furthermore, the results confirm the saturation of the active sites from the single attachment from the MCNC-TEMPO-PEI surface material during adsorption, hence, following PSO kinetics [11]. Using the slope and intercept from the graphs, the calculated adsorption capacity at equilibrium was found to be 2,18 mg/g. The results agree with Qhubu *et al* [28], where the equilibrium adsorption was also obtained at 2.64 mg/g and the interaction following PSO reaction [28]. Moreover, other studies also reported that the PSO was followed when removing the Cr (VI) ions from water which is also corroborated to this study [4,29]. To further understand the chemisorption interaction, the mechanism of action for adsorption was discussed.

4.5.8 Mechanism of action

To understand the adsorption mechanism Cr (VI) is complexed and oxidizes by the DPC to form a Cr-DPCA complex through a redox reaction [38-39]. The oxygen atom and two of the nitrogen atoms in DPC act as donors (O and N-donors) that bind selectively with Cr (VI) [50, 51][38-39]. This is caused by the complexation reaction, under the chelation process that binds the Cr (VI) ions to the surface material during the adsorption process [38-39]. The chromophore, enhances its colorimetric property, leading to a higher removal of Cr (VI) ions [1-2,4]. This mechanism is also understood and presented in **Fig. 4.1.** In an acidic medium condition, the materials surface of MCNC-TEMPO-PEI is protonated, the release of the Cr (VI) is eminent due to the formation of the $HCrO_4^-$ and CrO_4^{2-}via the electrostatic interaction. This depends on the surface charges which occurred after protonation of NH_3^+ from the amine groups (NH_2^-), attracting the anionic charged Cr ions ($HCrO_4^-$ and CrO_4^{2-}) and using the chemisorption interaction [37]. This was confirmed by the Langmuir adsorption isotherms corroborating the chemisorption interaction fitting the PSO kinetic model. This is in addition to the magnetic forces forming an ionic bond caused by the metal complex adsorption attracting negative ions from the analyte from the positively charged surface adsorbent [34,37].

4.5.9 The thermodynamic studies

The thermodynamic interaction reaction was evaluated and experimented between 20 - 40 ºC and the results are presented in **Fig. 4.17**.

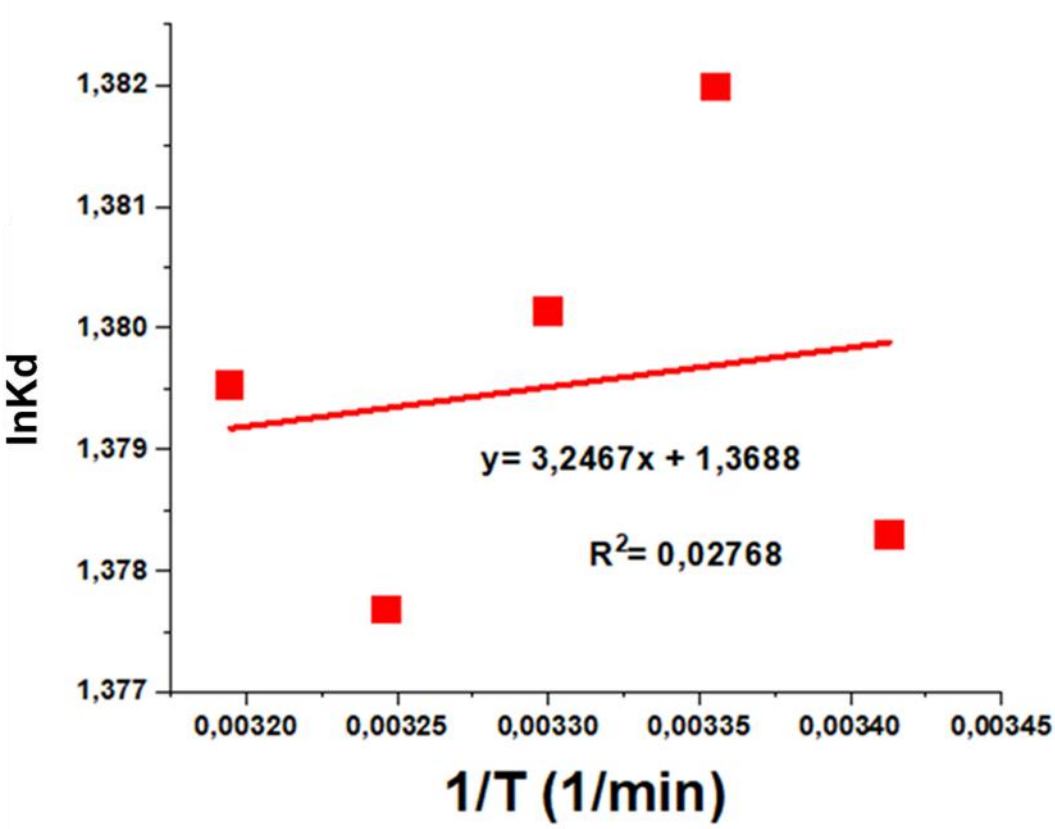

Figure 4.17: The thermodynamic studies of MCNC-TEMPO-PEI

In **Fig. 4.17**, the results confirm a positive slope with a positive intercept, exhibiting the thermodynamic parameters (ΔG, ΔS and ΔH) for the adsorptive removal of Cr (VI) ions using the MCNC-TEMPO-PEI. According to the results presented in **Fig. 4.17**, the Gibbs free energy was calculated using the slope and intercept from the ln Kd vs 1/T regression line. This displayed a positive change (ΔG) with a value of 26,8 kJ/mol, implying a non-spontaneous reaction, meaning that it might require a less amount of energy for the reaction to occur [28,34]. Thus, an optimal temperature condition of 25 ºC was obtained. Moreover, the enthalpy change (ΔH) was also calculated and found to be 27 kJ/mol, a positive ΔH, confirming that the reaction is endothermic [5]. The value of 0,1645 J/mol/K of the entropy change (ΔS) indicated an

increase within the irregular process of the adsorbent during adsorption. A summary of isotherms, kinetics and thermodynamics are exhibited in **Table 4.1**.

Table 4.1: Some essential factors affecting the isotherms and kinetics plots

Langmuir			
Qmax	Kl	R_L	R^2 value
0,04693 mg/g	-2,14473	-0,10284	0,93378
Freundlich	1/n	Kf	R^2 value
	18,90622	5643779	0,76965
PFO	K_1	Qe	R^2
	-0,00323	0,344387mg/g	0,20673
PSO	K_2	Qe	R^2
	21,54673	2,175758 mg/g	0,55404
Thermodynamic	ΔH	ΔS	ΔG
	27,02 KJ/mol	0,164638 J/mol/T	26,8 KJ/mol

4.5.10 The reusability studies of the MCNC-TEMPO-PEI against Cr (VI) ion

The stability of the MCNC-TEMPO-PEI was further analysed for reusability and the results are presented in **Fig. 4.18.** The investigation was subjected to perform 9 cycles using the validated conditions of the initial concentration of 5 ppm with 30 mg of the adsorbent dosage at pH = 2 for 15 min maintained at 25 ºC during the adsorptive removal of Cr (VI) ions and the results are exhibited in **Fig. 4.18**. According to the results, the performance of the MCNC-TEMPO-PEI was stable for the first four (4) cycles with the removal above 90 % and a slight decrease from the 5^{th} cycle until the 8^{th} cycle (87 – 77%) was noted and thereafter a drastic reduction in efficiency till 20 % was recorded.

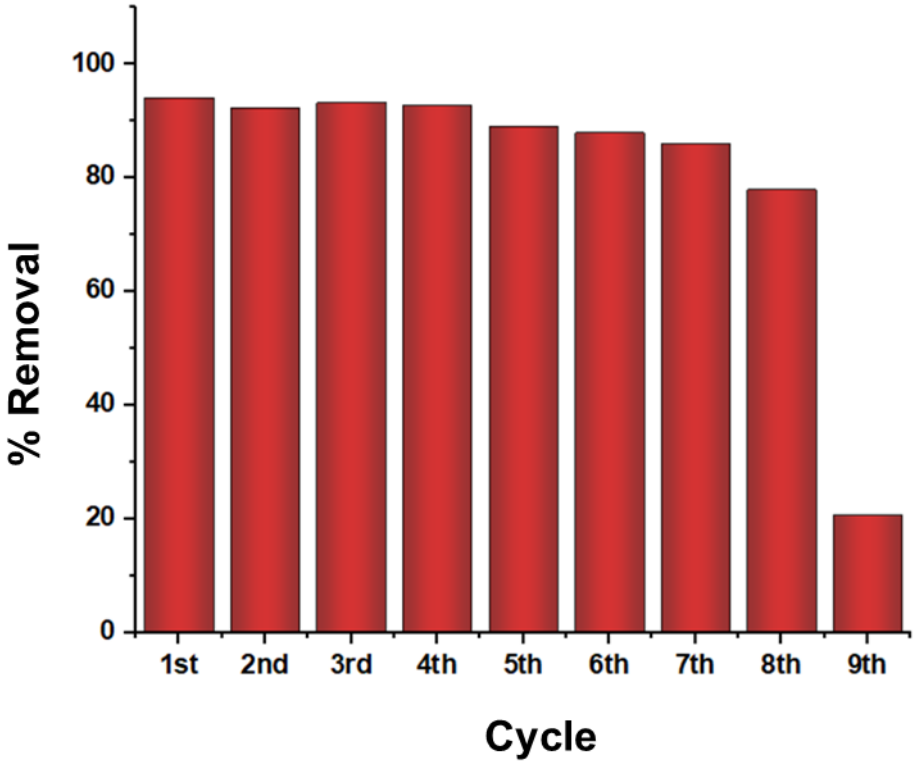

Figure 4.18: Reusability cycle of MCNC-TEMPO-PEI against Cr (VI) ions

These results indicate that Fe_3O_4 was not leached from the adsorbent surface material resulting from a chemical reaction during the elution process. When recovering the adsorbent, it maintained the stability and efficiency until the 8^{th} cycle. To further understand the stability and the effectiveness of iron from the surface of MCNC-TEMPO-PEI after the last reusability cycle, an investigation was conducted using the FTIR technique and the results obtained are exhibited in **Fig.4.19**.

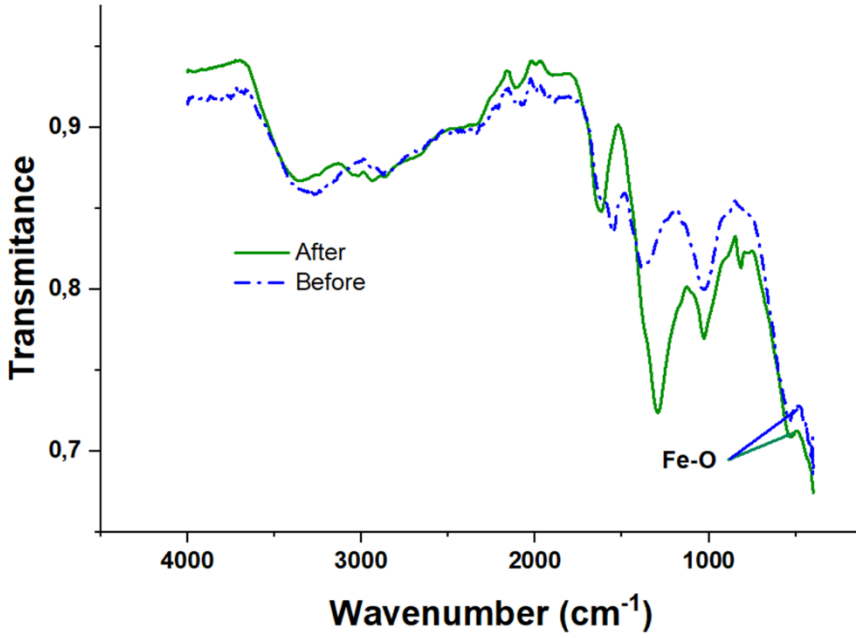

Figure 4.19: The FTIR analysis of MCNC-TEMPO-PEI before and after the last cycle

According to the results presented in **Fig. 4.19**, it showcased the presence of iron shown before and after the last cycles. This confirms the absence of the decomposition of iron after reusability studies. Furthermore, there were no traces of Fe_3O_4 that were observed in the analyte solution, which also supports that the MCNC-TEMPO-PEI was still attached to the magnetite and because of that, was proven stable during reusability studies. Moreover, other functional groups were retained even after the last cycle from the adsorbent before the first cycle as exhibited from the FTIR spectrum in **Fig. 4.19**. Since the stability of the MCNC-TEMPO-PEI was confirmed, a series wastewater samples were conducted to also investigate the efficiency of these adsorbents. According to the results, it was discovered that the concentration level from these real wastewater samples were below the detection point from the UV-Vis spectrophotometer. This confirms that none of these sources contained Cr (VI) ions even before adsorption, hence, the concentration was undetected. These results are similar to the research done by Pourmortazavi *et al* [39] where Cr (VI) ions were undetected [39]. The results found from this study were also used to check the efficiency of the material as compared to the other materials used for the removal of the same analyte. **Table 4.2** was

used to capture a few studies with different magnetic adsorbents using the UV-Vis spectrophotometer as the detection technique for the adsorptive removal of Cr (VI) ions.

Table 4.2: Different adsorbents for the removal of Cr (VI) and Pb (II) ions

Adsorbent	Quantification technique	Cycles	Ci (ppm)	Adsorption capacity (mg/g)	% Removal	Ref
Cr (VI)						
DPC-SBA-15	UV-Vis	-	50	0,85mmol/g	86	[6]
NIP-Cr (VI)(4VP-co-EGDMA)	UV-Vis	10	14	3,4	96	[7]
AF-Fe_2O_3	UV-Vis	-	10	8,38	-	[13]
Fe_2O_3@CTAB	UV-Vis	10	1	12	95	[14]
CMPBC	UV-Vis	-	5	14,6	75	[23]
ACM	UV-Vis	-	2,5	6,1		[28]
MCMGO	UV-Vis	15	15	0,75	-	[40]
Zn-NiF@PBC	UV-Vis	5	100	29,7	95	[41]
Fe_3O_4@PVA/CS	UV-Vis	-	100	0,239 g/g	-	[42]
MCNC-TEMPO-PEI	UV-Vis	9	5	4,41	98	This work
Pb (II)						
MCNC@Zn-BTC	AAS	5	200	558	80	[43]
GTD 2	FAS	-	100	192	-	[44]
m-CNF+ PAN	UV	3	100	138	-	[27]
CCN-Fe3O4	AAS	5	50	64	-	[45]
MCNC	ICP	4	1	47	97	This work

Looking at the studies presented in Table 4.2, it can be assumed that the initial concentration and the type of the detection technique has played a role in the adsorption capacity. The majority of the studies presented in Table 4.2 have used UV-Vis as a quantification technique for Cr(VI) and obtained a lower adsorption capacity even though the % removal was efficient. This could have been due to the detection limit obtained at lower concentrations when using a UV-Vis technique. Unlike when the other quantification techniques like ICP-OES and AAS techniques that have the ability to detect higher concentration ranges resulting in the higher adsorption capacities. Moreover, it was also discovered in this study that the presence of iron within the surface material could have also contributed to the efficiency in the higher % removal from these adsorbents hence the majority followed PSO and Langmuir adsorption isotherms just like in this study. In contrast to our study, these reports were able to achieve a higher adsorption capacity for Pb(II) despite the technique they employed. Nonetheless, the results from this study displayed higher percentage removal. Which might have been impacted by the initial concentration being

employed at a lower concentration level. Therefore, even though the materials employed in this investigation were different, Pb(II) produced a larger percentage efficiency than Cr(VI) ion.

4.5.11 Conclusion

The MCNC-TEMPO-PEI was successfully synthesized using a co-precipitation method after the crosslinking of TEMPO in the presence of the cross-linking reagents glutaraldehyde (GLA). Further grafted with the second polymer polyethyleneimine (PEI) via Schiff base reaction. The final nanocomposite was characterised and confirmed by the FTIR, P-XRD, TEM, SEM and EDS. The optimised parameters were proved to be 5 ppm for the initial concentration, with the dosage of 30 mg within the acidic medium of pH 2 at 25 ºC for 15 min. The adsorption isotherms, kinetics and thermodynamic revealed a chemisorption interaction governed by the electrostatic forces combined with ionic and magnetic interactions. A regression correlation of 0,93 with the highest adsorption capacity of 4 mg/g with the removal of 98% was reported. The results further confirmed a favourable and endothermic reactions. It was further tested for stability and the results revealed that it is stable up until the 8^{th} cycle owing to the magnetic interaction and the addition of amine groups from the surface.

4.6 References

1 Samuel, M.S., Shah, S.S., Subramaniyan, V., Qureshi, T., Bhattacharya, J., Pradeep Singh, N.D.: Preparation of graphene oxide/chitosan/ferrite nanocomposite for Chromium(VI) removal from aqueous solution. Int. J. Biol. Macromol. 119, 540–547

2 Owlad, M., Aroua, M.K., Daud, W.A.W., Baroutian, S.: Removal of hexavalent chromium-contaminated water and wastewater: A review. Water. Air. Soil Pollut. 200, 59–77 (2009).

3 Nchoe, O.B., Klink, M.J., Mtunzi, F.M., Pakade, V.E.: Synthesis, characterization, and application of β-cyclodextrin-based ion-imprinted polymer for selective sequestration of Cr(VI) ions from aqueous media: Kinetics and isotherm studies. J. Mol. Liq. 298, (2020).

4 Pakade, V.E., Tavengwa, N.T., Madikizela, L.M.: Recent advances in hexavalent chromium removal from aqueous solutions by adsorptive methods, (2019)

5 Bagheri, V., Naseri, A., Sajedi-Amin, S., Soylak, M., Zhang, Z.: Using Fe3O4-graphene oxide-modified chitosan with melamine magnetic nanocomposite in the removal and magnetic dispersive solid-phase microextraction of Cr (VI) ion in aquatic samples. Chem. Pap. (2023).270.

6 Mumtaz, K., Iqbal, S., Shahida, S., Shafique, M.A., Wasim, M., Ahmad, B.: Synthesis and performance evaluation of diphenylcarbazide functionalized mesoporous silica for selective removal of Cr(VI). Microporous Mesoporous Mater. 326, 111361 (2021).

7 Neolaka, Y.A.B., Lawa, Y., Naat, J.N., Pau Riwu, A.A., Darmokoesoemo, H., Supriyanto, G., Holdsworth, C.I., Amenaghawon, A.N., Kusuma, H.S.: A Cr(VI)-imprinted-poly(4-VP-co-EGDMA) sorbent prepared using precipitation polymerization and its application for selective adsorptive removal and solid phase extraction of Cr(VI) ions from electroplating industrial wastewater. React. Funct. Polym. 147, (2020).

8 Huang, R., Ma, X., Li, X., Guo, L., Xie, X., Zhang, M., Li, J.: A novel ion-imprinted polymer based on graphene oxide-mesoporous silica nanosheet for fast and efficient removal of chromium (VI) from aqueous solution. J. Colloid Interface Sci. 514, 544–553 (2018).

9 Kumar, S., Alveroğlu, E., Balouch, A., Talpur, F.N., Jagirani, M.S., Abdullah, Mahar, A.M., Pato, A.H., Mal, D., Lal, S.: Fabrication of chromium-imprinted polymer: A real magneto-selective sorbent for the removal of Cr(vi) ions in real water samples. New J. Chem. 44, 18668–18678 (2020).

10 Nan, Y., Gomez-Maldonado, D., Whitehead, D.C., Yang, M., Peresin, M.S.: Comparison between nanocellulose-polyethylenimine composites synthesis methods towards multiple water pollutants removal: A review. Int. J. Biol. Macromol. 232, 123342 (2023).

11 Wang, M., Chen, Y., Zhang, Y., Wei, S., Zhao, X., Zhao, K., Xu, L., Feng, X.: Selective removal of Cr(VI) from solution by polyethyleneimine modified hydrochar loaded nanoscale zero-valent iron with high adsorption capacity. Sep. Purif. Technol. 329, 125150 (2024).

12 Liu, P., Oksman, K., Mathew, A.P.: Journal of Colloid and Interface Science Surface adsorption and self-assembly of Cu (II) ions on TEMPO-oxidized cellulose nanofibers in aqueous media. J. Colloid Interface Sci. 464, 175–182 (2016).

13 Juturu, R., Murty, V.R., Selvaraj, R.: Efficient adsorption of Cr (VI) onto hematite nanoparticles: ANN, ANFIS modelling, isotherm, kinetic, thermodynamic studies and mechanistic insights. Chemosphere. 349, 140731 (2024).

14 Naous, M., Halfadji, A.: Comparative adsorption study of functionalized magnetite and maghemite nanoparticles coated with ctab surfactant for efficient chromium removal from wastewater. J. Water Environ. Nanotechnol. 9, 73–89 (2024).

15 Sun, X., Yang, L., Xing, H., Zhao, J., Li, X., Huang, Y., Liu, H.: High capacity adsorption of Cr(VI) from aqueous solution using polyethylenimine-functionalized poly(glycidyl methacrylate) microspheres. Colloids Surfaces A Physicochem. Eng. Asp. 457, 160–168 (2014).

16 Riva, L., Fiorati, A., Punta, C.: Synthesis and application of cellulose-polyethyleneimine composites and nanocomposites: A concise review. Materials (Basel). 14, 1–22 (2021).

17 Boyrazlı, M., Güler, S.H.: Synthesis of carbon nanostructures from corn stalk using mechano-thermal method. J. Mol. Struct. 1199, (2020).

18 Zhao, J., Yu, L., Ma, H., Zhou, F., Yang, K., Wu, G.: Corn stalk-based activated carbon synthesized by a novel activation method for high-performance adsorption of hexavalent chromium in aqueous solutions. J. Colloid Interface Sci. 578, 650–659 (2020).

19 Hegazi, H.A.: Removal of heavy metals from wastewater using agricultural and industrial wastes as adsorbents. HBRC J. 9, 276–282 (2013).

20 Nordin, A.H., Wong, S., Ngadi, N., Mohammad Zainol, M., Abd Latif, N.A.F., Nabgan, W.: Surface functionalization of cellulose with polyethyleneimine and magnetic nanoparticles for efficient removal of anionic dye in wastewater. J. Environ. Chem. Eng. 9, (2021).

21 Omer, A.M., Abd El-Monaem, E.M., Eltaweil, A.S.: Novel reusable amine-functionalized cellulose acetate beads impregnated aminated graphene oxide for adsorptive removal of hexavalent chromium ions. Int. J. Biol. Macromol. 208, 925–934 (2022).

22 Abou-zeid, R.E., Dacrory, S., Ali, K.A., Kamel, S.: International Journal of Biological Macromolecules Novel method of preparation of tricarboxylic cellulose nano fi ber for ef fi cient removal of heavy metal ions from aqueous solution. Int. J. Biol. Macromol. 119, 207–214 (2018).

23 Perera, H.M., Rajapaksha, A.U., Liyanage, S., Ekanayake, A., Selvasembian, R., Daverey, A., Vithanage, M.: Enhanced adsorptive removal of hexavalent chromium in aqueous media using chitosan-modified biochar: Synthesis, sorption mechanism, and reusability. Environ. Res. 231, 115982 (2023).

24 Buchman, Y.K., Lellouche, E., Zigdon, S., Bechor, M., Michaeli, S., Lellouche, J.P.: Silica nanoparticles and polyethyleneimine (PEI)-mediated functionalization: A new method of pei covalent attachment for siRNA delivery applications. Bioconjug. Chem. 24, 2076–2087 (2013).

25 Xing, X., Li, W., Zhang, J., Wu, H., Guan, Y., Gao, H.: TEMPO-oxidized cellulose hydrogel for efficient adsorption of Cu2+ and Pb2+ modified by polyethyleneimine. Cellulose. 28, 7953–7968 (2021).

26 Zhao, F., Repo, E., Song, Y., Yin, D., Hammouda, S. Ben, Chen, L., Kalliola, S., Tang, J., Tam, K.C., Sillanpää, M.: Polyethylenimine-cross-linked cellulose nanocrystals for

highly efficient recovery of rare earth elements from water and a mechanism study. Green Chem. 19, 4816–4828 (2017).

27 Zhang, Y., Yang, W., Luo, R., Shang, H.: Preparation of carbon nanospheres by non-catalytic chemical vapor deposition and their formation mechanism. New Carbon Mater. 31, 467–474 (2016).

28 Qhubu, M.C., Mgidlana, L.G., Madikizela, L.M., Pakade, V.E.: Preparation, characterization and application of activated clay biochar composite for removal of Cr(VI) in water: Isotherms, kinetics and thermodynamics. Mater. Chem. Phys. 260, 124165 (2021).

29 Lesaoana, M., Mlaba, R.P.V., Mtunzi, F.M., Klink, M.J., Edijike, P., Pakade, V.E.: Influence of inorganic acid modification on Cr(VI) adsorption performance and the physicochemical properties of activated carbon. South African J. Chem. Eng. 28, 8–18 (2019).

30 Sun, Y., Wu, Y., Fu, Y., Yang, C., Jiang, J., Yan, G., Hu, J.: Rapid and high selective removal of Hg(II) ions using tannic acid cross-linking cellulose/polyethyleneimine functionalized magnetic composite. Int. J. Biol. Macromol. 182, 1120–1129 (2021).

31 Sun, Y., Zhang, H., Li, Q., Vardhanabhuti, B., Wan, C.: High lignin-containing nanocelluloses prepared via TEMPO-mediated oxidation and polyethylenimine functionalization for antioxidant and antibacterial applications. RSC Adv. 12, 30030–30040 (2022).

32 Guo, Z., Yang, R., Yang, F., Sun, L., Li, Y., Xu, J.: Fabrication of polyethylenimine functionalized magnetic cellulose nanofibers for the sorption of Ni(II), Cu(II) and Cd(II) in single-component and multi-component systems. Int. J. Biol. Macromol. 184, 68–78 (2021).

33 Meng, Q., Li, H., Fu, S., Lucia, L.A.: Reactive & Functional Polymers The non-trivial role of native xylans on the preparation of TEMPO-oxidized cellulose nanofibrils. React. Funct. Polym. 85, 142–150 (2014).

34 Zhang, K., Li, H., Xu, X., Yu, H.: Synthesis of reduced graphene oxide/NiO

nanocomposites for the removal of Cr(VI) from aqueous water by adsorption. Microporous Mesoporous Mater. 255, 7–14 (2018).

35 Thangadurai, T.D., Manjubaashini, N., Thomas, S., Maria, H.J.: Nanostructured Materials for Environmental Remediation. (2020)

36 Anirudhan, T.S., Jalajamony, S., Suchithra, P.S.: Improved performance of a cellulose-based anion exchanger with tertiary amine functionality for the adsorption of chromium(VI) from aqueous solutions. Colloids Surfaces A Physicochem. Eng. Asp. 335, 107–113 (2009).

37 Lace, A., Ryan, D., Bowkett, M., Cleary, J.: Chromium monitoring in water by colorimetry using optimised 1,5-diphenylcarbazide method. Int. J. Environ. Res. Public Health. 16, (2019).

38 Marczenko, Z., Balcerzak, M.: Separation, preconcentration and spectrophotometry in inorganic analysis. Elsevier (2000)

39 Pourmortazavi, S.M., Sahebi, H., Zandavar, H., Mirsadeghi, S.: Fabrication of Fe3O4 nanoparticles coated by extracted shrimp peels chitosan as sustainable adsorbents for removal of chromium contaminates from wastewater: The design of experiment. Compos. Part B Eng. 175, 107130 (2019).

40 Moges, A., Nkambule, T.T.I., Fito, J.: The application of GO-Fe 3 O 4 nanocomposite for chromium adsorption from tannery industry wastewater. J. Environ. Manage. 305, 114369 (2022).

41 Masuku, M., Nure, J.F., Atagana, H.I., Hlongwa, N., Nkambule, T.T.I.: Advancing the development of nanocomposite adsorbent through zinc-doped nickel ferrite-pinecone biochar for removal of chromium (VI) from wastewater. Sci. Total Environ. 908, 168136 (2024).

42 Yan, E., Cao, M., Jiang, J., Gao, J., Jiang, C., Ba, X., Yang, X., Zhang, D.: A novel adsorbent based on magnetic Fe3O4 contained polyvinyl alcohol/chitosan composite nanofibers for chromium (Ⅵ) removal. Solid State Sci. 72, 94–102 (2017).

43 Wang, N., Ouyang, X. K., Yang, L. Y., & Omer, A. M. Fabrication of a magnetic cellulose nanocrystal/metal–organic framework composite for removal of Pb (II) from water. ACS Sustainable Chemistry & Engineering, 5(11), 10447-10458, (2017).

44 Yang, Rui, Katherine B. Aubrecht, Hongyang Ma, Ran Wang, Robert B. Grubbs, Benjamin S. Hsiao, and Benjamin Chu. "Thiol-modified cellulose nanofibrous composite membranes for chromium (VI) and lead (II) adsorption." Polymer 55, no. 5: 1167-1176, (2014)

45 Lu Jiao, Lu Jiao, Jin RuNa Jin RuNa, Liu Chao Liu Chao, Wang YanFei Wang YanFei, and Ouyang XiaoKun Ouyang XiaoKun. "Magnetic carboxylated cellulose nanocrystals as adsorbent for the removal of Pb (II) from aqueous solution." 547-556, (2016):

CHAPTER V: (OVERALL CONCLUSION, LIMITATIONS & FUTURE RECOMMENDATIONS)

PREAMBLE

In Chapter VI, the overall study conclusions, limitations, and future work are highlighted. The first section discusses a detailed summary of the overall observations and the results obtained from this study. Details on the characterizations of the nano adsorbent, the MCNC and MCNC-TEMPO-PEI are highlighted; the adsorption capacity of Pb (II) and Cr (VI) are summarized and discussed, respectively. The challenges encountered during the study are also outlined in the limitation section, and the future perspectives are discussed with an emphasis on giving the directive about the gaps that are left out to be covered in future work.

5.1 Overall conclusion

The magnetic cellulose nanocrystal (MCNC) and its derivatives (magnetite and cellulose nanocrystals) were successfully synthesised and confirmed with FTIR, P-XRD, UV-Vis, TEM, SEM-EDS, TGA and BET characterization techniques. The FTIR data revealed the presence of COOH, CH and OH band frequencies which confirmed the successful functionalization of CNCs and additionally, the Fe_3O_4 stretching band were also highlighted. The P-XRD diffractograms confirmed the crystalline monoclinic type 1 cellulose with 1β lattice and magnetite cubic spinel phases. The elemental composition from EDS confirmed the presence of Fe, O, and traces of C from the SEM analysis. The spherical and rod-like morphology of the nanocomposite was also observed with SEM and TEM analysis. BET analysis demonstrated a large surface area of 56 m^2/g with a sufficient pore volume of 0,1465 $cm^3/g.Å$ and pore size of 98 Å for the MCNC enhanced after the CNCs were functionalised with magnetite. The influential parameters were determined successfully using the 2^n-level half factorial design used for the adsorptive removal of Pb (II) ion from the multivariate analysis. The optimum conditions obtained, using the response surface where dosage = 60 mg, concentration = 100 ppb, time = 5 min, temperature 60 ºC and pH=6. The maximum adsorption capacity for Pb (II) obtained was 47 mg/g with the highest removal efficiency of 96 %. The adsorption capacity of

the three materials (Magnetite, CNC and MCNC) was validated and the order of increased adsorption capacity was found to be CNC<magnetite<MCNC. The adsorption isotherms revealed a physisorption interaction and a heterogeneous multilayer surface interaction governed by the weak van der Waals forces as the Freundlich adsorption and the PFO model are described. The thermodynamic parameters exhibited a spontaneous and exothermic thermodynamic reaction.

Furthermore, the modified MCNC-TEMPO-PEI was successfully synthesized, and the characterization techniques confirmed the formation of the synthesized nano-adsorbent material. The FTIR confirmed the deposition of amine groups in addition to the previously verified functional groups available on the surface of the material of MCNC nano adsorbent. The P-XRD exhibited an amorphous material from the MCNC-TEMPO-PEI contrary to the crystalline structure from the MCNC obtained from the P-XRD. The TEM, SEM and EDS confirmed the deposition of the amine groups in addition to the carboxylic and the hydroxyl groups. The morphology of the nano adsorbents was observed to be smooth, oval, needle-like and an irregular morphology for the MCNC-TEMPO-PEI, confirming the presence of Fe_3O_4, TEMPO and PEI after CNCs functionalization. The adsorption performance of MCNC-TEMPO-PEI on Cr (VI) was investigated by univariate optimization tools and the optimal parameters were captured as dosage = 30 mg, concentration = 5 ppm, temperature = 25 ºC, contact time = 15 minutes and pH = 2. The MCNC-TEMPO-PEI indicated a higher efficiency in terms of capacity and adsorptive removal of 4,4mg/g with a 98 %, removal efficiency respectively, as compared to the other tested adsorbents. These results revealed the chemisorption of the electrostatic interaction from the monolayer of the Langmuir adsorption isotherm with the PSO kinetic model against the Cr (VI) ions. The thermodynamic interaction was favourable, and a non-spontaneous endothermic reaction was observed. The adsorbent could be reused at least 8 times with a removal efficiency above 75 %. The results revealed that the real wastewater sample that was analysed from this study did not contain Cr (VI) ions.

The surface modification of the CNCs by grafting with amine groups and magnetite was to improve the adsorption capacity and removal efficiency of MCNC-TEMPO-PEI against the anionic Cr (VI) ions. However, the results demonstrated a low adsorption capacity which may be due to experimental setup (detection method) and the surface chemistry of the adsorbent.

5.2 General limitations

The limitation of this study could be attributed to the use of the UV-Vis technique for the quantification of the reaction which could have contributed towards the minimal adsorptive performance of the MCNC-TEMPO-PEI against the removal of Cr (VI) ions. This was discovered that the detection limit was lower at concentration ranges of 1-5 ppm and this was justified by some literature studies that opted to use UV-Vis owing to its reliability, precision and accuracy of the results after the complexed Cr (VI) ion. Literature has indicated that these results only attained a low adsorption capacity even when the adsorptive removal results were above 90 %.

The second limitation might have been due to the material surface chemistry. It could be suspected that the material surface binding sites were reduced due to further functionalization quenching the ability for the material to perform at optimal capacity. The availability of the carbonyl groups due to TEMPO oxidation reactions may have also contributed to the reduced adsorption capacity of the nanocomposites respectively.

5.3 Future recommendations

For future work, more emphasis will be placed on characterization techniques like BET and zeta potential that can predict the surface area, pore size and pore volume, as well as the surface charge of the MCNC-TEMPO-PEI nanocomposite material. Moreover, to improve the adsorption capacity by introducing more polymer materials like molecular imprinted polymer that have demonstrated to have trapping capacity of heavy metals. Furthermore, to study the adsorption capacity using different analytical techniques such as ICP-OES and AAS with improved detection limit. In contrast, to this study, where the adsorption capacity of the materials would be higher obtained during adsorption against higher concentrations of the

analyte. Moreover, the real wastewater analysis of MCNC against the adsorptive removal of Pb (II) ions to assess the surface capacity and selectivity of the adsorbent material.

APPENDIX

Table S1: The average crystalline size (D) calculation

Material	Peak Numbers	hkl values	Peak position (2θ)	FWHM	Crystalline size− D(nm)	Average D(nm)
CNC	1	*1,1,0*	11,54	0,44	17,78	9,56
	2	*1,1,0*	16,90	53,38	0,15	
	3	*0,0,2*	22,60	0,72	10,84	
	4	*2,2,0*	29,84	0,35	21,73	
	5	*0,2,1*	25,86	81,67	0,09	
	6	*0,0,4*	29,14	0,48	15,91	
	7	*0,4,0*	36,76	15,85	0,48	
M	1	*0,0,2*	22,18	5,41	1,44	4,98
	2	*2,2,0*	30,06	0,69	11,13	
	3	*3,1,1*	35,44	1,09	6,93	
	4	*4,0,0*	57,08	35,04	0,20	
	5	*4,2,2*	57,08	1,31	5,31	
	6	*4,4,0*	62,70	1,40	4,85	
MCNC	1	*1,1,0*	21,96	3,35	2,33	6,79
	2	*2,2,0*	21,84	0,57	13,71	
	3	*3,1,1*	35,47	0,77	9,83	
	4	*4,0,0*	36,08	52,46	0,14	
	5	*4,2,2*	57,08	0,89	7,84	
	6	*4,4,0*	62,74	0,99	6,86	

The average particles sizes of the three materials (CNC, M and MCNC) were calculate using the Debye Scherrer equation: $D = k\lambda / \beta \cos \theta$, where k is the shape factor constant and = 0,9; the λ is the wavelength and equates to 0.154 nm; β is the full width at half maximum (FWHM) and were measured at the highest tip peaks of all these materials and were captured on this table, θ is the de Bragg's angle which was also measured and displayed on this table as 2θ, so to calculate the particle size this angle was divided by 2 converted to radians. The calculated average particle size of each material were 9,56 nm, 4,98 nm and 6,79 nm,

respectively for CNC, M and MCNC materials and their peak intensities differs based on their functionalism that was conducted on each material. Therefore, these results confirm the formation of the three materials (CNC, M and MCNC) and also verify that they are indeed nano materials. Moreover, the results also corroborate with various studies for the formation, the crystallinity and the phase identification of the materials Half factorial screening design results with percentage removal

Table S2: The adsorptive isotherms models, kinetic studies, and thermodynamic calculations of MCNC against the removal of Pb (II) ions.

Data for Langmuir and Freundlich Isotherm Plots									
Experiment No	C_i (µg/mL)	C_i (mg/L)	C_e (mg/L)	$1/C_e$ (L/mg)	Log C_e	Ln C_e	q_e (mg/g)	$1/q_e$ (g/mg)	Log q_e
1	50	0.05	1.98821	0.502965	0.298462	0.687234736	8.001965	0.124969	0.903197
2	100	0.1	3.12987	0.319502	0.495526	1.14099147	16.14502	0.061939	1.208039
3	150	0.15	4.89596	0.204250	0.689838	1.588410375	24.18401	0.041350	1.383528
4	200	0.2	5.27124	0.189709	0.721913	1.662265629	32.45479	0.030812	1.511279
5	400	0.4	6.98921	0.143078	0.844428	1.944367531	50.79536	0.019687	1.705824
6	500	0.5	10.0922	0.099086	1.003986	2.311762848	81.65130	0.012247	1.911963
			Langmuir model calculation						
	Intercept	**Slope**	**q_{max}**	**K_L**	**R_L**	**R^2**			
	-0.0192	0.2786	52.0833	-0.06892	0.21245	0.9865			
			Freundlich model calculation						
	Intercept	**Slope**	**1/n**	**n**	**K_F**	**R^2**			
	0.4743	1.4252	1.4252	0.702	2.98057	0.9889			
Experiment No	Time, t (min)	C_i (mg/L)	C_e (mg/L)	q_e (mg/g)	q_t (mg/g)	t/q_t (min/mg/g)	q_e-q_t	Ln (q_e-q_t)	
1	0	0.1	0.442741	16.14502	-0.05712	0	16.20214	2.785143	
2	5	0.1	1.69822	16.14502	-0.26637	-18.7709	16.41139	2.797976	
3	10	0.1	8.51103	16.14502	-1.40184	-7.13349	17.54686	2.864875	
4	15	0.1	3.92564	16.14502	-0.63761	-23.5255	16.78263	2.820344	
5	20	0.1	1.5934	16.14502	-0.2489	-80.3536	16.39392	2.796911	
6	25	0.1	3.65993	16.14502	-0.59332	-42.1357	16.73834	2.817702	
7	30	0.1	1.12441	16.14502	-0.17074	-175.711	16.31576	2.792132	
			Pseudo-First-order kinetic calculation						
Intercept	Slope	qe (mg/g)	k_1	R^2					
2.9293	-0.0068	18.7145	0.0068	0.9689					
			Pseudo-Second-order kinetic calculation						
Intercept	Slope	q_e (mg/g)	$(q_e)^2$ (mg/g)^2	k_2	R^2				
72.826	-7.322	-0.13657	0.01865	0.73627	0.9077				

Table.S3: The thermodynamics calculations of the MCNC against the removal of Pb (II) ions

T(K)	Ci (µg/L	Ci(mg/L)	Ce (mg/L	Ce(mg/L)	qe(mg/g)	kd	lnkd	1/T
298	100	0,1	0,093	0,000093	0,016651167	0,179044803	-1,720119209	0,003355705
303	100	0,1	0,097	0,000097	0,0166505	0,171654639	-1,762270732	0,00330033
313	100	0,1	0,088	0,000088	0,016652	0,189227273	-1,664806485	0,003194888
323	100	0,1	0,0722	0,0000722	0,016654633	0,230673592	-1,46675159	0,003095975
333	100	0,1	0,089	0,000089	0,016651833	0,187099251	-1,676116049	0,003003003
343	100	0,1	0,077	0,000077	0,016653833	0,21628355	-1,531165002	0,002915452

Table S.4: Particle size calculation for the three adsorbents

Material	Peak numbers	Peak position 2θ	FWHM	Crystalline size D (nm)	Average D (nm)
CNC-TEMPO	1	8,8497	0,44467	17,81233	
	2	19,03994	0,5185	15,11067	
	3	22,58665	0,8618	9,039763	
	4	24,72381	0,60309	12,86723	
	5	27,05615	0,67151	11,50225	
	6	31,39817	1,27293	6,008135	12,2997
	7	45,25566	0,533	13,75753	
CNC-TEMPO-PEI	1	16,6002	7,64602	1,028127	1,03
MCNC-TEMPO-PEI	1	17,64492	7,66147	1,024646	0,432245
	2	41,70105	46,29033	0,16038	
	3	17,64492	70,2747	0,111709	

Table S2: The adsorptive isotherms and the kinetic study models the removal of Cr (VI) ions using MCNC-TEMPO-PEI

Data for Langmuir and Freundlich adsorption isotherms											
Exp no	**Theoretical Ci (mg/L)**	**Intercept**	**slope**	**Ci (mg/L)**	**Ce (mg/L)**	**1/Ce**	**Log Ce**	**Ln Ce**	**qe (mg/g)**	**1/qe**	**Logqe**
1	1	0,1061	0,3888	1,658951	0,418724	2,388206	-0,37807	-0,87054	0,413409	2,418913	-0,38362
2	3	0,1061	0,3888	3,444959	0,451903	2,212863	-0,34495	-0,79429	0,997685	1,00232	-0,00101
3	5	0,1061	0,3888	5,260545	0,450103	2,221714	-0,34669	-0,79828	1,603481	0,623643	0,205064
4	7	0,1061	0,3888	6,563014	0,457047	2,187957	-0,34004	-0,78297	2,035322	0,491323	0,308633
5	9	0,1061	0,3888	9,870628	0,454218	2,201586	-0,34274	-0,78918	3,138803	0,318593	0,496764
Langmuir											
		Intercept	**Slope**	**q_{max}**	**KL**	**RL**	**R^2 value**				
		-21,307	9,93458	0,04693	-2,14473	-0,10284	0,93378				
Freundlich											
		Intercept	**Slope**	**qe**	**1/n**	**Kf**	**R^2 value**				
		6,75157	18,9062		18,90622	5643779	0,76965				
Adsorption studies for Pseudo first and second order kinetics											
Exp	**Time (min)**	**Intercept**	**slope**	**Ci (mg/g)**	**Ce(mg/g)**	**qe(mg/g)**	**qt (mg/g)**	**qe-qt (mg/g)**	**Ln(qe-qt)**	**t/qt**	
1	5	0,0406	0,24515	5,52886	0,438507	1,72154	1,696784	0,024755	-3,69871	2,946751	
2	10	0,0406	0,24515	5,52886	2,525801	1,72154	1,00102	0,72052	-0,32778	9,989813	
3	15	0,0406	0,24515	5,52886	3,115643	1,72154	0,804405	0,917134	-0,0865	18,64731	
4	20	0,0406	0,24515	5,52886	0,399347	1,72154	1,709838	0,011702	-4,44797	11,69702	
5	25	0,0406	0,24515	5,52886	0,418519	1,72154	1,703447	0,018093	-4,01224	14,67613	
6	30	0,0406	0,24515	5,52886	0,418519	1,72154	1,703447	0,018093	-4,01224	17,61135	
Pseudo Second Order											
		Intercept	**Slope**	**K1**	**qe(mg/g)**	**R^2**					
		-1,06599	-0,09704	-0,00323	0,344387	0,20673					
Pseudo Second Order											
		intercept	**Slope**	**qe**	**qe^2**	**K_2**		**R^2**			
		4,55156	0,45961	2,175758	4,733922	21,54673		0,55404			